Schriftenreihe des Instituts für Pflanzenbau und Pflanzenzüchtung Christian-Albrechts-Universität zu Kiel

Series of the Institute of Crop Science and Plant Breeding Kiel University

Acker- & Pflanzenbau

Agronomy & Crop Science

Katja Holzhauser

Cover Crops for Sustainable Silage-Maize Production: Enhancing Resource Use Efficiency through Modelling and Remote Sensing

118

Schriftenreihe des Instituts für Pflanzenbau und Pflanzenzüchtung
der Christian-Albrechts-Universität zu Kiel, Heft 118, 2025

Series of the Institute of Crop Science and Plant Breeding
at Kiel University, No 118, 2025

veröffentlicht mit Genehmigung
der Agrar- und Ernährungswissenschaftlichen Fakultät

Institut für Pflanzenbau und Pflanzenzüchtung
Agrar- und Ernährungswissenschaftliche Fakultät
Christian-Albrechts-Universität zu Kiel
Christian-Albrechts-Platz 4
24118 Kiel, Germany

ISSN: 1435-2613

Aus dem Institut für Pflanzenbau und Pflanzenzüchtung
der Christian-Albrechts-Universität zu Kiel

Cover Crops for Sustainable Silage-Maize Production

Enhancing Resource Use Efficiency through Modelling and Remote Sensing

---

Dissertation
zur Erlangung des Doktorgrades
der Agrar- und Ernährungswissenschaftlichen Fakultät
der Christian-Albrechts-Universität zu Kiel
vorgelegt von

M.Sc. Katja Holzhauser
aus St. Ingbert
Kiel, 2025

Dekan: Prof. Dr. Tim Diekötter

1. Berichterstatter: Prof. Dr. Henning Kage
2. Berichterstatterin: Prof.in Dr.in Sandra Spielvogel

Tag der mündlichen Prüfung: 21.05.2025

Table of Content

Chapter 1

General Introduction

Silage maize (*Zea mays*), also referred to as *"green maize"*, encompasses all forms of maize harvested as whole plant, primarily for silage but also for direct animal consumption or renewable energy production. Its versatility as high-energy livestock fodder and as key resource for biogas production underlines its central role in European agriculture. In the European Union, 5-6 million hectares of maize are cultivated annually (5.8 Mio ha in 2024), with Germany contributing approximately 2 Mio ha (Statistisches Bundesamt, 2024). The productivity of maize cultivation increased in recent decades (Food and Agriculture Organization of the United Nations, 2025), as a result of plant breeding, optimised managements as well as climate change (Lauer et al., 2001; Olesen et al., 2011; Taube et al., 2020). In parallel, the European Common Agricultural Policy (CAP, 2023-2027) has increasingly emphasised the need for a transition toward more climate-resilient and environmentally sustainable agricultural systems. Key objectives include reducing overfertilization and greenhouse gas emissions, enhancing soil health, and improving biodiversity. By promoting practices like diversifying crop rotations and integrating cover crops the CAP aims to foster agricultural resilience while mitigating climate change. Given its prominent role in European agriculture, silage maize is likely to substantially contribute to these efforts, balancing productivity with sustainable use of resources (European Commission, 2023).

For a better understanding and management of these dynamics, crop growth models have become an indispensable tool in agricultural research. They provide critical insights into crop development, yield potential, resource allocation, and the below-ground dynamics of soil water balance and rhizosphere. By comprehending these fundamental processes, it becomes feasible to promote efficient resource utilisation, thereby enabling the realisation of high yields at limited fertilisation or changed climatic conditions. Furthermore, crop simulation models enable the assessment of yield potential and food security under future climate scenarios, particularly for key crops like wheat, rice, and maize (Gavasso-Rita et al., 2023). For maize, various crop growth models such as CERES-Maize (Jones and Kiniry, 1986), DSSAT (Jones et al., 2003), and APSIM (Keating et al., 2003) have been developed globally, though primarily for grain maize. Silage maize, in Europe mainly grown in France and Germany, requires models tailored to earlier harvests and European cultivation conditions. To address this, a crop growth component for silage maize HUME component library was developed. Within this library other crop growth components have already been developed for winter wheat (Neukam et al., 2016), oilseed rape

(Böttcher et al., 2016) and sugar beet (Stephan et al., 2020).This work is documented as chapter two of this thesis and is subject to submission. – was adapted for silage maize in the initial part of this thesis.

However, an advanced crop management should not consider maize cultivation in isolation, but as a part of a holistic crop rotation. A common strategy to diversify spring crop production systems, such as silage maize, also recommended in the CAP (2023-2027), is to grow winter cover crops in advance. Cover crops offer numerous benefits for agriculture and soil health by providing key environmental services, including increase of soil organic matter, erosion control, weed suppression, and prevention of nitrogen (N) leaching (Thorup-Kristensen et al., 2003; Blanco-Canqui et al., 2011; Abdalla et al., 2019). Furthermore, cover crops are widely documented to improve soil physical properties, as they reduce soil compaction, enhance porosity, and increase water infiltration (Blanco-Canqui and Ruis, 2020). In particular, the cultivation of cover crop mixtures is becoming increasingly important, as functional diversity can improve resource utilisation efficiency and system stability (Tilman, 2013; Florence and McGuire, 2020). However, the optimisation of such mixtures represents a scientific challenge, as the pure number of species does not necessarily correlate with higher productivity (Wortman et al., 2012; Smith et al., 2014). Studies on cover crops show varying impacts on maize yields. While some report no effects or even negative impacts from monoculture cover crops (Tonitto et al., 2006; Kühling et al., 2023), others highlight benefits (Marcillo and Miguez, 2017), especially when legumes or mixed-species cover crops are used, which may increase yields (Abdalla et al., 2019). However, yield improvement may not always be the primary goal; rather, enhancing resource efficiency within the system could be more relevant. A well-structured soil resulting from cover crop use may improve water access, thereby increasing water use efficiency (Blum, 2009). Additionally, improved nutrient availability, particularly N, provided by cover crop residues generally supports maize growth and green area development, which in turn enhances radiation interception. Therefore, the third chapter of this thesis comprises an empirical study of cover crop mixtures subsequent impact on the maize yield development and its resource efficiency.

To better understand the effects of cover crops on maize growth and N availability in spring, it is important to look at the cover crop period itself, as they perform their essential functions during the winter. Accurate monitoring of the cover crop growth is therefore crucial, especially when mixtures with functional diversity are used. Advances in technology have provided various platforms for spectral data acquisition, including earth-orbiting satellites like Landsat and Sentinel (Clevers and Gitelson, 2013), handheld multispectral or hyperspectral sensors (Rose et al., 2023), and unmanned aerial vehicle (UAV)-mounted systems, which allow for high-resolution and high-throughput data collection. Remote sensing for essential crop parameters

green area index (GAI), dry matter (DM), or N uptake in cash crops such as maize (Kira et al., 2016; Bukowiecki et al., 2024) and wheat (Bukowiecki et al., 2019), are well-documented. The visual light spectrum primarily reflects chlorophyll content, with green light being reflected and red light absorbed during photosynthesis. Meanwhile, near infrared (NIR) reflectance provides structural information about the canopy, such as leaf architecture and thickness (Viña et al., 2011). Combining these wavelengths into vegetation indices (VI) like the normalised difference vegetation index (NDVI) or simple ratios improves the accuracy of monitoring plant development and biomass. However, the UAV-based monitoring of cover crops present additional challenges, due to the short growing-season under often difficult weather conditions and the heterogeneous spectral responses of cover crop mixtures in contrast to cash crop monocultures. Thus, in the fourth chapter of the thesis, calibrations for a UAV-based estimation of above ground canopy parameters for various cover crop sole stands as well as mixtures were developed.

By employing a diverse methodological approach, this thesis explores key aspects of a sustainable and resource-efficient silage maize cultivation, with a particular focus on the integration of cover crops:

1. The calibration and evaluation of the HUME model for silage maize allows the precise simulation of growth and yield dynamics, considering different climatic and site-specific conditions.
2. A detailed empirical analysis of silage maize after deep-rooted cover crop mixtures clarifies the potential impacts on yield formation, regarding radiation uptake and the use of soil water resources.
3. In light of nitrogen use efficiency of the regarded system, calibration of multispectral reflectance data enables the precise estimation of biomass and nitrogen uptake by different winter cover crops and diverse mixtures. (Published in *Remote Sensing*)

The integration of the three presented studies provides a comprehensive framework for optimizing the resource efficiency of crop rotation systems involving winter cover crops and silage maize. The empirical analysis of multiannual field trials, alongside data acquisition using modern remote sensing technology, establishes a robust database and process comprehension for future model enhancements. Moreover, the data and process understanding developed herein can serve as a foundation for further works, such as the refinement of the HUME-Maize model. These implications underline the dissertation's potential to support the development of a resource efficient agricultural systems capable of addressing both current and future challenges.

References

Abdalla, M., Hastings, A., Cheng, K., Yue, Q., Chadwick, D., Espenberg, M., Truu, J., Rees, R.M., Smith, P., 2019. A critical review of the impacts of cover crops on nitrogen leaching, net greenhouse gas balance and crop productivity. Global change biology 25, 2530–2543.

Blanco-Canqui, H., Mikha, M.M., Presley, D.R., Claassen, M.M., 2011. Addition of Cover Crops Enhances No-Till Potential for Improving Soil Physical Properties. Soil Science Society of America Journal 75, 1471–1482.

Blanco-Canqui, H., Ruis, S.J., 2020. Cover crop impacts on soil physical properties: A review. Soil Sci. Soc. Am. j. 84, 1527–1576.

Blum, A., 2009. Effective use of water (EUW) and not water-use efficiency (WUE) is the target of crop yield improvement under drought stress. Field Crops Research 112, 119–123.

Böttcher, U., Rampin, E., Hartmann, K., Zanetti, F., Flenet, F., Morison, M., Kage, H., 2016. A phenological model of winter oilseed rape according to the BBCH scale. Crop Pasture Sci. 67, 345.

Bukowiecki, J., Rose, T., Ehlers, R., Kage, H., 2019. High-Throughput Prediction of Whole Season Green Area Index in Winter Wheat With an Airborne Multispectral Sensor. Frontiers in plant science 10, 1798.

Bukowiecki, J., Rose, T., Holzhauser, K., Rothardt, S., Rose, M., Komainda, M., Herrmann, A., Kage, H., 2024. UAV-based canopy monitoring: Calibration of a multispectral sensor for green area index and nitrogen uptake across several crops. Precision Agric 28, 345.

Clevers, J., Gitelson, A.A., 2013. Remote estimation of crop and grass chlorophyll and nitrogen content using red-edge bands on Sentinel-2 and -3. International Journal of Applied Earth Observation and Geoinformation 23, 344–351.

European Commission, 2023. Common Agricultural Policy 2023-2027: Overview. https://agriculture.ec.europa.eu/common-agricultural-policy/cap-overview/cap-2023-27_de#legalbases. Accessed 15 January 2025.

Florence, A.M., McGuire, A.M., 2020. Do diverse cover crop mixtures perform better than monocultures? A systematic review. Agronomy Journal 112, 3513–3534.

Food and Agriculture Organization of the United Nations, 2025. FAOSTAT Statistical Database: Crop production data. https://www.fao.org/faostat/en/#data/QCL. Accessed 15 January 2025.

Gavasso-Rita, Y.L., Papalexiou, S.M., Li, Y., Elshorbagy, A., Li, Z., Schuster-Wallace, C., 2023. Crop models and their use in assessing crop production and food security: A review. Food and Energy Security 1, 27.

Jones, C.A., Kiniry, J.R., 1986. CERES-Maize. A simulation model of maize growth and development. Texas A. and M. University Press, Collage station.

Jones, J., Hoogenboom, G., Porter, C., Boote, K., Batchelor, W., Hunt, L., Wilkens, P., Singh, U., Gijsman, A., Ritchie, J., 2003. The DSSAT cropping system model. European Journal of Agronomy 18, 235–265.

Keating, B., Carberry, P., Hammer, G., Probert, M., Robertson, M., Holzworth, D., Huth, N., Hargreaves, J., Meinke, H., Hochman, Z., McLean, G., Verburg, K., Snow, V., Dimes, J., Silburn, M., Wang, E., Brown, S., Bristow, K., Asseng, S., Chapman, S., McCown, R., Freebairn, D., Smith, C., 2003. An overview of APSIM, a model designed for farming systems simulation. European Journal of Agronomy 18, 267–288.

Kira, O., Nguy-Robertson, A.L., Arkebauer, T.J., Linker, R., Gitelson, A.A., 2016. Informative spectral bands for remote green LAI estimation in C3 and C4 crops. Agricultural and Forest Meteorology 218-219, 243–249.

Kühling, I., Mikuszies, P., Helfrich, M., Flessa, H., Schlathölter, M., Sieling, K., Kage, H., 2023. Effects of winter cover crops from different functional groups on soil-plant nitrogen dynamics and silage maize yield. European Journal of Agronomy 148, 126878.

Lauer, J.G., Coors, J.G., Flannery, P.J., 2001. Forage Yield and Quality of Corn Cultivars Developed in Different Eras. Crop Science 41, 1449–1455.

Marcillo, G.S., Miguez, F.E., 2017. Corn yield response to winter cover crops: An updated meta-analysis. Journal of Soil and Water Conservation 72, 226–239.

Neukam, D., Böttcher, U., Kage, H., 2016. Modelling Wheat Stomatal Resistance in Hourly Time Steps from Micrometeorological Variables and Soil Water Status. J Agro Crop Sci 202, 174–191.

Olesen, J.E., Trnka, M., Kersebaum, K.C., Skjelvåg, A.O., Seguin, B., Peltonen-Sainio, P., Rossi, F., Kozyra, J., Micale, F., 2011. Impacts and adaptation of European crop production systems to climate change. European Journal of Agronomy 34, 96–112.

Rose, M., Rose, T., Kage, H., 2023. Spectral reflection and crop parameters: can the disentanglement of primary and secondary traits lead to more robust and extensible prediction models? Precision Agric 24, 607–626.

Smith, R.G., Atwood, L.W., Warren, N.D., 2014. Increased productivity of a cover crop mixture is not associated with enhanced agroecosystem services. PLOS ONE 9, e97351.

Statistisches Bundesamt, 2024. Ackerland nach Hauptfruchtgruppen und Fruchtarten. https://www.destatis.de/DE/Themen/Branchen-Unternehmen/Landwirtschaft-Forstwirtschaft-Fischerei/Feldfruechte-Gruenland/Tabellen/ackerland-hauptnutzungsarten-kulturarten.html. Accessed 23 October 2024.

Stephan, H., Böttcher, U., Sieling, K., Kage, H., 2020. Yield potential of non-bolting winter sugar beet in Germany. European Journal of Agronomy 115, 126035.

Taube, F., Vogeler, I., Kluß, C., Herrmann, A., Hasler, M., Rath, J., Loges, R., Malisch, C.S., 2020. Yield Progress in Forage Maize in NW Europe—Breeding Progress or Climate Change Effects? Front. Plant Sci. 11, 473.

Thorup-Kristensen, K., Magid, J., Jensen, L.S., 2003. Catch crops and green manures as biological tools in nitrogen management in temperate zones. Advances in Agronomy, 227–302.

Tilman, D., 2013. Functional Diversity. In: Levin, S.A. (Ed.) Encyclopedia of biodiversity, 2nd ed. Academic Press, Amsterdam, pp. 587–596.

Tonitto, C., David, M.B., Drinkwater, L.E., 2006. Replacing bare fallows with cover crops in fertilizer-intensive cropping systems: A meta-analysis of crop yield and N dynamics. Agriculture, Ecosystems & Environment 112, 58–72.

Viña, A., Gitelson, A.A., Nguy-Robertson, A.L., Peng, Y., 2011. Comparison of different vegetation indices for the remote assessment of green leaf area index of crops. Remote Sensing of Environment 115, 3468–3478.

Wortman, S.E., Francis, C.A., Lindquist, J.L., 2012. Cover Crop Mixtures for the Western Corn Belt: Opportunities for Increased Productivity and Stability. Agronomy Journal 104, 699–705.

Chapter 2

HUME-Maize: A dynamic crop growth model for silage maize (*Zea mays* L.)

Katja Holzhauser[a *], Babette Wienforth[a], Martin Komainda[b], Antje Herrmann[c], Iris Zimmermann[d], Michaela Dippold[e], Sandra Spielvogel[d], Henning Kage[a], Josephine Bukowiecki[a]

a Institute of Crop Science and Plant Breeding, Agronomy and Crop Science, Kiel University, Germany
b Department of Crop Sciences, Grassland Science, Georg-August-University of Göttingen, Germany
c Hessen Department of Agriculture Affairs, Germany
d Institute of Plant Nutrition and Soil Science, Soil Science, Kiel University, Germany
e Department of Geoscience, Geo-Biosphere Interactions, University of Tübingen, Germany

Corresponding author.: holzhauser@pflanzenbau.uni-kiel.de (Katja Holzhauser)

Keywords: *Zea mays* L., crop growth model, yield prediction, dry matter partitioning, drought stress

Abstract

Modelling crop growth is crucial for agricultural research. Including detailed processes of plant growth and water uptake enable the analysis on effects of breeding progress on plant allometry, of crop sequences and soil textures on root growth and water uptake, thus enabling forecasts of potential crop yields under current and changing climate conditions. This study endeavors to establish a foundational framework for a dynamic growth model, specifically tailored for silage maize within European climate contexts, termed HUME-Maize. The model considers drought stress and focussed on the mid-early maturity group and sufficient nitrogen supply. Data from multi-annual field trials conducted under a huge gradient of climatic conditions and contrasting soil types served as basis for calibration and an independent model evaluation. Parameters of the model components *development, dry matter production, partitioning, root growth, evapotranspiration* and *soil water balance* were determined by linear regression or derived by literature research. Model performance in terms of dry matter production resulted in R^2 of 0.97 and 0.95 for calibration and evaluation datasets, respectively. Despite differing sowing dates, growth stages were simulated with high confidence during the whole season with RMSE of 8.83 d for calibration and 4.43 d evaluation datasets. The resultant HUME-Maize model emerges as a valuable tool for comprehending and predicting silage maize growth under European climate conditions. Furthermore, it serves as a foundation for future investigations, with potential expansions to include nitrogen limitations or differences in cultivar specific phenotypes.

1. Introduction

The modelling of crop growth stands as a pivotal effort in agricultural research, providing not only insights into the underlying processes of plant growth but also holding significant implications for optimizing crop yields and promote sustainable agricultural practices. Being able to assess potential yields for future scenarios, crop simulation models are important tools for forecasting food security and yield gaps under climate change conditions (Gavasso-Rita et al., 2023; van Wart et al., 2013). In the past decades, several crop growth models for wheat, rice and maize have been developed and tested globally (Basso et al., 2016; Gavasso-Rita et al., 2023; Qin et al., 2023).

For maize (*Zea mays*, L.), CERES-Maize (Jones and Kiniry, 1986) can be regarded as the origin of process orientated plant growth simulation. The model runs by weather data and is based on the approach that plant growth is dependent on the product of photosynthetic active radiation (PAR) and the light use efficiency (LUE). Further growth stages are separated into important physiological timepoints, such as silking or grain filling, but eventually depending on temperature. Later on, Jones et al. (2003) developed a more generic model called DSSAT, providing a user-friendly platform that enables farmers and researchers to analyse different scenarios and improve their decision-making in the field of agriculture. Yang et al. (2004) modified CERES-Maize with regard to cultivar-specific effects and recently improved root growth and water deficit responses to the model named HYBRID-Maize. As both models were developed in the United States, Australian researchers developed a growth model named APSIM adjusted to their respective site conditions (Keating et al., 2003). Nowadays, APSIM is used worldwide and is adaptable to various site conditions and crops (Brown et al., 2019; Holzworth et al., 2014).

However, these maize growth models were developed for the simulation of grain maize growth. Whereas in Northwest Europe, maize is mainly harvested as green maize or silage maize, hence earlier in the vegetation period (European Commission, 2023). Main European silage maize growing regions are situated in France and Germany (European Commission, 2023). Recently, Morel et al. (2020) reparametrized APSIM-Maize for silage maize and for higher latitudes in Northern Europe. Yet, their model distinctly underestimated biomass production. Morel et al. (2020) traced this back to missing adjustments to climatic conditions, especially concerning radiation uptake and day lengths, and concluded a large need for further data acquisition. However, it could be a more efficient approach to adapt an already well-performing crop model under Northern European conditions to silage maize. The crop growth and soil simulation model approach HUME (Kage and Stützel, 1999b) was already successfully applied to model yield

formation of winter wheat (Henke et al., 2008; Johnen et al., 2014; Ratjen et al., 2018) and of winter oilseed rape (Böttcher et al., 2020) under German conditions.

Therefore, the aim of this paper was the development of a dynamic growth model for silage maize suited for the climate conditions of the main European silage maize growing area. For this purpose, the model approach HUME was adjusted crop-specific and developed further. Data of multiannual field trials at different German sites formed the basis for calibration and independent evaluation. With the idea of conducting further studies advancing the resulting HUME-Maize model, this study focusses on growth conditions without any nitrogen limitations and on silage maize of one maturity group only.

2. Material and Methods

2.1. Datasets

The data basis comprises sets of field trials conducted across four distinct sites in Northern to Central Germany under temperate agro-climatic conditions over four consecutive years (Table 1; data set 1-14), focusing on mid-early silage maize cultivars. The trials had a randomised block design (4 replications) ensuring adequate N fertilization. Geographical positioning, soil texture, year of study, and sowing dates varied across trial sites, as detailed in Table 1. Meteorological data was retrieved of the nearest DWD weather station (Deutscher Wetterdienst, 2023) exhibiting notable discrepancies between sites and across different years (Table 1). In order to facilitate an unbiased assessment, the data was divided into a calibration dataset and an evaluation dataset. Both datasets encompass field observations from two distinct years and at least two sites, each exhibiting significant variations in weather conditions.

2.1.1. Calibration datasets

All model parameters for above-ground plant growth were calibrated by dataset 1-6 (Table 1). The field trials for this were conducted at two sites (Hohenschulen and Karkendam, experimental farms of Kiel University) in Northern Germany in 2007 and 2008 (Table 1) as part of a research project focusing on nitrogen use efficiency in biogas production systems. The experimental farm Hohenschulen is located on a sandy loam soil (Luvisol) and the soil at Karkendam is sand (Gleyic Podzol). Both study sites are influenced by the maritime climate of the Baltic Sea. Weather conditions during the observed growing seasons are shown in Table 1. From the different trial treatments, plots of two different crop rotations and therefore different sowing dates were chosen (Table 1). From each crop rotation, two treatments of highest nitrogen levels were used for model calibration (240, 300 kg N ha^{-1}) in order to exclude N limitation. Within this study, no cultivar-specific differences were considered. The grown cultivar was KWS Ronaldinio from a mid-early maturity group.

Calibration of the *root growth* parameters was done by data of a research project examining the root growth of maize after different winter cover crops (dataset 8 and 12). The trials took place at the above described experimental farm Hohenschulen during summer 2021 and 2022. However, above ground measurements of dataset 8 and 12 were used for model evaluation.

2.1.2. Evaluation datasets

The model was evaluated with data of set 7-14. All field trials were conducted in 2021 and 2022. The trials providing dataset 7, 8, 11 and 12 were conducted at the experimental farm Hohenschulen (site A), but differed in the sowing date and the year of cultivation. The field trials

for dataset 9 and 13 were located in the Northwest of Germany at the experimental farm Wehnen of the Agricultural Chamber of Lower Saxony and coordinated by the University of Göttingen (site C). Dataset 10 and 14 were compiled by field trials at Bad Hersfeld in Central Germany, managed by the Hessen department of agriculture (site D). In addition to climatic differences, soil types of location C and D were sand and sandy silt, respectively. The field trials of datasets 7, 9, 10, 11, 13 and 14 were conducted within a research project focussing on the nitrogen use efficiency of maize (Table 1). The N levels chosen for the present study were 180, 240 and 300 kg N ha^{-1}, to ensure sufficient N supply. Mid-early maturity groups were selected for evaluation datasets as well (KWS Gunnario: 7,9,10,11,13,14; KWS Stefano: 8, 12).

2.1.3. Data sampling

Aboveground biomass was consistently measured sequentially over several dates of the growing season by means of destructive manual sampling. Therefore, at least 10 plants per plot were harvested and weighted. In order to assign the dry matter weights to a specific area, length of harvested maize rows were determined to form a parallelogram and consequently its area. An aliquot of the harvested plants was fractionated into the organs, leaf, stem and cob (DM_{leaf}, DM_{stem}, DM_{cob}). As small generative organs, husk and panicle were assigned to cob dry matter. For all organs, DM was determined and summarized to DM_{shoot}. For each sampling, GAI was determined by scanning the leaves (LAI) and stems (SAI) using the LAI-3100 (LI-COR, Inc., Lincoln, NE, USA).

In the field trials used for evaluation, GAI was additionally monitored by drone-based multispectral measurements with a Sequoia™ camera (Parrot Sequoia, Parrot Drones SAS, 143 Paris, France) and a corresponding GAI calibration for silage maize (Bukowiecki et al. 2024). Crop height, BBCH (Lancashire et al. 1991) and number of leaves (only for 2008) were determined frequently during the growing season.

Root growth was measured in the field trials providing dataset 8 and 12 (Table 1). In both trial years root length (RL) and root length density (RLD) were monitored to a soil depth of 120 cm, either by soil pits or by soil cores. Soil cores were sampled at silking and grain filling and divided into 10 cm sections. After washing the samples, extracted roots were scanned using the Epson Perfection V850 Pro. The scans were analysed using RhizoVision Explorer v2.0.3 (Seethepalli et al., 2021). Rooting depth (zr) was investigated at four timepoints during the growing period of 2022 (dataset 12) measuring the deepest visible root in the soil pit.

Table 1 Datasets used for calibration and evaluation. The datasets differ in their location (Site A: Hohenschulen, Site B: Karkendam, Site C: Wehnen, Site D: Bad Hersfeld), soil type, trial year and sowing dates. Temperature is averaged and precipitation is summed up over the growing season (sowing till harvest date).

Data use			Dataset	Site	Geographical position	Soil type	Trial year	Sowing date	Temperature [°C]	Precipitation [mm]
Calibration		Evaluation shoot growth								
Shoot growth	Root growth									
X			1	A	54.18°N, 9.58°E	sandy loam	2007	2007/04/19	14.8	496.5
X			2	A	54.18°N, 9.58°E	sandy loam	2007	2007/05/15	15.4	452.4
X			3	B	53.55°N, 9.56°E	sand	2007	2007/04/20	15.1	520.7
X			4	A	54.18°N, 9.58°E	sandy loam	2008	2008/04/24	14.5	370.6
X			5	A	54.18°N, 9.58°E	sandy loam	2008	2008/04/30	14.6	357.9
X			6	B	53.55°N, 9.56°E	sand	2008	2008/04/28	15.1	371.4
		X	7	A	54.18°N, 9.58°E	sandy loam	2021	2021/04/28	15.4	461.8
	X	X	8	A	54.18°N, 9.58°E	sandy loam	2021	2021/05/20	16.0	389.7
		X	9	C	51.49°N, 9.93°E	sand	2021	2021/05/01	15.5	524.3
		X	10	D	51.59°N, 9.85°E	sandy silt	2021	2021/05/31	15.6	322.7
		X	11	A	54.18°N, 9.58°E	sandy loam	2022	2022/04/28	16.2	238.7
	X	X	12	A	54.18°N, 9.58°E	sandy loam	2022	2022/04/29	15.7	273.5
		X	13	C	51.49°N, 9.93°E	sand	2022	2022/05/02	17.3	182.5
		X	14	D	51.59°N, 9.85°E	sandy silt	2022	2022/05/09	18.4	132.5

2.2. The model

The silage maize crop growth model is built in the modelling environment HUME (Kage and Stützel (1999b). It is an object-orientated component library, based on the software development technology Delphi® /C++ Builder®. Within HUME, there are several components depicting different parts of the soil-water-atmosphere-plant continuum. These can be linked to a main component and fitted crop-specifically to model crop growth of winter wheat (Johnen et al., 2014; Kage et al., 2003; Neukam et al., 2016) or winter oilseed rape (Böttcher et al., 2020). The components of this library used for the maize crop growth model are *evapotranspiration*, *dry matter production*, *dry matter partitioning*, *root growth* and *soil water balance* described in the following chapters. All components are linked to a main model component, which provides the simulation and a basic statistical analysis. A component includes *variables*, *state variables*, *parameters* and *external variables*. The latter describes variables, which are either exchanged between the components or input variables, to start the model (e.g. temperature, global radiation).

Crop-specific modifications of components and crop-specific fits of parameters were either derived by chosen scientific studies or computed by linear regression based on the calibration data (Table 1). A table of these model parameters, their value, description and source can be found in Appendix B (Table B 1). Model performance was tested with regard to above-ground shoot growth and the partitioning to the organs, as well as the plant development. Therefore, root mean squared errors (RMSE), intercepts, slope sand R^2 between the measured vs. simulated regressions were calculated for the calibration and evaluation. Model equations (E) are listed in Appendix A. Parameter calibration and model evaluation was carried out using the software R (R Core Team, 2023). The performance was assessed with slope and intercept of the regression between measured and simulated data, R^2 and root mean square error (RMSE).

2.2.1. Development

Maize development is regulated by the effective temperature (T_{eff}) – derived by the positive difference of daily mean temperature and a defined base temperature (T_1) of 6°C in agreement with Pagès and Pellerin (1994), Verheul et al. (1996), R. Bonhomme et al. (1994)). Furthermore, the development process is separated into five stages further named XStage, following HYBRID-Maize, based on the approach of Yang et al. (2016). The XStages represent the development stages emergence, tassel initiation, silking, effective grain filling and maturity (Figure 1). Development rates between sowing and emergence (DevRateS0), emergence and tassel initiation (DevRateS1), tassel initiation and silking (DevRateS2), silking and grain filling (DevRateS3) are calculated as simple ratio of T_{eff} and the temperature sum (GDD) between the respective XStages (E1-E4). Compared to the approach of Yang et al. (2016), an additional GDD

is introduced from emergence till silking (GDD_{silk}) to calculate the development rate from grain filling until maturity (DevRateS4, E5).The GDDs are defined cultivar specific parameters assigned according to the assumptions of Bignon (1990) for a mid-early cultivar at a soil with medium warming dynamics, harvested at the dough stage, which is the harvest date of whole crop silage maize with a typical DM content of 35%.

Growth of leaf number is calculated according to the approach of HYBRID- and CERES-Maize (Jones and Kiniry, 1986; Yang et al., 2016). Thereby, leaf growth is the ratio between T_{eff} and the parameter phyllochron (phy, E6). For the early growth period in which the plant has less than five leaves (< BBCH15), growth rate is assumed to be higher. Therefore, a factor (f_{phy}) is reducing phy (E7). However, in the field trials, growth stages were recorded according to the BBCH scale of Lancashire et al. (1991), hence, were converted into XStages for model evaluation (Figure 1).

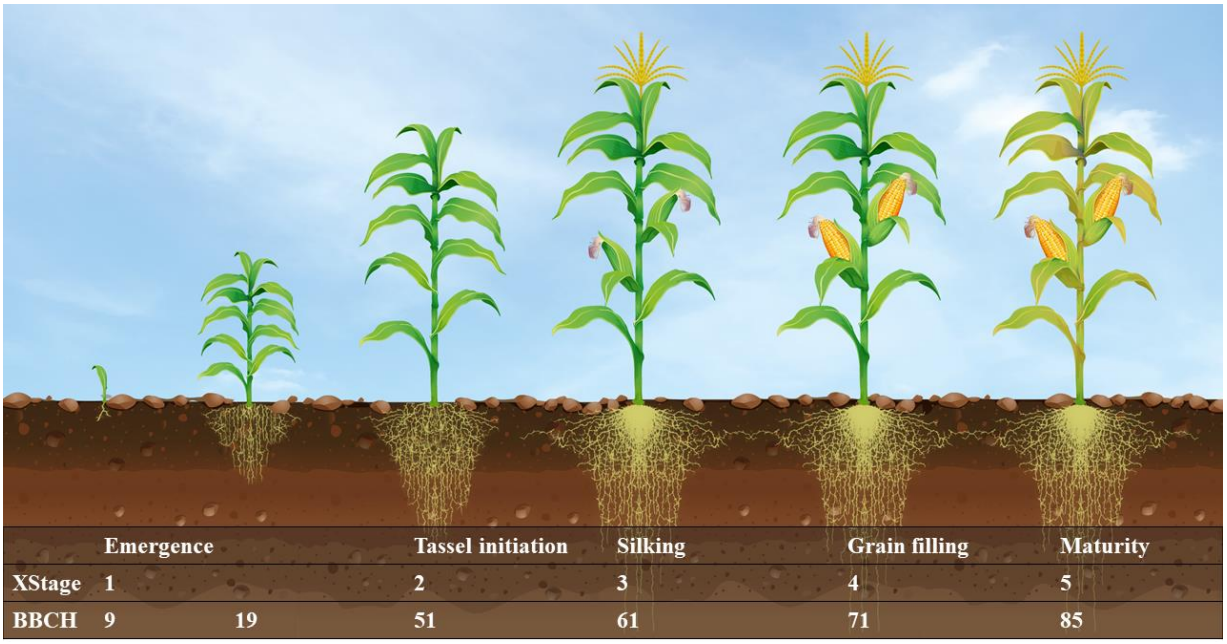

Figure 1 The XStages 1-5 represent the development stages emergence, tassel initiation, silking, effective grain filling and maturity. XStages can be converted to respected values of BBCH scale (Lancashire et al., 1991)

2.2.2. Dry matter production

Total dry matter production (DM_{tot}) is initialised at emergence by DM_{ini}, which is the weight of the seed (DM_{seed}) corrected by the weight fraction of the hypocotyl (f_{hypo}) and the loss due to transformation and translocation processes (f_{trans}, E8). The DM_{ini} decreases constantly after sowing (E18). The DM_{seed} is always subtracted from total dry matter production (DM_{tot}, E9).

Within season, dry matter production is driven by absorbed photosynthetic radiation (Q) and potential light use efficiency (LUE). Potential LUE is reduced to actual LUE by a factor for photosynthetic activity (f_T) and a factor for soil water deficit (f_{SWDF}, E10-E13), introducing

drought stress into the model. Q corresponds to the photosynthetic active radiation (PAR) which is commonly known as half of global radiation (GR, Szeicz, 1974), reduced by the radiation reflected by the canopy. It is calculated by the extinction coefficient k_{PAR} and the GAI according to the Beer-Lambert law (Monsi, 1953, E11). Therefore, GAI is provided by the *dry matter partitioning component* as external value to the *dry matter production component*.

Potential LUE was optimised by the model-internal Levenberg-Marquard algorithm to 3.6 g MJ^{-1}, remaining constant during the growing season. k_{PAR} is also assumed to be constant. f_T ranges from 0 to 1 and is calculated with a trapezoidal function (Marshall and Squire, 1996; Porter and Gawith, 1999). f_{SWDF} is calculated within the model as the ratio of actual transpiration to potential transpiration (E13).

2.2.3. Dry matter partitioning

In the first step, the *dry matter partitioning component* apportions the daily produced DM_{tot} (in the *dry matter production component*) between shoot dry matter (DM_{shoot}) and root dry matter (DM_{root}, E14, E15). Thereby, the increase of DM_{root} through the season is determined by the allocation coefficient (AC_{root}), calculated according to Yang et al. (2016), including a upper limit of root growth shortly after silking (DS_{stop}, E16, E17). DM_{shoot} is further distributed between leaf dry matter (DM_{leaf}), stem dry matter (DM_{stem}) and cob dry matter (DM_{cob}, E19) by dry matter allocation factors (E30): f_{leaf} describes the allocation to the leaves and f_{cob} to the cob (E21, E23).

f_{leaf} is the ratio of DM_{leaf} to DM_{shoot} increase between two sampling dates. f_{leaf} is assumed to increase linearly across the XStages starting at emergence with increasing XStages, described by the regression parameters $f_{leafslope}$ and f_{leaf0} (E22, Figure 2 A). Due to translocation processes from leaf to stem, DM_{leaf} is assumed to decrease after silking (XStage3) or if the maximum GAI (GAI_{max}) has been reached. This decay is described through a f_{leaf} derived from a decreasing power function with two parameters ($decay_a$, $decay_b$, E22, Figure 2 B). f_{cob} is calculated as the ratio of DM_{cob} increase to the sum of DM_{cob} and DM_{stem} increase between two sampling dates (E24, Figure 2 C). If f_{cob} exceeds 1, dry matter is translocated from stem to cobs. As soon as DM_{stem} accounts for less than 24.8% ($f_{stemmin}$) of the DM_{shoot}, f_{cob} is set to 1 (E24). $f_{stemmin}$ is the calculated average dry matter remaining in the stem at harvest. In a last step, stem growth rate can be derived by the combination of f_{leaf} and f_{cob} (E25).

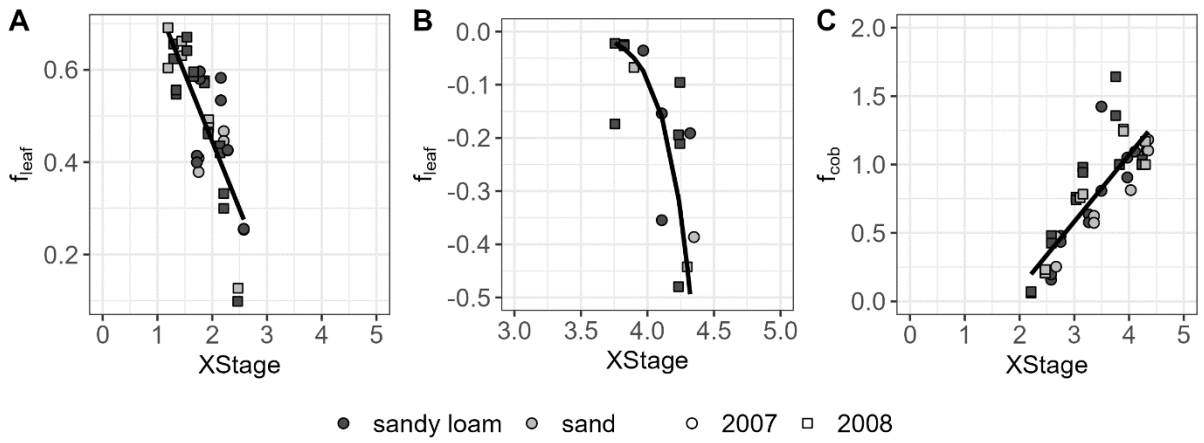

Figure 2 Calibration of the partitioning variables f_{leaf} and f_{cob} describing the dry matter growth rate of leaves and stems, by generating regressions to XStages. Depicted are the different soil types (sandy loam, sand) and trial years (2007, 2008). ***A:*** *f_{leaf} is described by the parameters $f_{leafslope}$ and f_{leaf0} until LAI_{max} is reached ($f_{leaf}=f_{leaf0}+f_{leafslope}*XStage$, $f_{leaf0}= 1.032$, $f_{leafslope}= -0.293$);* ***B:*** *For XStage>3 leaf decay due to translocation processes is described by a power function regression of f_{leaf} and XStages ($f_{leaf}=decay_a*XStage^{decayb}$; $decay_a= -3.232 * 10^{-15}$, $decay_b= 22.32$);* ***C:*** *f_{cob} is decribed by a linear regression utilising the parameters f_{cob0} and $f_{cobslope}$ ($f_{cob}=f_{cob0}+f_{cobslope}*XStage$; $f_{cob0}= -1.095$, $f_{cobslope}= 0.5687$)*

GAI expansion and its growth rate is calculated as the sum of its compartments (LAI, SAI, E26) and their growth rates (E27), respectively. Growth rate of LAI is the product of the specific leaf area SLA and DM_{leaf} (E28, E32). Thereby, SLA is assumed to be the negative exponential function of LAI (E30, Figure 3 A). The functions were fitted with the calibration datasets and slopes, exponents, upper and lower limits were set as model parameters (Table B 1). The same applies for SAI and specific stem area (SSA, E29, E31, E33, Figure 3 B). The proportion of senescent leaf area is depicted by the factor f_{sen}, increasing exponentially from the time of silking (XStage3, E34, E35). Parameters for f_{sen} computation are sen_a, sen_b (E35). Thereby, it is assumed, that the ratio of the measured GAI values towards the highest measured GAI is the proportion of senescent leaf area.

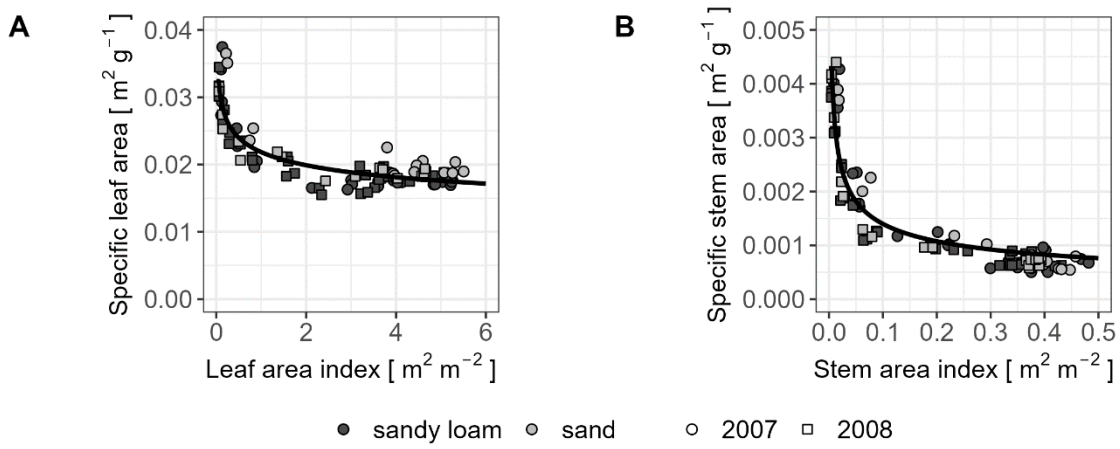

*Figure 3: Calibration of model parameters for **A:** specific leaf area (SLA) and **B:** specific stem area (SSA), assuming, that both, SLA and SSA are decreasing with increasing leaf area index (LAI) and stem area index (SAI), respectively. SLA and SSA are restricted by an upper and a lower limit. Depicted are the different soil types (sandy loam, sand) and trial years (2007, 2008).*

Plant height was derived from DM_{shoot}, using a quadratic function (E36) with the model parameters $height_a$, $height_b$ and $height_c$ (Table B 1).

2.2.4. Evapotranspiration

Required input for this component are weather data; daily mean temperature, global radiation (GR), windspeed, precipitation and vapour pressure deficit (VPD). Necessary external variables are provided by the *dry matter partitioning* component (GAI, crop height) and by the *dry matter production* component (k_{PAR}).

Potential evapotranspiration (ET_{pot}) is calculated by the Pennman-Monteith equation (Monteith, 1973), being the sum of potential transpiration (T_{pot}), potential evaporation (E_{pot}) and interception (I) (E39). E_{pot} is calculated by the fraction of radiation, which is transmitted, calculated with an exponential function of GAI and k_{PAR}. Calculation of interception is described in Kage et al. (2003). T_{pot} is derived as the difference of E_{pot} and I from ET_{pot}.

2.2.5. Soil water dynamics

Vertical soil water movement is calculated based on Richards equation (E40) along an diffusion approach, more detailed by Johnen et al. (2014), Neukam et al. (2016) and Böttcher et al. (2020). Soil textures are set site-specific and were determined in the field using the DINXX method and set for each of four defined soil layers (Eckelmann et al., 2005). The van Genuchten (1980) parameters following Mualem (1976) parameterisation (α,θs, θr, n) and saturated hydraulic conductivity Ks are derived from soil textures (Renger et al., 2014). To each soil layer, a sink term S[i] considering the water uptake by plants, is calculated by splitting T_{pot} (as external variable from the *evapotranspiration component*) across the four soil layers (E41). The

distribution of T_{pot} is oriented on the prevailing root length of each soil layer (i). A parameter for root competition (CompF) is added, to explain reduced water uptake due to root competition (Ehlers et al., 1991; Kage et al., 2003; Kage and Ehlers, 1996). Soil water potential may limit the water uptake as well, if it exceeds the critical soil water potential (ψ_{crit}). Therefore, n reduction factor $f_{sinkred}$ is included when estimating S[i], following the assumptions of Feddes (1980) and Belmans et al. (1983) (E42). Actual transpiration (T_{act}) is the sum of the soil layers sink terms (E43). Actual evaporation (E_{act}) is determined by reducing E_{pot} when the soil water potential in the top soil layer ($\psi_{arr[1]}$) falls below a critical threshold ($\psi_{critevap}$, E44, E45).To ensure an adequate representation of starting values, model was already started at the first of November of the previous year, respectively.

2.2.6. Root growth

The root growth component was introduced first by Kage et al. (2000) for cauliflower. Hence, all components were refitted for silage maize. As a function of DM_{root} and specific root length (SRL, Figure 4 C), root length (RL_{tot}) increases linear until maximum root depth (zr_{max}) or until DS_{stop} is reached (E46). DS_{stop} was introduced in the *dry matter partitioning* component and zr_{max} is a site-specific model parameter for the maximum rooting depth. Root depth growth starts with sowing depth (zr_0) and proceeds in a linear manner with a temperature dependent fitted parameter (k_{zr}, E47, Figure 4 A).

The exponential decrease of root length density with soil depth, depicting the vertical root distribution, is calculated with the coefficients kr, and RLD_0 (E48, Figure 4 B). RLD_0 is the RLD at zr = 0. kr is the fractional decrease with increasing soil depth z, determined by ratio between RLD_{zr} and RLD_0 (E49). To avoid iterative steps, the ratio is set as a fix parameter r_{RLD} (Table B 1).

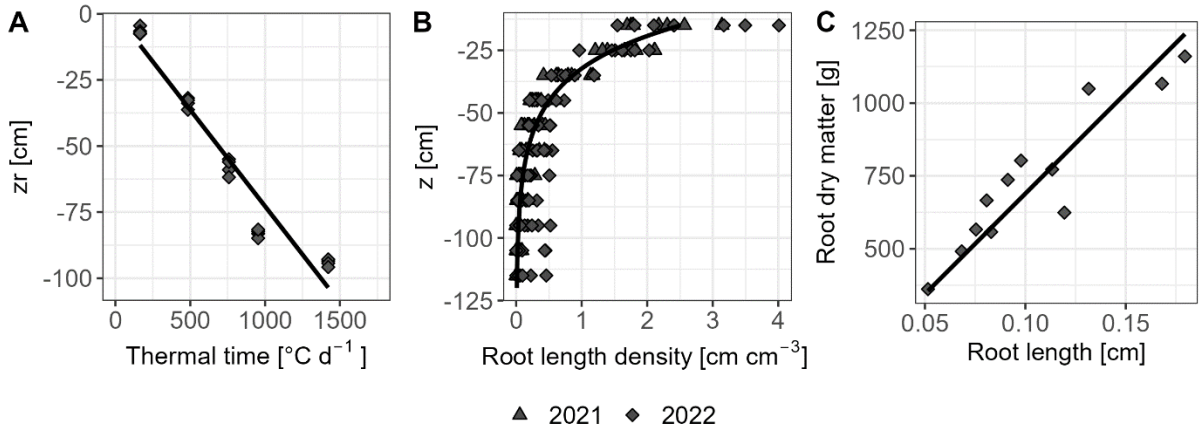

Figure 4 ***A:*** *Root depth growth. Linear relation of root depth z to thermal time ($dzr/dt = k_{zr}*T_{eff}$, $k_{zr}=0.703$).* ***B:*** *Vertical root growth is described by an exponential function over soil depth z ($RLD=RLD_0*e^{kr*zr}$).* ***C:*** *Specific root length (SRL) depicted as the regression between root dry matter [g m^{-2}] (DM_{root}) and root length (RL).*

3. Results

3.1. Parameterisation

For the final model, 20 silage maize-specific parameters for aboveground plant growth and three parameters for root growth were fitted (Appendix B – List of model parameters). Potential LUE was optimised by the model intern Levenberg-Marquard algorithm, as described in model description. Parameters for the plant development, phy, and soil water dynamic components were derived from literature. A detailed list of all parameters containing their description, value and source can be found in Appendix B (Table B 1).

3.2. Development

Plant development describing XStages, translated to BBCH (Lancashire et al., 1991) was simulated sufficiently with R^2 of 0.93 and 0.98 in calibration and evaluation (Table 2), respectively. Variations due to different sowing dates, geographical position and soil types were well estimated (Figure 5). Inaccuracies occurred during BBCH 50 and 65, as the period of tassel initiation to silking may be difficult to quantify in the field.

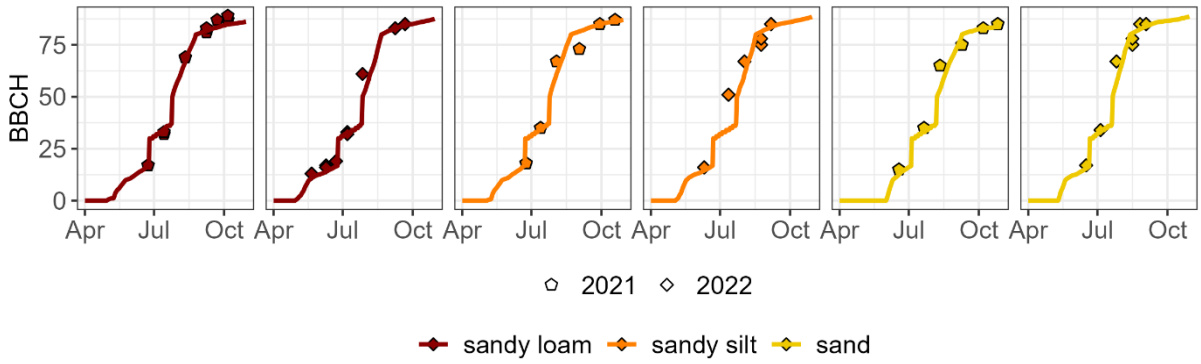

Figure 5 Model simulation of BBCH development stages (line) and measured BBCH of the evaluation datasets (point) over the vegetation period of maize. Depicted are evaluation datasets of 7, 11 (site A), 9, 13 (site C) and 10, 14 (site D) with their individual soil types starting at different sowing dates.

3.3. Dry matter production

With the calibration dataset, a strong fit was achieved for whole-season DM_{shoot} (R^2 = 0.97, Table 2) including measurement data of the whole season (n=83). The productivity on sandy loam sites was underestimated in 2008 and overestimated in 2007. However, predictions for the sandy site were accurate for both calibration years (Figure 6, A). In the evaluation, prediction accuracy of DM_{shoot} was still high with R^2 of 0.95 and a RMSE of 239.28 g m^{-2} (Table 2). In 2021, high yields harvested at both sandy loam and sandy sites were underestimated by the model. Due to severe drought stress at the sandy and sandy silt site in 2022, harvest was conducted

one month earlier (2022/09/06 and 2022/09/02, respectively), explaining the low yields (Figure 6, B).

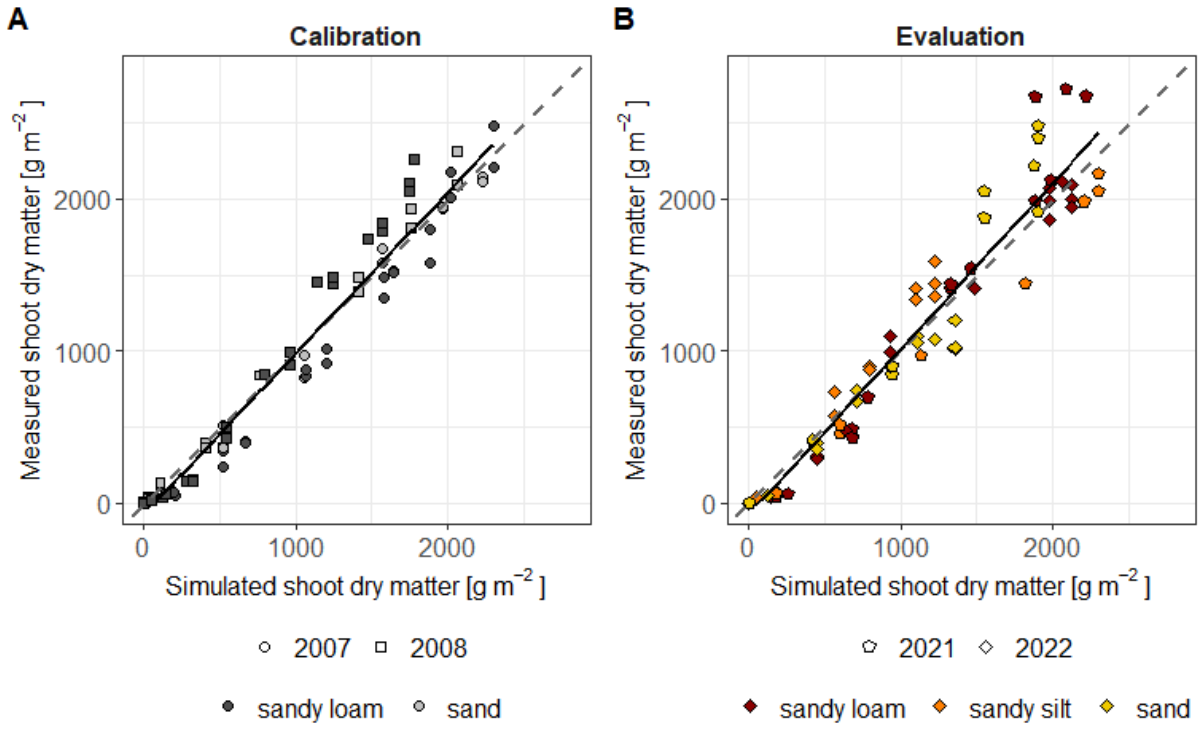

Figure 6 Dry matter estimation in calibration (grey) and evaluation (colourful) exhibit by simulated shoot dry matter [g m^{-2}] against measured data of the evaluation datasets (7-12). Dashed line is the 1:1 line. Solid line is the regression between measured and simulated shoot dry matter [g m^{-2}].

3.4. Dry matter partitioning

Partitioning into leaves, stems and cobs was well calibrated with R^2 of 0.82, 0.92 and 0.83, respectively, and regression slopes close to 1 (Table 2). However, simulating dry matter partitioning of evaluation datasets led to inaccuracies caused by over- and underestimation for DM_{leaf} and DM_{stem} (slopes: 0.83 and 1.65), followed by high RMSE's of 78.21 g m^{-2} and 217.9 g m^{-2}, respectively. Nevertheless, evaluation of DM_{cob} outperformed calibration with a slope of 0.98 and a R^2 of 0.91.

The GAI simulation depicted measurements well within the calibration (Table 2; R^2 = 0.73, slope = 0.92, RMSE = 1.08). Accuracy for its compartments LAI and SAI was even higher with RMSE's of 0.98 and 0.05, respectively. Since LAI and SAI of evaluation datasets were calculated based on the imprecise simulated dry matter partitioning, the deviation continued for evaluation with R^2 of 0.50 and 0.56, respectively. However, the slopes for both compartments were high, with a slight overestimation (0.85 and 0.94). GAI, as the sum of LAI and SAI, achieved a reasonable fit with a slope of 0.85, an intercept of 0.87 and a R^2 of 0.63, indicating a moderate level of explained variability (n=212).

Crop height was simulated with a low RMSE of 0.24 m and an overestimation of high values (slope = 0.88). Evaluation datasets were predicted well (R^2=0.97) although the base is a small n of 19.

Table 2 Results of model evaluation and calibration (in brackets) for development (BBCH), aboveground dry matter production (DM_{shoot}), dry matter partitioning into plant organs and the derived green area indices (DM_{leaf}, DM_{stem}, DM_{cob}, GAI, LAI, SAI) and of crop height. Performance was assessed with slope and intercept of the regression between measured and simulated data, R^2 and root mean square error (RMSE). n is the number of measurements.

Parameter	Unit	Slope	Intercept	R^2	n	RMSE
BBCH	[d]	0.99 (0.94)	2.13 (7.66)	0.98 (0.93)	51 (183)	4.28 (8.83)
DM_{shoot}	[g m^{-2}]	1.14 (1.08)	-102.91 (-73.91)	0.95 (0.97)	63 (83)	239.28 (157.41)
DM_{leaf}	[g m^{-2}]	0.83 (0.89)	27.17 (-5.70)	0.44 (0.82)	33 (83)	78.21 (53.94)
DM_{stem}	[g m^{-2}]	1.65 (1.00)	-105.75 (-31.30)	0.83 (0.92)	34 (83)	217.9 (85.04)
DM_{cob}	[g m^{-2}]	0.98 (1.04)	-41.47 (61.81)	0.91 (0.83)	22 (43)	173.61 (206.07)
GAI	[-]	0.85 (0.92)	0.5 (0.08)	0.63 (0.73)	212 (81)	1.18 (1.08)
LAI	[-]	0.85 (0.90)	0.12 (-0.11)	0.5 (0.8)	30 (81)	1.27 (0.98)
SAI	[-]	0.94 (0.92)	0.03 (-0.01)	0.56 (0.92)	30 (81)	0.1 (0.05)
Crop height	[m]	1.39 (0.88)	-0.51 (-0.20)	0.97 (0.96)	19 (111)	0.43 (0.24)

3.5. Evapotranspiration and soil water dynamics

At the time of sowing, soil was water-saturated at all study sites and years. During the season, the model depicted strong variations in the soil water balance. In 2021 on the sandy silt site and in 2021 and 2022 on the sandy loam site, optimal water availability was modelled (Figure 7). In 2007 and in 2021 on the sandy site, drought stress occurred only briefly in mid-June. A strong restriction of growth due to drought stress in 2022, particularly in sandy and sandy silt locations, as well as in 2008, in sandy loam and sandy areas (Figure 7). For example, the average f_{SWDF} on the sandy site in 2022 was 0.66, meaning that the potential LUE was reduced by one third.

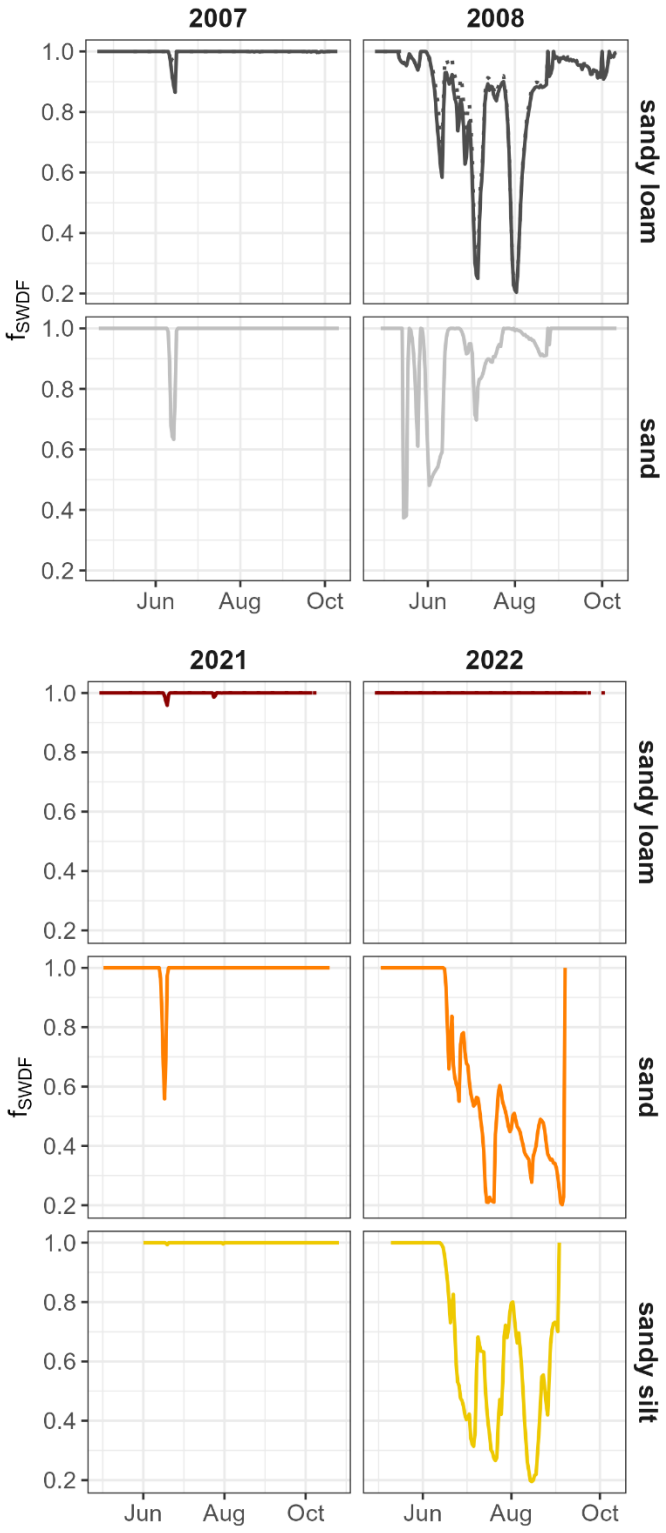

Figure 7 Soil water deficit factor (f_{SWDF}) as the ratio of actual and potential transpiration during the vegetation period, introducing drought stress to the model. Depicted is the f_{SWDF} for all datasets (calibration: grey; evaluation: colourful), arranged in trial years (columns) and soil types (rows). Start and end of line represent sowing and harvest date, each. Sandy loam site (site A) comprise each two datasets (Table 1) with differing sowing dates in each year. If their f_{SWDF} do not match, the dataset with the delayed sowing date is displayed by a dotted line.

4. Discussion

The target of this study was the development of a fundamental structure of a dynamic growth modelling for silage maize under the climate conditions of its European main growing area. The model was parameterised for growth conditions without nitrogen limitations. The fitted parameters can be regarded as first HUME-Maize-driven insights in silage maize growth. The requirements were, establishment of an easy adjustable model providing already reasonable results for different year/site-combinations within Germany.

4.1. Development

The *development* component is based on the assumptions of HYBRID-Maize (Yang et al., 2004). However, the growth conditions between Northern America (environment in which HYBRID-Maize was developed) and Europe differ. Furthermore, HYBRID-Maize focusses on grain maize whereas whole-crop silage maize is already harvested green and breaded with regard to shorter growing seasons. In consequence, several parameters in the *development* module of HUME-Maize had to be adjusted. The base temperature (T_1) was decreased from 8 °C respectively 10 °C (Jones and Kiniry, 1986; Yang et al., 2016) to 6°C following European studies on maize physiology (Pagès and Pellerin, 1994; R. Bonhomme et al., 1994). Alterations in the base temperature not only impact the effective temperature but also influence all GDD's and consequently affecting the timing of XStages. All GDD's to calculate the XStages were derived from the results of (Bignon, 1990) for mid-early cultivars. As the study focusses on silage maize, XStage5, describing the dough stage where whole crop silage maize is usually harvested, was selected at a dry matter content of 35 %. Measured and modelled BBCH growth stages correlate well in calibration (R^2 = 0.93, Table 2) and evaluation (R^2: 0.98, Table 2, Figure 5). The R^2 for BBCH estimations are distinctly higher than those obtained by Morel et al. (2020) refitting APSIM for silage maize growth under North European conditions (R^2: 0.81). As Bignon (1990) provided also GDDs for early- and late -cultivars, extending the model for further maturity groups should be feasible.

Additionally, the parameter phy, describing the phyllochron [°Cd], has been recalculated, experiencing an increase from 38.9 °Cd in Yang et al. (2016) to 50.8 °Cd (Table B 1). The results are corroborated by the study conducted by Dos Santos et al. (2022), which determined an average phyllochron of 51.5 °Cd by linear regression method. However, Dos Santos et al. (2022) suggest a bilinear relation for leaf number simulation, receiving an improvement of model efficiency by 3%.

4.2. Dry matter production

Similar to CERES-Maize, total dry matter production in HUME-Maize is driven by radiation uptake, for which potential LUE was set to a constant value of 3.6 g MJ PAR^{-1}. This value differs strongly from the proposal of 4.33 g MJ PAR^{-1} by Kiniry et al. (1997) for grain maize. This can be traced back to the lower sowing density in grain maize, or at least in datasets of CERES-Maize, with 6 plants per m² (Kiniry et al., 1989) than in dense sown silage maize (10 plants per m²).

Drought stress occurs, if soil water storage cannot cover the demand of the growing plant (Draye et al., 2010). Within the model, potential LUE is reduced by f_{SWDF}, as it is the ratio between potential and actual transpiration, thus f_{SWDF} is determined by the soil water dynamics, thus by soil texture and the resultant water holding capacity and van Genuchten parameters (E10, Figure 7). For calibration datasets the approach of LUE correction through f_{SWDF} seems to work well for the sandy site but not for sandy loam, as drought in 2008 led to a shift of underestimation. However, 2007 was slightly overestimated for sandy loam site without water limitation (Figure 6). Despite severe drought events as well as sufficient water supply in evaluation datasets, no clear shifts due to soil type and water limitation were found (Figure 6, Figure 7), indicating that potential LUE of 3.6 g MJ PAR^{-1} was reliable.

The fitted k_{PAR} of 0.67 matches well to Jones and Kiniry's (1989) k_{PAR} of 0.65. In literature, k_{PAR} ranges between 0.4 and 0.7, depending on the cultivar and measurement method (Lacasa et al., 2021). Morel et al. (2020) traced their underestimation of North European silage maize yields (RMSE = 5.2 t ha^{-1}) back to an inadequate combination of LUE, k_{PAR} and row spacing within their model. The problem is solved by optimising potential LUE and refitting k_{PAR} within European climate conditions within the HUME modelling environment.

4.3. Dry matter partitioning

Partitioning into the plant organs within HUME-Maize is controlled by the factors f_{leaf}, f_{stem} and f_{cob}, fitted as a function of XStages (Jones et al., 2003; Keating et al., 2003). The R^2 for the calibration data were high (R^2 for DM_{leaf}: 0.85, DM_{stem}: 0.81, DM_{cob}: 0.93, Table 2). For evaluation datasets, dry matter partitioning to leaves and stems was over- and underestimated, respectively (slopes: 0.83 and 1.65, Table 2). This could be traced back to the time lag between calibration and evaluation datasets of about 14 years. Investigating the yield increase of maize during the past 40 years, Taube et al. (2020) found a higher leave number of younger maize cultivars. As an adaption to changing climate conditions, breeding changed the dry matter partitioning towards a higher radiation interception. In this study, differences in cultivars were not considered, but the release year of the cultivar in the calibration data set (KWS Ronaldinio)

and in the evaluation data set – KWS Gunnario and KWS Stefano – differs by 13 and 12 years, respectively.

Dry matter partitioning driven by coefficients depending on thermal time, as the XStages used here (Jones et al., 2003; Keating et al., 2003), was long considered as standard simulation method. An alternative approach for calculating the partitioning into the plant organs leaf, stem and cob is the allometric concept (Fukuyama and Sakurai, 2019). Kage and Stützel (1999a) developed and successfully tested an allometric algorithm in a cauliflower growth model. Ratjen et al. (2018) found a satisfactory allometric relation between leaf and stem biomass in silage maize utilising the current calibration data set. However, in this study, the approach with parameters of Ratjen et al. (2018) has been tested (not shown), but did not overpass the here presented results of the linear regressions for growth of all organs (f_{leaf}, f_{stem}, f_{cob}) depending on the XStages.

Lizaso et al. (2003) discussed the importance of an appropriate depiction of leaf growth and senescence for a precise forecasting of maize yields so far not depicted in CERES-Maize and proposed an approach on leaf level. The calculated leaf area per plant is afterwards scaled up, which results in a tendency to overestimate leaf area on canopy scale. This shift was found to depend on sowing density and cultivar selection (Lizaso et al. 2003). In HUME-Maize, senescence is depicted similarly on plant level, but already at the calculation of leaf dry matter, as leaf decay is modelled as exponential decrease of f_{leaf}, describing the translocation of dry matter to the stem (Figure 2).

Computation of leaf area expansion is calculated with an allometric approach based on the approach of Ratjen et al. (2018), stating that GAI is described best by SLA, instead of thermal time or XStages. The decrease of the exponential model of Ratjen et al. (2018) can be interpreted as shading effects of deeper leaf layers, connecting single leaf growth with canopy leaf growth. RMSE of complete GAI was 1.08, matching to the results of studies testing CERES-Maize (Basso et al., 2016).

4.4. Root growth

The depiction of linear and vertical root growth is based on the approach of Kage et al. (2000) for cauliflower. Therefore, the parameters k_{zr} for linear depth growth and r_{RLD} for vertical depth growth had to be re-parametrised for whole-crop silage maize, as the latter study investigated the fine root growth of cauliflower. Authors introduced the model parameter ratio for calculating the coefficient k_r for vertical root growth (E49, E48). To avoid iterative steps and due to a lack of data, Kage et al. (2000) optimised the parameter and received a very small value. In this study, it was possible to calculate the parameter with data of experiments 8 and 12 recording a much

higher value for r_{RLD} (r_{RLD}: 0.128, Table B 1). Kage et al. (2000) found 0.021 for all years and soil conditions combined.

Maximal rooting depth zr_{max} is a site-specific parameter, which can be changed manually depending on the site conditions. Deeper root growth may result in higher amount of water uptake and consequently higher T_{act}. In general, root growth and water uptake are currently driven by thermal time, independent of soil texture, potentially impacting root depth expansion, particularly in drought conditions (Jorda et al., 2022). Subsequent model enhancements may incorporate soil texture-specific root growth.

4.5. Evapotranspiration and soil water dynamics

Modelling of evapotranspiration in HUME follows the approach of Monteith (1973). Hereby, the model parameter rc_0 was modified to 75 s m^{-1} according to assumptions of Rochette et al. (1991), Sinclair et al. (1975), Irmak and Mutiibwa (2008), instead of common stomatal resistance of 50 s m^{-1} (Neukam et al., 2016) to depict the capability of maize as a C_4 plant, of fixing higher amounts of CO_2.

The soil water component was adopted from previously published HUME models; HUME-Wheat (Neukam et al. 2016; Johnen et al. 2014) and HUME-OSR (Böttcher et al., 2020; Johnen et al., 2014; Neukam et al., 2016). However, the parameters ψ_{crit}, $\psi_{critEvap,}$ ψ_{crit} and CompF, guiding and restricting the water uptake by roots were adapted for HUME-Maize. Pivot point of the component is the selection of soil textures for each soil layer, allowing the model to adjust to any soil conditions. van Genuchten parameters following Mualem (1976) parameterisation (α,θs, θr, n) and saturated hydraulic conductivity Ks were selected according to the soil texture (Renger et al., 2014).

Currently, general soil texture assumptions were set for each location, irrespective of the small scale variation at field scale. Koehler et al. (2022) emphasised the importance of soil texture, altering the hydraulic properties and consequently the transpiration rate of a plant. As a result, they found that the critical water content until transpiration decreases, is depending on texture. A more detailed look into soil hydraulic properties for small-scale soil texture variations may allow a precision of T_{act} and consequently f_{SWDF}.

This accuracy of estimation silage maize growth for contrasting soils and climate conditions demonstrates that the model is suited for the application for differing European cultivation conditions, also with regard to changing climatically conditions.

5. Conclusion

This study aimed to develop a dynamic growth model for the simulation of silage maize yield grown under European climate conditions. This involves not only average climatic conditions, but also severe drought. Whole-crop silage maize phenology, particularly the timepoint of silage maize maturity were simulated satisfactorily. The developed HUME-Maize serves as a robust base, to build on within future studies. For instance, drought stress was implemented by a simple approach driven by soil water dynamics, which was reliable for first steps in HUME-Maize but could be adapted even more precisely to small-scale soil texture differences. Further studies could also include the yield quality in order to predict optimal harvest dates in the future. In addition, nitrogen limitation and cultivar specific phenological differences, as important factors of nitrogen fertilizer efficiency and allometric growth strategies, were not modelled, setting the foundation for future investigations.

References

Basso, B., Liu, L., Ritchie, J.T., 2016. A Comprehensive Review of the CERES-Wheat, -Maize and -Rice Models' Performances. Elsevier. 10.1016/bs.agron.2015.11.004, 27-132.

Belmans, C., Wesseling, J.G., Feddes, R.A., 1983. Simulation model of the water balance of a cropped soil: SWATRE. Journal of Hydrology 63 (3), 271–286. 10.1016/0022-1694(83)90045-8.

Bignon, J., 1990. Agrométéorologie et physiologie du maïs grain dans la communauté Européenne. CEC.

Böttcher, U., Weymann, W., Pullens, J.W.M., Olesen, J.E., Kage, H., 2020. Development and evaluation of HUME-OSR: A dynamic crop growth model for winter oilseed rape. Field Crops Research 246, 107679. 10.1016/j.fcr.2019.107679.

Brown, H.E., Huth, N.I., Holzworth, D.P., Teixeira, E.I., Wang, E., Zyskowski, R.F., Zheng, B., 2019. A generic approach to modelling, allocation and redistribution of biomass to and from plant organs. in silico Plants 1 (1), 57. 10.1093/insilicoplants/diy004.

Deutscher Wetterdienst, 2023. Wetter und Klima. https://www.dwd.de/EN/Home/home_node.html;jsessionid=F8DD474BF98FB06D685EF8994FD620D9.live21073. Accessed 14 December 2023.

Dos Santos, C.L., Abendroth, L.J., Coulter, J.A., Nafziger, E.D., Suyker, A., Yu, J., Schnable, P.S., Archontoulis, S.V., 2022. Maize Leaf Appearance Rates: A Synthesis From the United States Corn Belt. Front. Plant Sci. 13, 872738. 10.3389/fpls.2022.872738.

Draye, X., Kim, Y., Lobet, G., Javaux, M., 2010. Model-assisted integration of physiological and environmental constraints affecting the dynamic and spatial patterns of root water uptake from soils. Journal of experimental botany 61 (8), 2145–2155. 10.1093/jxb/erq077.

Eckelmann, W., Sponagel, H., Grottenthaler, W., 2005. Bodenkundliche Kartieranleitung: Mit 41 Abbildungen, 103 Tabellen und 31 Listen, 5th ed. Bundesanstalt für Geow. und Rohstoffe, Hannover, 438 str.

Ehlers, W., Hamblin, A.P., Tennant, D., van der Ploeg, R. R., 1991. Root system parameters determining water uptake of field crops. Irrig Sci 12 (3), 115–124. 10.1007/BF00192282.

European Commission, 2023. Green maize by area, production and humidity - Data Europa EU. https://data.europa.eu/data/datasets/7gxelzhficlf0wcrbpzfog?locale=en. Accessed 13 December 2023.

Feddes, R.A., 1980. Simulation of field water use and crop yield. Field Crops Research 3, 95–96. 10.1016/0378-4290(80)90010-6.

Fukuyama, R., Sakurai, G., 2019. Comparison of the robustness of methods for estimating leaf development for crop growth models. J. Agric. Meteorol. 75 (2), 76–83. 10.2480/agrmet.D-17-00034.

Gavasso-Rita, Y.L., Papalexiou, S.M., Li, Y., Elshorbagy, A., Li, Z., Schuster-Wallace, C., 2023. Crop models and their use in assessing crop production and food security: A review. Food and Energy Security 1, 27. 10.1002/fes3.503.

Henke, J., Böttcher, U., Neukam, D., Sieling, K., Kage, H., 2008. Evaluation of different agronomic strategies to reduce nitrate leaching after winter oilseed rape (Brassica napus L.) using a simulation model. Nutr Cycl Agroecosyst 82 (3), 299–314. 10.1007/s10705-008-9192-0.

Holzworth, D.P., Huth, N.I., deVoil, P.G., Zurcher, E.J., Herrmann, N.I., McLean, G., Chenu, K., van Oosterom, E.J., Snow, V., Murphy, C., Moore, A.D., Brown, H., Whish, J.P.M., Verrall, S., Fainges, J., Bell, L.W., Peake, A.S., Poulton, P.L., Hochman, Z., Thorburn, P.J., Gaydon, D.S., Dalgliesh, N.P., Rodriguez, D., Cox, H., Chapman, S., Doherty, A., Teixeira, E., Sharp, J., Cichota, R., Vogeler, I., Li, F.Y., Wang, E., Hammer, G.L., Robertson, M.J., Dimes, J.P., Whitbread, A.M., Hunt, J., van Rees, H., McClelland, T., Carberry, P.S., Hargreaves, J.N.G., MacLeod, N., McDonald, C., Harsdorf, J., Wedgwood, S., Keating, B.A., 2014. APSIM – Evolution towards a new generation of agricultural systems simulation. Environmental Modelling & Software 62 (9), 327–350. 10.1016/j.envsoft.2014.07.009.

Irmak, S., Mutiibwa, D., 2008. Dynamics of photosynthetic photon flux density and light extinction coefficient to assess radiant energy interactions for maize canopy. Transactions of the ASABE 51: 1663-1673.

Johnen, T., Boettcher, U., Kage, H., 2014. An analysis of factors determining spatial variable grain yield of winter wheat. European Journal of Agronomy 52, 297–306. 10.1016/j.eja.2013.08.005.

Jones, C.A., Kiniry, J.R., 1986. CERES-Maize. A simulation model of maize growth and development. Texas A. and M. University Press, Collage station.

Jones, J.W., Hoogenboom, G., Porter, C.H., Boote, K.J., Batchelor, W.D., Hunt, L.A., Wilkens, P.W., Singh, U., Gijsman, A.J., Ritchie, J.T., 2003. The DSSAT cropping system model. European Journal of Agronomy 18 (3), 235–265. 10.1016/S1161-0301(02)00107-7.

Jorda, H., Ahmed, M.A., Javaux, M., Carminati, A., Duddek, P., Vetterlein, D., Vanderborght, J., 2022. Field scale plant water relation of maize (Zea mays) under drought – impact of root hairs and soil texture. Plant and Soil 478 (1-2), 59–84. 10.1007/s11104-022-05685-x.

Kage, H., ALT, C., Stützel, H., 2003. Aspects of nitrogen use efficiency of cauliflower I. A simulation modelling based analysis of nitrogen availability under field conditions. J. Agric. Sci. 141 (1), 1–16. 10.1017/S0021859603003344.

Kage, H., Ehlers, W., 1996. Does transport of water to roots limit water uptake of field crops? Zeitschrift für Pflanzenernährung und Bodenkunde 159 (6), 583–590. 10.1002/jpln.1996.3581590609.

Kage, H., Kochler, M., Stützel, H., 2000. Root growth of cauliflower (Brassica oleracea L. botrytis) under unstressed conditions: Measurement and modelling. Plant and Soil 223 (1), 133–147. 10.1023/A:1004866823128.

Kage, H., Stützel, H., 1999a. A simple empirical model for predicting development and dry matter partitioning in cauliflower (Brassica oleracea L. botrytis). Scientia Horticulturae 80 (1), 19–38. 10.1016/S0304-4238(98)00226-X.

Kage, H., Stützel, H., 1999b. HUME: An object oriented component library for generic modular modelling of dynamic systems. European Society of Agronomy, 299–300.

Keating, B.A., Carberry, P.S., Hammer, G.L., Probert, M.E., Robertson, M.J., Holzworth, D., Huth, N.I., Hargreaves, J.N.G., Meinke, H., Hochman, Z., McLean, G., Verburg, K., Snow, V., Dimes, J.P., Silburn, M., Wang, E., Brown, S., Bristow, K.L., Asseng, S., Chapman, S., McCown, R.L., Freebairn, D.M., Smith, C.J., 2003. An overview of APSIM, a model designed for farming systems simulation. European Journal of Agronomy 18 (3), 267–288. 10.1016/S1161-0301(02)00108-9.

Kiniry, J.R., Jones, C.A., O'toole, J.C., Blanchet, R., Cabelguenne, M., Spanel, D.A., 1989. Radiation-use efficiency in biomass accumulation prior to grain-filling for five grain-crop species. Field Crops Research 20 (1), 51–64. 10.1016/0378-4290(89)90023-3.

Kiniry, J.R., Williams, J.R., Vanderlip, R.L., Atwood, J.D., Reicosky, D.C., Mulliken, J., Cox, W.J., Mascagni, H.J., Hollinger, S.E., Wiebold, W.J., 1997. Evaluation of Two Maize Models for Nine U.S. Locations. Agron.j. 89 (3), 421–426. 10.2134/agronj1997.00021962008900030009x.

Koehler, T., Moser, D.S., Botezatu, Á., Murugesan, T., Kaliamoorthy, S., Zarebanadkouki, M., Bienert, M.D., Bienert, G.P., Carminati, A., Kholová, J., Ahmed, M., 2022. Going underground: Soil hydraulic properties impacting maize responsiveness to water deficit. Plant Soil 478 (1), 43–58. 10.1007/s11104-022-05656-2.

Lacasa, J., Hefley, T.J., Otegui, M.E., Ciampitti, I.A., 2021. A practical guide to estimating the light extinction coefficient with nonlinear models-a case study on maize. Plant methods 17 (1), 60. 10.1186/s13007-021-00753-2.

Lancashire, P., Bleiholder, H., van den Boom, T., Langelüddeke, P., Strauss, R., Weber, E., Witzenberger, A., 1991. A uniform decimal code for growth stages of crops and weeds. Annals of Applied Biology 119 (3), 561–601. 10.1111/j.1744-7348.1991.tb04895.x.

Marshall, B., Squire, G.R., 1996. Non-linearity in rate-temperature relations of germination in oilseed rape. J Exp Bot 47 (9), 1369–1375. 10.1093/jxb/47.9.1369.

Monsi, M., 1953. The light factor in plant communities and its significance for dry matter production. Japanese Journal of Botany 14, 22.

Monteith, J.L., 1973. Principles of environemental physics. Edward Arnold, London, 13 + 241 s.

Morel, J., Parsons, D., Halling, M.A., Kumar, U., Peake, A., Bergkvist, G., Brown, H., Hetta, M., 2020. Challenges for Simulating Growth and Phenology of Silage Maize in a Nordic Climate with APSIM. Agronomy 10 (5), 645. 10.3390/agronomy10050645.

Mualem, Y., 1976. A new model for predicting the hydraulic conductivity of unsaturated porous media. Water Resources Research 12 (3), 513–522. 10.1029/WR012i003p00513.

Neukam, D., Böttcher, U., Kage, H., 2016. Modelling Wheat Stomatal Resistance in Hourly Time Steps from Micrometeorological Variables and Soil Water Status. J Agro Crop Sci 202 (3), 174–191. 10.1111/jac.12133.

Pagès, L., Pellerin, S., 1994. Evaluation of parameters describing the root system architecture of field grown maize plants (Zea mays L.). Plant Soil 164 (2), 169–176. 10.1007/BF00010068.

Porter, J.R., Gawith, M., 1999. Temperatures and the growth and development of wheat: A review. European Journal of Agronomy 10 (1), 23–36. 10.1016/S1161-0301(98)00047-1.

Qin, M., Zheng, E., Hou, D., Meng, X., Meng, F., Gao, Y., Chen, P., Qi, Z., Xu, T., 2023. Response of Wheat, Maize, and Rice to Changes in Temperature, Precipitation, CO2 Concentration, and Uncertainty Based on Crop Simulation Approaches. Plants (Basel, Switzerland) 12 (14). 10.3390/plants12142709.

R Core Team, 2023. R: A language and environment for statistical computing. R foundation for statistical computing, Vienna, Austria.

R. Bonhomme, M. Derieux, G. O. Edmeades, 1994. Flowering of Diverse Maize Cultivars in Relation to Temperature and Photoperiod in Multilocation Field Trials. Crop Science 34 (1), 156–164. 10.2135/cropsci1994.0011183X003400010028x.

Ratjen, A.M., Lemaire, G., Kage, H., Plénet, D., Justes, E., 2018. Key variables for simulating leaf area and N status: Biomass based relations versus phenology driven approaches. European Journal of Agronomy 100, 110–117. 10.1016/j.eja.2018.04.008.

Renger, M., Bohne, K., Wessolek, G., 2014. Bodenphysikalische Kennwerte und Berechnungsverfahren für die Praxis, Teil II.

Rochette, P., Pattey, E., Desjardins, R.L., Dwyer, L.M., Stewart, D.W., Dubé, P.A., 1991. Estimation of maize (Zea mays L.) canopy conductance by scaling up leaf stomatal conductance. Agricultural and Forest Meteorology 54 (2-4), 241–261. 10.1016/0168-1923(91)90008-E.

Seethepalli, A., Dhakal, K., Griffiths, M., Guo, H., Freschet, G.T., York, L.M., Cahill, J., 2021. RhizoVision Explorer: Open-source software for root image analysis and measurement standardization. AoB PLANTS 13 (6), 945. 10.1093/aobpla/plab056.

Sinclair, T.R., Bingham, G.E., Lemon, E.R., Allen, L.H., 1975. Water Use Efficiency of Field-grown Maize during Moisture Stress. Plant physiology 56 (2), 245–249. 10.1104/pp.56.2.245.

Szeicz, G., 1974. Solar-radiation for plant-growth. Journal of Applied Ecology 11 (2). 10.2307/2402214.

Taube, F., Vogeler, I., Kluß, C., Herrmann, A., Hasler, M., Rath, J., Loges, R., Malisch, C.S., 2020. Yield Progress in Forage Maize in NW Europe—Breeding Progress or Climate Change Effects? Front. Plant Sci. 11, 473. 10.3389/fpls.2020.01214.

van Genuchten, M.T., 1980. A Closed-form Equation for Predicting the Hydraulic Conductivity of Unsaturated Soils. Soil Science Society of America Journal 44 (5), 892–898. 10.2136/sssaj1980.03615995004400050002x.

van Wart, J., Kersebaum, K.C., Peng, S., Milner, M., Cassman, K.G., 2013. Estimating crop yield potential at regional to national scales. Field Crops Research 143, 34–43. 10.1016/j.fcr.2012.11.018.

Verheul, M.J., Picatto, C., Stamp, P., 1996. Growth and development of maize (Zea mays L.) seedlings under chilling conditions in the field. European Journal of Agronomy 5 (1), 31–43. 10.1016/S1161-0301(96)02007-2.

Yang, H.S., Dobermann, A., Cassman, K.G., Walters, D.T., Grassini, P., 2016. Hybrid Maize (ver. 2016): A Simulation Model for Corn Growth and Yield. Nebrasca Cooperative Extension, Lincoln, NE, 102 pp.

Yang, H.S., Dobermann, A., Lindquist, J.L., Walters, D.T., Arkebauer, T.J., Cassman, K.G., 2004. Hybrid-maize—a maize simulation model that combines two crop modeling approaches. Field Crops Research 87 (2), 131–154. 10.1016/j.fcr.2003.10.003.

6. Appendix A – Model equations

6.1. Development component

E1. $$DevRateS0 = \frac{T_{eff}}{GDD_{emer}}$$

DevRateS0: Development rate between sowing and emergence, T_{eff}: effective temperature, GDD_{emer}: corresponding growing degree days

E2. $$DevRateS1 = \frac{T_{eff}}{GDD_{tasini}}$$

DevRateS1: Development rate between emergence and tassel initiation, T_{eff}: effective temperature, GDD_{tasini}: growing degree days from emergence till tassel initiation

E3. $$DevRateS2 = \frac{T_{eff}}{GDD_{S2}}$$

DevRateS2: Development rate between tassel initiation and silking, T_{eff}: effective temperature, GDD_{S2}: growing degree days from tassel initiation till silking

E4. $$DevRateS3 = \frac{T_{eff}}{GDD_{S3}}$$

DevRateS3: Development rate silking and grain filling T_{eff}: effective temperature, GDD_{S3}: growing degree days from silking till grain filling

E5. $$DevRateS4 = \frac{T_{eff}}{GDD_{total} - GDD_{emer} - GDD_{silk} - GDD_{S3}}$$

DevRateS4: Development rate between grain filling and maturity, T_{eff}: effective temperature, GDD_{total}: growing degree days from sowing till maturity, GDD_{emer}: growing degree days from sowing till emergence, GDD_{silk}: growing degree days from emergence till silking, GDD_{S3}: growing degree days from silking till grain filling

E6. $$\frac{dLeaf_{No}}{dt} = \frac{Teff}{phy * f_{phy}}$$

$Leaf_{No}$: number of leaves, T_{eff}: effective temperature, phy: phyllochron, f_{phy}: reduction factor for early growth phase.

E7. $$f_{phy} = \begin{cases} 0.66 + 0.068 * Leaf_{No} & | \; Leaf_{No} < 5 \\ 1 & | \; Leaf_{No} \geq 5 \end{cases}$$

f_{phy}: reduction factor for early growth phase, $Leaf_{No}$: number of leaves, constants (0.66, and 0.068) are parameters according to Yang et al. (2016), Jones and Kiniry (1986).

6.2. Dry matter production

E8. $DM_{ini}=DM_{seed}-(DM_{seed}*f_{trans})-(DM_{seed}*f_{hypo})$

DM_{ini}: initial dry matter value for starting the model, DM_{seed}: seed dry matter, f_{trans}: fraction of seed dry matter lost by transformation processes, f_{hypo}: fraction of the hypocotyl

E9. $$\frac{dDM_{tot}}{dt}=\frac{dDM_{tot}}{dt}-\frac{dDM_{ini}}{dt}$$

DM_{ini}: initial dry matter value, DM_{tot}: total dry matter

E10. $$\frac{dDM_{tot}}{dt}=Q*LUE*f_T*f_{SWDF}$$

DM_{tot}: total dry matter, Q: absorbed radiation, LUE: light use efficiency, f_T: temperature weight factor for photosynthetic activity, f_{SWDF}: soil water deficit factor

E11. $$Q=PAR*\left(1-e^{-k_{PAR}*GAI}\right)$$

Q: absorbed radiation, PAR: photosynthetic active radiation (0.5 * global radiation), k_{PAR}: extinction coefficient, GAI: green area index

E12. $$f_T=\begin{cases}0 & |T_{mean}<T_1\\ \frac{T_{mean}-T_1}{T_2-T_1} & |T_1\le T_{mean}\le T_2\\ 1 & |T_2<T_{mean}\le T_3\\ \frac{T_4-T_{mean}}{T_4-T_3} & |T_3<T_{mean}\le T_4\\ 0 & |T_{mean}>T_4\end{cases}$$

f_T: temperature weight factor for photosynthetic activity, T_{mean}: daily averaged effective temperature, T_1: base temperature, T_2, T_3, T_4: cardinal temperatures of trapezoid function.

E13. $$f_{SWDF}=\frac{T_{act}}{T_{pot}}$$

f_{SWDF}: soil water deficit factor, T_{act}: actual transpiration, T_{pot}: potential transpiration

6.3. Dry matter partitioning

E14. $DM_{tot}=DM_{root}+DM_{shoot}$

DM_{tot}: total dry matter, DM_{root}: root dry matter, DM_{shoot}: shoot dry matter

E15. $$\frac{dDM_{tot}}{dt}=\frac{dDM_{root}}{dt}+\frac{dDM_{shoot}}{dt}$$

DM_{tot}: total dry matter, DM_{root}: root dry matter, DM_{shoot}: shoot dry matter

E16. $$AC_{root}=ACE_{root}-DS*\frac{ACE_{root}}{DS_{stop}}$$

AC_{root}: proportion of root dry matter, ACE_{root}: allocation coefficient of root dry matter proportion, DS: development stage of root growth, DS_{stop}: highest development stage of root growth

E17. $$\frac{dDM_{root}}{dt} = \frac{dDM_{tot}}{dt} * AC_{root}$$

DM_{root}: root dry matter, DM_{tot}: total dry matter, AC_{root}: proportion of root dry matter

E18. $$\frac{dDM_{shoot}}{dt} = \frac{dDM_{tot}}{dt} * (1 - AC_{root})$$

DM_{shoot}: shoot dry matter, DM_{tot}: total dry matter, AC_{root}: proportion of root dry matter

E19. $$DM_{shoot} = DM_{leaf} + DM_{stem} + DM_{cob}$$

DM_{shoot}: shoot dry matter, DM_{leaf}: leaf dry matter, DM_{stem}: stem dry matter, DM_{cob}: cob dry matter

E20. $$\frac{dDM_{shoot}}{dt} = \frac{dDM_{leaf}}{dt} + \frac{dDM_{stern}}{dt} + \frac{dDM_{cob}}{dt}$$

DM_{shoot}: shoot dry matter, DM_{leaf}: leaf dry matter, DM_{stem}: stem dry matter, DM_{cob}: cob dry matter

E21. $$\frac{dDM_{leaf}}{dt} = \frac{dDM_{shoot}}{dt} * f_{leaf}$$

DM_{leaf}: leaf dry matter, DM_{shoot}: shoot dry matter, f_{leaf}: fraction of leaf dry matter

E22. $$f_{leaf} = \begin{cases} XStage * f_{leafslope} + f_{leaf0} & | \ XStage > 1 \\ decay_a * XStage^{decay_b} & | \ GAI > GAI_{max} \end{cases}$$

$f_{leaf:}$ fraction of leaf dry matter, $f_{leafslope}$: slope of linear leaf dry matter growth, f_{leaf0}: intercept of linear leaf dry matter growth, $decay_a$: coefficient of leaf dry matter decay, $decay_b$: power coefficient of leaf decay, GAI: green area index, GAI_{max}: maximum green area index, at which leaf dry matter starts decreasing.

E23. $$\frac{dDM_{cob}}{dt} = \frac{dDM_{shoot}}{dt} * (1 - f_{cob})$$

DM_{cob}: cob dry matter, DM_{shoot}: shoot dry matter, f_{cob}: proportion of cob dry matter

E24. $$f_{cob} = \begin{cases} XStage * f_{cobslope} + f_{cob0} & | \ \frac{DM_{stem}}{DM_{shoot}} > f_{stemmin} \\ 1 & | \ \frac{DM_{stem}}{DM_{shoot}} \leq f_{stemmin} \end{cases}$$

f_{cob}: proportion of cob dry matter, $f_{cobslope}$: slope of the linear cob dry matter growth, f_{cob0}: intercept of the linear cob dry matter growth, $f_{stemmin}$: threshold of dry matter allocated in the stem

E25. $$\frac{dDM_{stem}}{dt} = \frac{dDM_{shoot}}{dt} * (1 - f_{leaf}) * (1 - f_{cob})$$

DM_{stem}: stem dry matter, DM_{shoot}: shoot dry matter, f_{leaf}: proportion of leaf dry matter, f_{cob}: proportion of cob dry matter

E26. $GAI=LAI+SAI$

GAI: green area index, LAI: green area index of leaves, SAI: green area index of stems

E27. $$\frac{dGAI}{dt}=\frac{dLAI}{dt}+\frac{dSAI}{dt}$$

GAI: green area index, LAI: green area index of leaves, SAI: green area index of stems

E28. $$\frac{dLAI}{dt}=\frac{d(SLA*DM_{leaf})}{dt}$$

LAI: green area index of leaves, SLA: specific leaf area, $DM_{leaf:}$ leaf dry matter

E29. $$\frac{dSAI}{dt}=\frac{d(SSA*DM_{stem})}{dt}$$

SAI: green area index of stems, SSA: specific stem area, DM_{stem}: stem dry matter

E30. $$SLA=\begin{cases} SLA_{ini} & |SLA \geq SLA_{ini} \\ SLA_a * LAI^{-SLAb} & |SLA_{ini}>SLA>SLA_{min} \\ SLA_{min} & |SLA<SLA_{min} \end{cases}$$

SLA: specific leaf area, SLA_{ini}: upper limit of SLA, SLA_{min}: lower limit of SLA, SLA_a: coefficient of exponential decrease of SLA, SLA_b: power coefficient of exponential decrease of SLA

E31. $$SSA=\begin{cases} SSA_{ini} & |SSA \geq SSA_{ini} \\ SSA_a * SAI^{-SSAb} & |SSA_{ini}>SSA>SSA_{min} \\ SSA_{min} & |SSA<SSA_{min} \end{cases}$$

SSA: specific stem area, SSA_{ini}: upper limit of SSA, SSA_{min}: lower limit of SSA, SSA_a: coefficient of exponential decrease of SSA, SSA_b: power coefficient of exponential decrease of SSA

E32. $$\frac{dLAI}{dt}=\left(SLA_a*LAI^{-SLAb}-SLA_a*SLA_b*LAI^{-SLAb}\right)*\frac{dDM_{leaf}}{dt}$$

LAI: green area index of leaves, SLA_a, SLA_b: coefficients of exponential decrease of SLA via LAI, DM_{leaf}: leaf dry matter

E33. $$\frac{dSAI}{dt}=\left(SSA_a*SAI^{-SLAb}-SSA_a*SSA_b*SAI^{-SLAb}\right)*\frac{dDM_{leaf}}{dt}$$

SAI: green area index of stems, SSA_a, SSA_b: coefficients of exponential decrease of SSA via SAI, DM_{stem}: stem dry matter

E34. $GAI=(1-f_{Sen})*GAI^*$

f_{sen}: proportion of green area turning to senescent plant material, GAI*: actual GAI

E35. $f_{Sen}=sen_a*XStage^{sen_b}$

f_{sen}: proportion of green area turning to senescent plant material, sen_a, sen_b: coefficients of exponential increase of senescent plant area

E36. $Cropheight=GAI^{*}*f_{cropheight}$

GAI*: actual GAI, $f_{cropheight}$: slope of linear regression between GAI and crop height

6.4. Evapotranspiration

E37. $ET_{pot}=\frac{\Delta*R_{net}+\rho*cp*\frac{VPD}{r_a}}{\Delta+\gamma*\left(1+\frac{rc_{min}}{r_a}\right)}*\frac{1}{\lambda}$

ET_{pot}: potential evapotranspiration, Δ: slope of relation between saturation vapor pressure and temperature, R_{net}: net radiation, ρ: air density, cp: specific heat of the air, VDP: , r_a: aerodynamic resistance, γ: psychometric constant, rc_{min}: minimal stomatal resistance, λ: latent heat of water vaporisation

E38. $E_{pot}=ET_{pot}*e^{-k_{PAR}*GAI}$

E_{pot}: potential evaporation, ET_{pot}: potential evapotranspiration, k_{PAR}: extinction coefficient, GAI: green area index

E39. $T_{pot}=ET_{pot}-E_{pot}-I$

T_{pot}: potential transpiration, ET_{pot}: potential evapotranspiration, E_{pot}: potential evaporation, I: interception

6.5. Soil water component

E40. $\frac{\partial\theta}{\partial t}=\frac{\partial}{\partial z}*\left[D_w(\theta)\left(\frac{\partial\theta}{\partial z}\right)+k(\theta)\right]-S(\psi)$

θ: volumetric soil water content, t: time, z: soil depth, D_w: diffusivity of water, k: unsaturated hydraulic conductivity, S: sink term for water uptake by plant roots, ψ: soil water potential

E41. $S[i]=T_{pot}*\frac{RL[i]^{CompF}}{\sum_j RL[j]^{CompF}}*f_{sinkred}$

S: sink term for water uptake by plant roots, T_{pot}: potential transpiration, RL: root length, i: certain soil layer, j: all soil layers, CompF: root competition factor, $f_{sinkred}$: reduction factor

E42. $f_{sinkred}[i]=\begin{cases}1 & |\ \psi_i<\psi_{crit}\\ \frac{\log(\psi_i)-\log(\psi_0)}{\log(\psi_{crit})-\log(\psi_0)} & |\ \psi_i\geq\psi_{crit}\end{cases}$

$f_{sinkred}[i]$: reduction factor for each soil layer i, ψ: soil water potential, ψ_0: soil water potential when water uptake is 0, ψ_{crit}: soil water potential from which water uptake decreases

E43. $T_{act} = \sum_j S[j]$

T_{act}: actual transpiration, S: sink term, j: all soil layers

E44. $E_{act} = E_{pot} * f_{evap}$

E_{act}: actual evaporation, E_{pot}: potential evaporation, f_{evap}: reduction factor

E45. $f_{evap} = \frac{-(\log(\psi_{arr[1]}) - 4.2)}{4.2 - \log(\psi_{critevap})}$

f_{evap}: reduction factor, correcting E_{pot} by low soil water content in the top soil layer, $\psi_{arr[1]}$: soil water potential in the top soil layer, $\psi_{critevap}$: soil water potential at which evaporation decreases.

6.6. Rooting component

E46. $RL_{tot} = DM_{root} * SRL$

RL_{tot}: total root length, DM_{root}: root dry matter, SRL: specific root length

E47. $\frac{dzr}{dt} = k_{zr} * T_{eff} \mid zr \leq zr_{max}$

zr: rooting depth, k_{zr}: slope of linear root depth growth, T_{eff}: effective temperature, zr_{max}: maximum root depth

E48. $RLD = RLD_0 * e^{-kr*z}$

RLD: root length density, RLD_0: root length density at zr=0, kr: exponential coefficient describing vertical root growth, z: soil depth

E49. $kr = \frac{-\ln\left(\frac{RLD_{zr}}{RLD_0}\right)}{zr}$

kr: rooting coefficient, describing vertical root growth, RLD_{zr}: root length density at rooting depth, RLD_0: root length density at zr=0, the ratio of RLD_{zr} and RLD_0 is fitted as a model parameter r_{RLD} to avoid iterative steps, zr: rooting depth

E50. $RLD_0 = \frac{RL_{tot} * kr}{1 - e^{-kr*zr}}$

RLD_0: root length density at zr=0, RL_{tot}: total root length, kr: rooting coefficient describing vertical root growth, zr: rooting depth

7. Appendix B – List of model parameters

In total, 20 crop-specific parameters for aboveground plant growth and three parameters for root growth were fitted with the calibration data set (Table 1). Parameters for the development, besides phy, and soil water dynamic components were derived from literature.

Table B 1 Model parameter values derived from literature and fitted by empirical regression (no literature entry). The table is structured following the model components: Evapotranspiration, Soil water dynamics, Development, Dry matter production, Dry matter partitioning and Root growth.

Parameter	Value	Unit	Description	Literature
Development				
T_1	6	[°C]	Base temperature for calculating T_{eff}	Pagès and Pellerin (1994), Verheul et al. (1996), R. Bonhomme et al. (1994)
GDD_{emer}	100	[°C d]	Temperature sum from sowing until emergence	All GDD's derived according to Bignon (1990)
GDD_{tasini}	320	[°C d]	Temperature sum from emergence until tassel initiation	
GDD_{S2}	510	[°C d]	Temperature sum from tassel initiation until silking	
GDD_{S3}	200	[°C d]	Temperature sum from silking until grain filling	
GDD_{silk}	830	[°C d]	Temperature sum from emergence till silking	
GDD_{total}	1890	[°C d]	Temperature sum from sowing till maturity	
phy	50.8	[°C d leaf^{-1}]	Phyllochron	
Dry matter production				
DM_{seed}	3.7	[g m^{-2}]	Weight of the sown seeds	
f_{hypo}	0.24	[-]	Weight fraction of the hypocotyl	
f_{trans}	0.3	[-]	Weight fraction lost by transformation and translocation	
T_2	16	[°C]	Cardinal temperatures of trapezoidal temperature function to calculate f_T	Yang et al. (2016)
T_3	28	[°C]		
T_4	34	[°C]		
LUE	3.6	[g MJ PAR^{-1}]	Light use efficiency	Optimised by the model internal Levenberg-Marquard algorithm
k_{PAR}	0.67	[-]	Constant extinction coefficient	
Evapotranspiration				
rc0	75	[s m^{-1}]	Stomatal conductance	Rochette et al. (1991), Sinclair et al.

				(1975), Irmak and Mutiibwa (2008)
Soil water dynamics				
psi_0	15000	[hPa]	Water tension at permanent wilting point	Neukam et al. (2016)
$psi_{critEvap}$	20	[hPa]		Beese et al. (1978)
psi_{cri}	500	[hPa]	Critical soil water potential	Neukam et al. (2016)
CompF	0.5	[-]	Root competition factor reducing water uptake	Ehlers et al. (1991)
Dry matter partitioning				
ACE_{root}	0.35	[-]	Dry matter allocation coefficient for root dry matter	Yang et al. (2016)
DS_{stop}	1.15	[-]	Development stage when root growth stops	Yang et al. (2016)
$f_{leafslope}$	-0.293	[-]	Slope of linear leaf growth (f_{leaf})	
f_{leaf0}	1.032	[-]	Intercept of linear leaf growth (f_{leaf})	
GAI_{max}	5.5	[m^2 m^{-2}]	maximum green area index, at which leaf dry matter starts decreasing	
$decay_a$	$3.232*10^{-15}$	[-]	Coefficients calculating f_{leaf}	
$decay_b$	22.32	[-]	after silking due to dry matter translocation to stem (f_{leaf})	
$f_{cobslope}$	0.5687	[-]	Slope of the linear growth of f_{cob}	
f_{cob0}	-1.095	[-]	Intercept of the linear growth of f_{cob}	
$f_{stemmin}$	0.248	[-]	Proportion of DM remaining in the stem at harvest	
SLA_{ini}	0.032	[m^2 g^{-1}]	Upper limit of the negative exponential relation between LAI and SLA	
SLA_{min}	0.016	[m^2 g^{-1}]	Lower limit of the negative exponential relation between LAI and SLA	
SLA_a	0.022	[m^2 g^{-1}]	Coefficients of the negative	
SLA_b	-0.135	[-]	exponential relation between LAI and SLA	
SSA_{ini}	0.004	[m^2 g^{-1}]	Upper limit of the negative exponential relation between SAI and SSA	
SSA_{min}	0.0006	[m^2 g^{-1}]	Lower limit of the negative exponential relation between SAI and SSA	
SSA_a	0.0006	[m^2 g^{-1}]	Coefficients of the negative	
SSA_b	-0.379	[-]	exponential relation between SAI and SSA	
sen_a	0.00013	[-]	Coefficients of exponential	
sen_b	1.734	[-]	growth of senescent proportion of GAI (f_{sen})	

$height_a$	0.2894	[-]	Coefficients of quadratic
$height_b$	0.0027	[-]	equation to calculate crop
$height_c$	$7.7982*10^{-7}$	[-]	height by DM_{shoot}
Root Growth			
zr_0	6	[cm]	Sowing depth
SRL	6790	[cm g^{-1}]	Specific root length
zr_{max}	120	[cm]	Maximum rooting depth
k_{zr}	0.703	[cm d^{-1} $°C^{-1}$]	Coefficient of linear root growth
r_{RLD}	0.128	[-]	Ratio between RLD_{zr} and RLD_0 for computing k_r

Chapter 3

Exploiting Deeper Soil Layers with Deep-Rooting Cover Crops: Which Mixtures Are Most Effective?

Katja Holzhauser[a, *], Josephine Bukowiecki[a], Iris Zimmermann[b], Michaela A. Dippold[c], Sandra Spielvogel[b], Henning Kage[a]

a Institute of Crop Science and Plant Breeding, Agronomy and Crop Science, Kiel University, Germany
b Institute of Plant Nutrition and Soil Science, Soil Science, Kiel University, Germany
c Geo-Biosphere Interactions, Department of Geoscience, University of Tübingen, Germany

* Corresponding author: holzhauser@pflanzenbau.uni-kiel.de, (Katja Holzhauser)

Keywords: Catch crop, Silage Maize, Subsoil, Soil water, Drought resilience

Abstract

Context: Cover crops are one essential component of sustainable agriculture, as it allows improving soil health, water management, and nutrient cycling, which strengthens resilience and yield stability in cropping systems. Given limited soil resources and increasing summer drought periods, efficient use of water and nutrient reserves in deeper soil layers has become a central agricultural challenge. Integrating deep-rooting cover crops into cropping systems may enhance the vertical exploitation of arable soils, enabling subsequent silage maize crops to access subsoil resources more efficiently.

Objective: This study aims to investigate the influence of deep-rooting cover crops on yield formation of silage maize. It was hypothesized that pre-formed biopores from deep-rooting cover crops enhance water access from deeper soil layers supporting maize yield.

Methods: Cover crops of different functional groups and rooting characteristics — brassicas, grasses, and legumes — were combined to three cover crop mixtures. Perennial alfalfa, with a longer growth period and therefore expected deeper roots than winter cover crops, was included as a variant to enhance effects on soil structure. Winter fallow served as a control. In a triannual trial (2021-2023) in Northern Germany their effects on silage maize yield were investigated, with a focus on radiation uptake (RU), changes in soil water content (ΔS), total water use (WU) and the resulting radiation and water use efficiencies (RUE, WUE) of silage, utilising soil sensors and remote sensing technique.

Results: Legume-grass and brassica-grass mixtures sustained high maize yields, while legume-brassica and perennial alfalfa variants reduced yields (-13.6% and -13.9%). Yield differences were unrelated to maize green area index, radiation uptake, or total water use. Subsoil (20–110 cm) water storage changes were significantly lower after legume-grass and brassica-grass mixtures than fallow, while deep subsoil (110–160 cm) moisture was generally reduced, significantly so for maize after legume-brassica. Radiation use efficiency was comparable to fallow for all mixtures except perennial alfalfa, while water use efficiency declined for the legume-brassica variant.

Conclusions: All tested cover crop mixtures facilitated maize access to deep subsoil water resources, with mixtures including grasses conserving subsoil moisture while maintaining yields comparable to those after fallow.

Implications: The study investigates innovative strategies for the composition of cover crop mixtures that integrate diverse functional traits by applying the ecological concept of niche complementarity.

1. Introduction

Cover crops play a crucial role in sustainable agriculture, influencing soil properties, water dynamics and nutrient cycling, consequently increasing the resilience of the cropping system to changing environmental conditions (Kaye and Quemada, 2017). The presence of cover crops in the rotation can have lasting effects on the performance of subsequent cash crops like maize (Marcillo and Miguez, 2017), by enhancing soil conditions and optimizing resource use. Thus, in Europe the use of winter cover crops became strongly recommended in some countries, primarily guided by the Common Agricultural Policy (CAP) for 2023-2027.

The wide range of cover crops can be categorized into functional groups, fulfilling various environmental services, such as prevention of nitrogen leaching, erosion control, weed suppression and nitrogen fixation by legumes (Daryanto et al., 2018; Abdalla et al., 2019). The combination of cover crops from different functional groups into cover crop mixtures may combine specific functions and eventually improve the adaptability to specific site conditions and management practices. According to ecological principles, such as resource competition, niche complementarity, or the diversity-stability hypothesis (Tilman, 2013), the use of diverse cover crop mixtures can enhance resource use efficiency and thereby ecosystem services, if the species involved complement each other and effectively use the available resources. Moreover, mixtures tend to establish more reliably than monocultures because they contain a greater variety of species, each of which can respond differently to varying climatic conditions across different growing seasons (Florence and McGuire, 2020b).

Cover crops have been widely documented to improve various soil physical properties, which play a crucial role in enhancing soil health and consequently crop productivity. Blanco-Canqui and Ruis (2020) highlights that cover crops reduce soil penetration resistance, a key indicator of soil compaction, enhance porosity, and consequently water infiltration. Villamil et al. (2006) specifically measured an increase in mesopores (50–0.5-µm) due to the presence of winter cover crops. Root channels left by cover crops, such as those observed by Williams and Weil (2004), facilitate deeper root growth of subsequent crops. For example, maize following alfalfa has been shown to recolonise the root channels formed by alfalfa (Rasse and Smucker, 1998). Brassica species, such as radish or rapeseed, have also been identified as effective in breaking through compacted soils and reaching deep soil layers, thereby providing greater access to deeper water reservoirs (Kristensen and Thorup-Kristensen, 2004a; Chen and Weil, 2010, 2011; Kemper et al., 2020). Furthermore, taproots and fibrous root systems of cover crop components were suggested to complement each other. Saleem et al. (2020) measured larger root length and root areas by mixing legume and brassica cover crops, than grown as monocultures.

Williams and Weil (2004) found similar patterns combining the non-legume/grass rye with forage radish. However, a recent review by Blanco-Canqui (2024) compared the effects of cover crop mixtures with their monoculture components on soil physical properties and found that mixtures did not outperform monocultures.

Silage maize is one of the most widely cultivated crops in Germany, alongside winter wheat and winter barley, covering approximately 2 million hectares in 2024 (Statistisches Bundesamt, 2024). While its significance in German agriculture is clear, the impact of preceding winter cover crops on silage maize yields remains a topic of debate in the literature. Some studies found no significant effects of cover crop monocultures on maize yield (Basche et al., 2016; Kühling et al., 2023), while others reported negative impacts (Tonitto et al., 2006; Abdalla et al., 2019). These contrasting findings could be traced back to the different types of considered cover crops. For example, Alvarez et al. (2017) and Marcillo and Miguez (2017) noted that legume cover crops tend to increase subsequent maize yields, in contrast to non-legumes, e.g. grasses or brassicas. Furthermore, their combination in cover crop mixtures have been found to increase yields of the following maize, about 13 % on average (Abdalla et al., 2019).

Even if cover crops do not consistently increase yields, their role in preserving productivity and enhancing the resilience of cropping systems under changing environmental conditions might be vital in future. Crop productivity is primarily driven by photosynthetically active radiation (PAR) , with the green area index (GAI) determining how much light is captured by the plant (de Wit, 1958; Duncan, 1971) and the radiation use efficiency (RUE) defining the conversion efficiency of PAR into biomass (Monteith, 1977). Following cover crops, an improved soil structure and nutrient availability could favour maize growth, by promoting GAI development and increasing the interception of light. If the GAI is sufficiently high, maize can maximize its RUE, especially under favourable water conditions (Earl and Davis, 2003).

Drought tolerance is primarily determined by a plant's ability to utilize soil water resources under dry conditions. Improved soil water availability through cover crop mixtures could increase water use (WU) and help mitigate yield losses during water stress periods (Blum, 2009). It is important to distinguish WU from water use efficiency (WUE), which refers to the productivity of a plant per unit of WU (Tanner, 1981; Kijne et al., 2003). High WUE indicates high yields with low total WU. However, in this study, increased water availability from cover crops may lead to higher WU while maintaining productivity, resulting in a reduced WUE (Blum, 2009). The use of cover crops may also result in a reduction in water availability for subsequent main crops, by the cover crops themselves. If their autumnal water uptake is not fully replenished by winter rainfall, transpiration during cover crops spring growth phase, may deplete the water resources.

However, this could subsequently lead to a reduction in WU of the main crop (Unger and Vigil, 1998).

Based on a triannual field trial, this study aims to enhance the understanding of the effects of cover crop mixtures on the yield formation of silage maize, with a focus on radiation uptake, soil water content changes (ΔS) in specific soil layers, and WU of the cash crop. We observed if cover crops, with different rooting characteristics, form biopores, which facilitate access to water resources of deeper soil layers. A longer growth period of cover crops is often suggested, to enhance their effects (Blanco-Canqui and Ruis, 2020). Therefore, the perennial cover crop alfalfa is included in the study, to ensure the formation of deep root channels. The hypotheses were that under the cultivation conditions in Northern Europe (1) silage maize yield is not affected by preceding winter cover crop mixtures, and that (2) WUE decreases and RUE increases, due to a (3) better water access after cover crop variants, total WU of maize is increased, especially in deep subsoil. (4) Hypothesis are emphasised by perennial alfalfa.

2. Material and Methods

2.1. Study site

The research took place at the Hohenschulen experimental farm of Kiel University (10.0° E, 54.3° N, 30 m ASL). The area has been shaped by glacial processes, leading to a diverse and small-scale heterogeneity of soil types. However, the dominant soil type at the site is a luvisol with a sandy loam texture. The region experiences a temperate oceanic climate, with long-term data (1991–2020) showing an average annual air temperature of 9.3°C and a sum of precipitation of 797 mm, respectively (Deutscher Wetterdienst, 2024). Data collection was conducted over three consecutive years, with maize harvest in 2021, 2022, and 2023. Weather conditions in the three trial seasons differed distinctly. Highest sum of precipitation was measured in 2021, caused by several heavy rainfalls throughout the season, followed by a very dry summer in 2022, with temperature peaks until 35.9°C. Due to drought, sowing and harvest in 2022 were conducted early for conditions of Northern Germany. The growing period of 2023, was shaped by dry conditions at the start, but experienced steady rainfall from July till September (Table 3).

Table 3 Description of the three growing periods of maize (2021-2022-2023) by sowing and harvest date and days of each growing period (n). Furthermore, listed are weather conditions: sum of precipitation (mm), mean, max and min air temperature (T, °C)

	2021	2022	2023
Sowing date	2021-05-20	2022-04-28	2023-05-25
Harvest date	2021-10-11	2022-09-13	2023-09-29
n	144	138	127
Precipitation	296	231.6	261.4
T_{mean}	16.2	16.1	16.9
T_{min}	4	0.7	3.8
T_{max}	31.6	35.9	29.8

2.2. Trial design

Winter cover crops were sown in late summer of the year preceding silage maize sowing. A winter fallow was used as control. The previous crop was uniformly summer barley. A total of six winter cover crop species were included in the study, classified in three functional groups: legumes, grasses, and brassicas. Each mixture combines two functional groups, with two

species from each group, which leads to the variants Legume-Grass; Legume-Brassica; Brassica-Grass (Table 4). To enhance the beneficial effects of cover crops, a longer growth period is often recommended; thus, the perennial cover crop alfalfa (*Medicago sativa*) was included in this study to promote the formation of deep root channels, due to the multi-year growth period (2 years). Since the trial began in August 2020 with the sowing of cover crops, alfalfa plots were not available for samplings conducted in the first trial year (2020/2021). After termination of cover crops in late spring, silage maize (KWS Stefano) was sown. As the study focusses on cover crop effects on silage maize water balance, maize was fertilised sufficiently (180 kg N/ha).

Table 4 Winter cover crops investigated in this study

Family	Cover crops	Botanical name	Legume-Grass	Legume-Brassica	Brassica-Grass
Brassicaceae	Oilseed Rape	*Brassica napus*		X	X
	Oilseed Radish	*Brassica sativus*		X	X
Leguminosae	Red clover	*Trifolium pratense*	X	X	
	White clover	*Trifolium repens*	X	X	
Poaceae	Ryegrass	*Lolium perenne*	X		X
	Tall fescue	*Festuca arundicaceae*	X		X
Leguminosae	Alfalfa	*Medicago sativa*			

2.3. Plant and soil samplings

Maize yield was determined by manual sampling at the end of the growing season. At least 10 plants per plot were harvested, dried (°60 C) and weighted. In order to assign the dry matter weights to a specific ground area, length of harvested maize rows were determined to form a parallelogram and consequently its area.

Green area index (GAI) was monitored biweekly by drone-based multispectral measurements with a Sequoia™ camera (Parrot Sequoia, Parrot Drones SAS, 143 Paris, France) and a corresponding GAI calibration for silage maize (Bukowiecki et al., 2024a). Development stages (BBCH, Lancashire et al. 1991) were determined frequently during the growing season and classified into the main stages leaf development, stem elongation, silking, grain filling, maturity. Furthermore, for each variant maximum and averaged GAI (GAI_{max}, GAI_{avg}) of each plot were calculated and averaged for each variant, respectively.

Soil moisture was determined weekly till biweekly by means of the Diviner2000 (Sentek Sensor Technologies, Stepney, South Australia), which is based on frequency domain reflectance (FDR). Measurement tubes were installed in each plot enabling measurement of volumetric soil moisture until a depth of 1.60 m, via 16 x 10 cm steps.

2.4. Data processing and statistical analysis

Data processing and statistical analysis were performed in R (R version 4.4.1. R Core Team, 2024).

2.4.1. Radiation uptake

Radiation uptake (RU) was calculated from the incoming photosynthetic active radiation (PAR) which is commonly estimated as half of global radiation (Szeicz, 1974), and the radiation extinction within the canopy. The latter was calculated according to the Beer-Lambert law (Monsi, 1953).

$$RU = PAR * \left(1 - e^{-k * GAI}\right) \quad \text{(E1)}$$

with the extinction coefficient (k) set to 0.65 and the GAI derived by spectral reflectance data (Bukowiecki et al., 2024a). Finally, RU was cumulated over the season. Radiation use efficiency (RUE) was calculated as follows:

$$RUE = \frac{Y}{RU} \quad \text{(E2)}$$

with the final yield Y and RU at the final harvest dates of each plot.

2.4.2. Water use

By identifying patterns in soil moisture distribution across the soil profile, hierarchical clustering was performed. Ward's method merges the clusters with the smallest increase in total variance. Resulting clusters were topsoil 0 – 20 cm, subsoil 20 – 110 cm and deep subsoil 110 – 160 cm. Volumetric water content was transformed to mass water content (SW) and summed for each layer as well as the whole soil profile, respectively. To assess the change in SW (ΔS), the initial measurement (SW_i) of each plot in each trial year was subtracted from every respective subsequent measurement (SW):

$$\Delta S = SW - SW_i, \quad \text{(E3)}$$

For seasonal analysis, ΔS per layer was grouped for the main development stages. The latter represents the whole season perspective.

Water use (WU) was calculated using simplified water balance formula, omitting the components runoff, drainage to groundwater, upward capillary and lateral groundwater flow:

$$WU = P_{sum} - \Delta S, \quad \text{(E4)}$$

with the sum of precipitation until a given time (P_{sum}) and ΔS of the whole soil profile. If water is extracted from the soil by plant, the ΔS becomes negative, indicating that both rainfall and soil moisture have been utilized. If more than sufficient rainfall occurs, resulting in inflow to the soil, the ΔS becomes positive and is consequently subtracted from P_{sum}.

According to the calculation of RUE, Water use efficiency (WUE) was calculated as:

$$WUE = \frac{Y}{WU}, \quad \text{(E5)}$$

with the final yield Y and WU at the final harvest dates of each plot.

2.4.3. Statistical analysis

Data evaluation started with the definition of appropriate statistical mixed models (Pinheiro and Bates, 2010). For the response variables Y, GAI_{avg}, GAI_{max}, WU, RU, WUE and RUE the effects of the cover crop variants (Table 2) were tested. Trial years and blocks are included as random effects, blocks nested within years. By including these random effects, the model also accounts for variability due to these grouping factors that are not directly explained by the fixed effects, especially for the variant perennial alfalfa, which was not included in the first trial year (E6):

$$\{\text{Yield}, GAI_{avg}, GAI_{max}, \text{WU}, \text{RU}, \text{WUE}, \text{RUE}\} \sim \text{Variant} + \text{random effects} \quad \text{(E6)}$$

For the response variables GAI an additional seasonal analysis was done, by adding the development stages as a fixed effect, as well as the interaction cover crop variant (E7). Same was conducted for WU with the addition of the clustered soil layers and their interaction term (E8).

$$GAI \sim \text{Variant} * \text{Development stage} + \text{random effects} \quad \text{(E7)}$$

$$WU \sim \text{Variant} * \text{Soil layer} * \text{Development stage} + \text{random effects} \quad \text{(E8)}$$

Residuals were found to be normally distributed and to be heteroscedastic with respect to the different levels of variant, layer and development stage. Based on these models, an analysis of variance (ANOVA) was conducted followed by a multiple contrast test (Hothorn et al., 2008; Bretz et al., 2011), in order to compare the several levels of influence factors, respectively.

3. Results

3.1. Silage maize yield

On average over the years, the highest dry matter yield of silage maize was achieved by maize after bare fallow with averaged 24.0 t ha^{-1}. Legume-brassica and alfalfa treatments yields were significantly lower, by 13.6 respectively 13.9 %. Yields of legume-grass and brassica-grass variants were not significantly different (22.0 and 22.6 t ha^{-1}) (Figure 8).

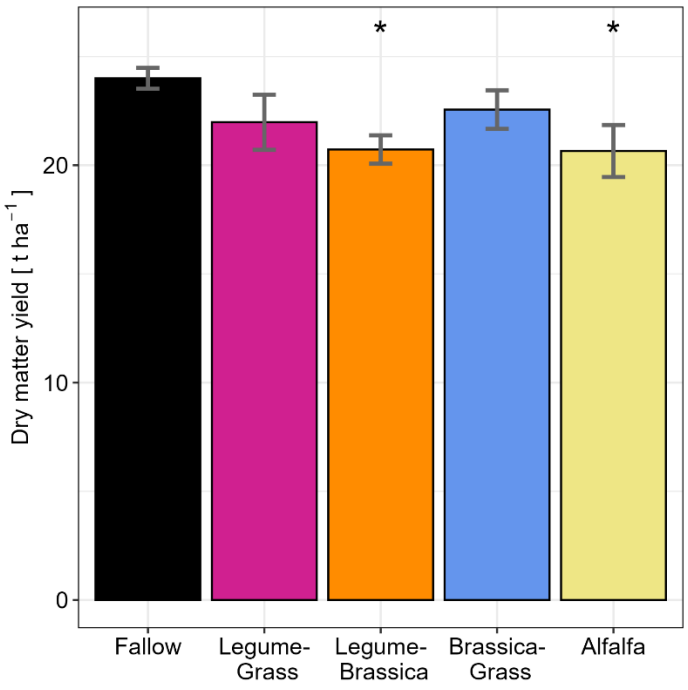

*Figure 8 Dry matter yield (g m^{-2}) of silage maize grown after fallow, cover crop mixtures and perennial alfalfa. Signif. codes: * 0.05*

3.2. Radiation uptake

GAI of maize after cover crop mixtures or perennial alfalfa were not significantly different to maize after fallow (n=616), neither at their maximal reached GAI (GAI_{max}), nor at specific BBCH stages throughout the season. GAI_{max} and GAI_{avg} were similar for all variants tested (Table 5). In general, GAI_{max} was reached after 87, 90 and 103 days after sowing, in 2021, 2022 and 2023, respectively, with the highest GAI's measured in 2021 (avg. 5.18 m^2 m^{-2}) and the lowest in 2023 (avg. 4.69. m^2 m^{-2}). Maize after perennial alfalfa reached GAI_{max} later (avg. 105 days after sowing, Figure 9) during the growing season, compared to the other variants (fallow: 93, legume-grass: 96, legume-brassica: 89, brassica-grass: 93 days after sowing, Figure 9). Except of alfalfa, all variants maintained a high GAI for a while, before declining due to senescence (Figure 9). Analogue to this, the RU was similar between the tested variants, as it is derived by

GAI. RU differs distinctly between the years. Sum of RU was highest in 2022 with and the lowest in 2021, with averaged 750.8 and 603.46 MJ, respectively (Table 5).

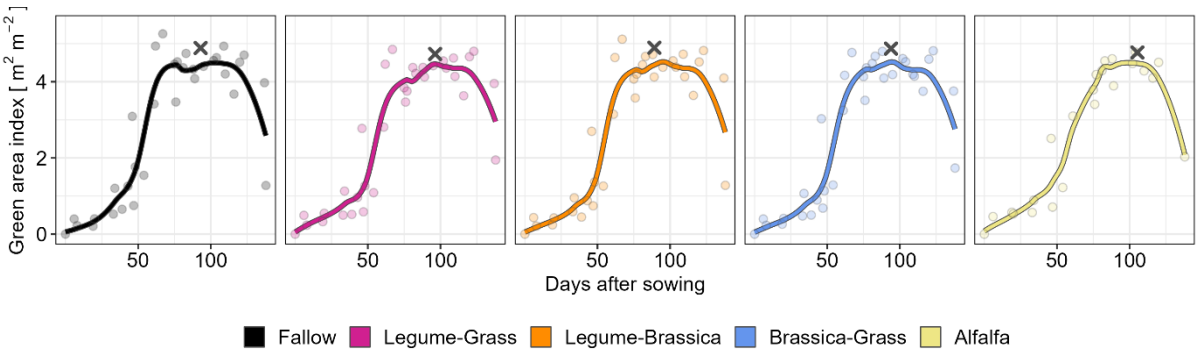

Figure 9 Spectrally derived green area index (GAI, m² m^{-2}) development of silage maize after bare fallow, cover crop mixtures and perennial alfalfa. Depicted is the average GAI of the trial years 2021, 2022 and 2023. Cross signs the maximum GAI (GAI$_{max}$).

3.3. Water use

Overall WU of silage maize after cover crop variants ranged from minimum 260 to maximum 294 mm, for alfalfa and legume-brassica variants respectively. The latter WU was about 3.6% higher than for maize after fallow. The other cover crop variants underperformed total WU of maize after fallow, yet without significant differences (Figure 10; legume-grass: -3.1%, brassica-grass: -5.2%, alfalfa: -8.4 %).

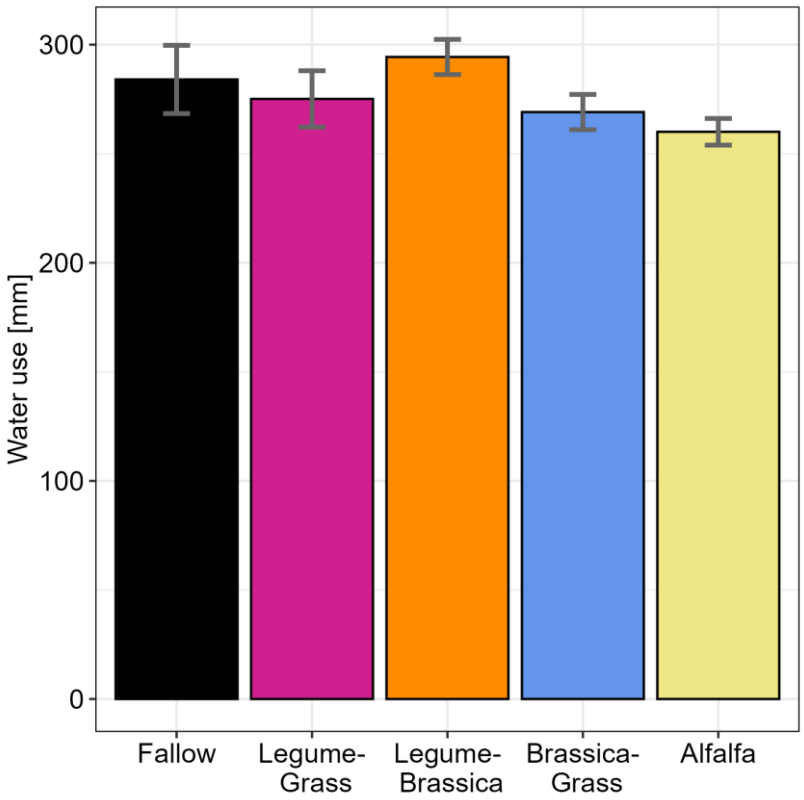

Figure 10 Averaged water use (WU, mm) of the growing period of silage maize after bare fallow, cover crop mixtures and perennial alfalfa. WU is the sum of precipitation and change in soil water storage (ΔS).

The cluster analysis divided soil moisture data into topsoil (0-20 cm) subsoil (20-110 cm) and deep subsoil (110-160 cm). Figure 11 illustrates the different cover crop variants ΔS across soil layers and maize growth stages. While no significant differences in WU were observed in the topsoil, subsoil and deep subsoil layers exhibit notable variation, particularly during silking, grain filling, and maturity.

In topsoil, ΔS was relatively small, across all development stages. In addition, there are no significant differences across the variants. The ΔS were positive, indicating an inflow of water into the topsoil layer by precipitation. Same applies for leaf development and stem elongation phases in subsoil.

First decreases in soil moisture of the subsoil of maize after fallow appear during silking. During grain filling and maturity measurements indicate crop water uptake for all variants. Thereby, decreases in soil moisture after legume-grass, and brassica-grass mixtures were significantly lower than maize / fallow variant. The effect appeared even earlier after legume-grass mixture, starting during grain filling.

In the deep subsoil, notable differences between the cover crop variants and the fallow variant become evident, particularly since stem elongation. During stem elongation and silking, all cover

crop mixtures show noticeable reduction in soil moisture indicating high water uptake, contrary to maize grown after fallow and alfalfa, where rather inflow of water was measured. Until grain filling, soil moisture of maize after fallow has almost not changed. Largest ΔS in deep subsoil occur at grain filling: Fallow, legume-grass, legume-brassica and brassica grass variants exhibit a reduction of soil moisture, with -7.71, -9.80, -24.99 and -9.81 mm, respectively (Figure 11). However, perennial alfalfa variant shows a significant increase in soil moisture (+5.75 mm). Soil moisture of maize after legume-brassica changes about averaged -29 mm regarding maturity stage. Since stem elongation phase, ΔS of legume-brassica variant differed significantly to fallow variant, indicating a higher water depletion in deep subsoil.

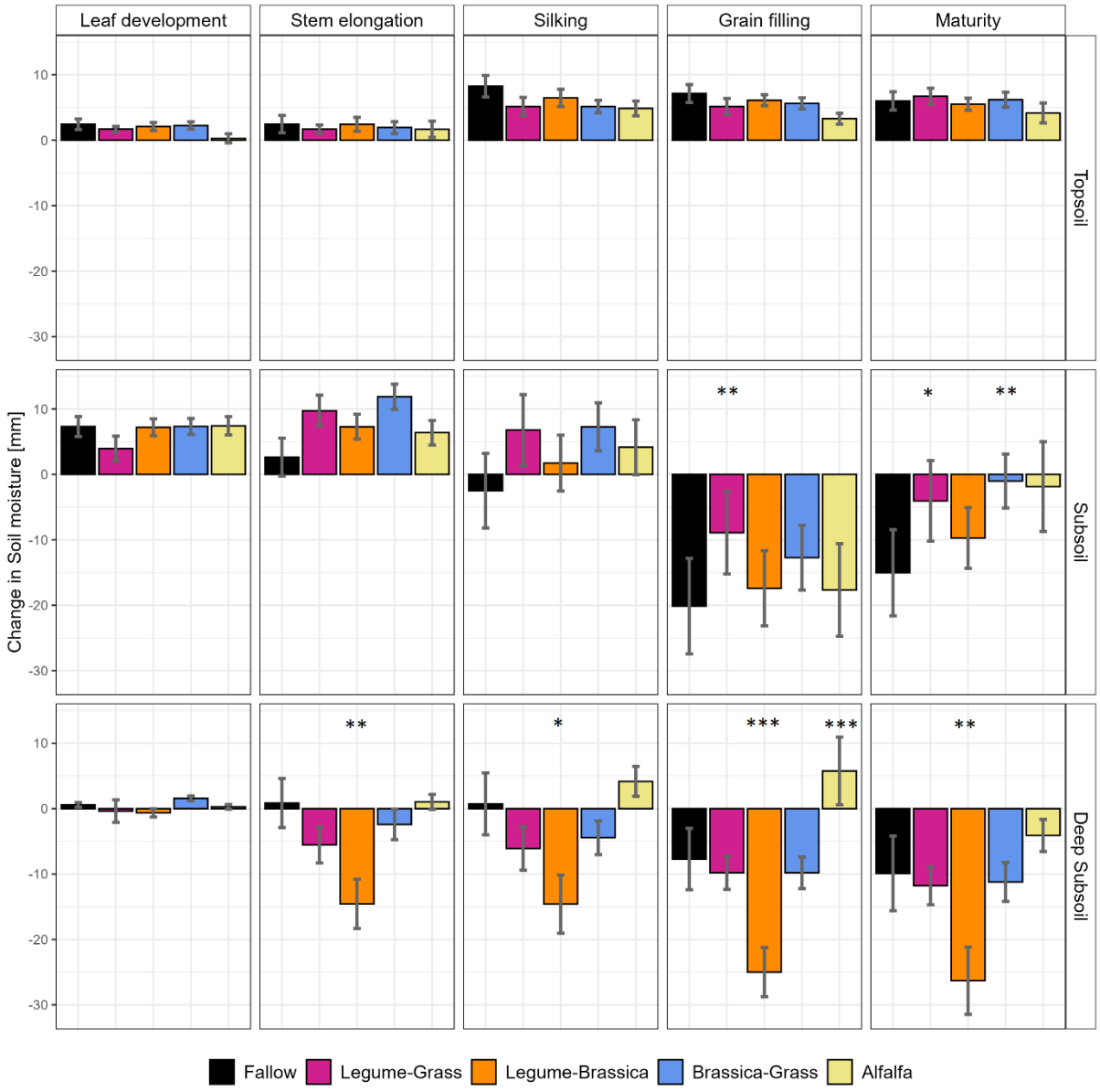

*Figure 11 Change in soil moisture (ΔS, mm) in topsoil (0-20 cm), subsoil (20-110 cm) and deep subsoil (110-160 cm) until leaf development, stem elongation, silking, grain filling an maturity. For each stage of development, the ΔS are related to the difference from the first measurement. Maturity stage represents the whole season perspective. Signif. codes: *** 0.001 ** 0.01* 0.05.*

Table 5 Means and standard deviation of yield (t ha^{-1}), water use (WU, mm), mean green area index (GAI, m² m^{-2}), maximal GAI and radiation use efficiency (RUE, g MJ $^{-1}$) and water use efficiency (WUE, g mm^{-1}) of silage maize after bare fallow, cover crop mixtures and perennial alfalfa

Variant	Yield	WU	GAI_{mean}	GAI_{max}	RUE	WUE
Unit	t ha^{-1}	mm	m² m^{-2}	m² m^{-2}	g MJ^{-1}PAR	g mm^{-1}
Fallow	24.0 ± 1.7	284 ± 54	2.7 ± 1.9	4.9	3.3 ± 0.3	8.3 ± 2.0
Legume-Grass	22.0 ± 4.4	275 ± 44	2.7 ± 1.8	4.7	3.1 ± 0.5	7.9 ± 2.5
Legume-Brassica	20.7 ± 2.2	294 ± 26	2.7 ± 1.8	4.9	3.0 ± 0.4	6.6 ± 1.0
Brassica-Grass	22.6 ± 3.1	269 ± 28	2.7 ± 1.8	4.9	3.2 ± 0.3	8.1 ± 1.8
Alfalfa	20.7 ± 3.4	260 ± 17	2.6 ± 1.7	4.7	2.8 ± 0.4	7.7 ± 1.4

3.4. Radiation and water use efficiencies

On average silage maize after fallow achieved the highest RUE of 3.34 g MJ^{-1}, followed by brassica-grass variant, with 3.21 g MJ^{-1}. Alfalfa variant was significantly lower with an averaged RUE of 2.78 g MJ^{-1} (Figure 12). Regarding the trial years, RUE of 2022 was low for all variants, ranging from a minimum 2.43 to maximum 2.86 g MJ^{-1} for legume-brassica and brassica-grass mixture, respectively. Notably, in this very dry summer (2022) alfalfa variant reached a comparably high RUE of 2.84 g MJ^{-1} as well. In the temperate trial years 2021 and 2023, the highest RUE's were calculated for maize after fallow and brassica-grass.

WUE's of respected variants was high, ranging from the significantly lower legume-brassica mixture to fallow variant, with 6.55 and 8.27 g l^{-1}, respectively. Similar to RUE pattern, brassica-grass mixture achieves a high WUE of 8.11 g l^{-1}. Highest WUE's were calculated in 2023, which experienced high precipitation during late summer, with an average of 9.58 g l^{-1}. During the dry year 2022, lowest WUE was found for legume-brassica (6.15 g l^{-1}) and the highest for brassica-grass variants (7.61 g l^{-1}).

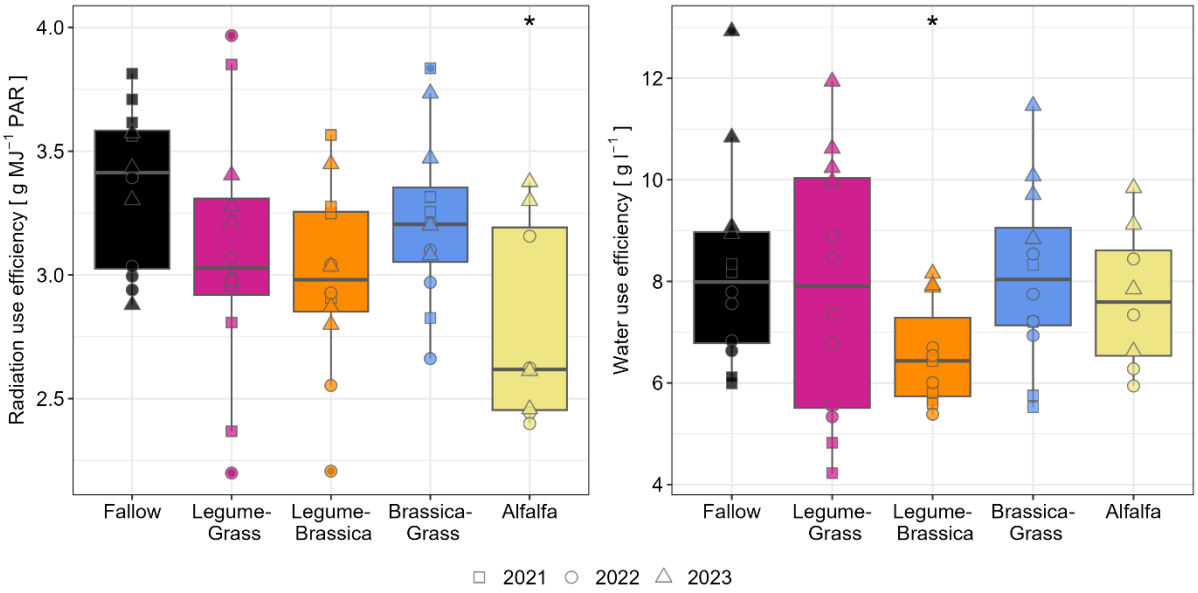

*Figure 12 Radiation use efficiency (RUE) and water use efficiency (WUE) of silage maize grown after fallow, cover crop mixtures and perennial fallow. Shapes illustrate the data from each trial year 2021 (rectangle), 2022 (circle) and 2023 (triangle). Signif. Codes * 0.05*

4. Discussion

Despite the common advantages of cover crops (e.g. minimising N leaching losses, sustaining humus contents of soils) their effects on yield and WU on the following main crops may be site specific (Wang et al., 2021). Reducing effects on WU and yield can occur if soil water replenishment over winter is incomplete or if the cover crops are consuming water after winter (Unger and Vigil, 1998). Positive effects on water use and yield may happen if cover crops enhance subsoil rooting.

4.1. Effect of cover crop variants on silage maize yield

Results of previous studies on the effect of cover crops on maize yield varied, from losses (Tonitto et al., 2006) to no significant effects (Basche et al., 2016; Hunter et al., 2021; Kühling et al., 2023) to even higher yields after cover crop monocultures (Chen and Weil, 2011; Niu et al., 2023) or mixtures (Abdalla et al., 2019; Florence and McGuire, 2020b). In this study, maize after brassica-grass in particular achieved a very high yield (22.6 t ha^{-1}). In the literature, the non-legume cover crops were often categorised as yield-reducing (Alvarez et al., 2017; Qin et al., 2021). However, in this study, the variants legume-grass and brassica-grass could sufficiently maintain the yield of maize at the same level as without cover crop (fallow), while legume-brassica mixture and perennial alfalfa reduced yield about 13.6 and 13.9 %, respectively.

These different findings might be explainable by different starting conditions for maize cultivation following cover crops. In drier regions, cover crops can have a depleting effect on the topsoil layers (Kaye and Quemada, 2017). Therefore, the effect of the termination date of cover crops on yield of the subsequent crop has been discussed in literature (Alonso-Ayuso et al., 2018). Several authors determine a late termination date for sufficient growing conditions of the subsequent crop (Stipešević and Kladivko, 2005), because of reduced risk of evaporation in spring and attenuation of nitrogen leaching. Stipešević and Kladivko (2005) found, that specifically young maize plants suffer under drought conditions and resource competition. This effect might have played a role in trial year 2023, following an unusually dry spring in northern Germany, with legume-brassica and perennial alfalfa reducing yields, while legume-grass and brassica-grass maintained them. In milder summer of 2021, this differentiation between cover crop mixtures (except alfalfa) did not appear. This indicates an increased resilience of maize to early water stress by preceding grass-mixtures. Alonso-Ayuso et al. (2018) found that a late termination date may cause competition, potentially explaining the yield reductions observed with alfalfa and legume-brassica mixtures. In contrast to their above-ground biomass, legume roots have been found to have a high C:N ratio and lignin content, resulting in slow root decomposition (Puget and Drinkwater, 2001; Jani et al., 2016). The remaining root biomass,

especially after enlarged growing period of alfalfa can suppress early maize root development, by a remaining physical barrier in the root channels.

4.2. Radiation uptake

RU is one factor in explaining yield formation, with the GAI determining the amount of radiation absorbed and subsequently converted into biomass (de Wit, 1958; Ullah et al., 2019). However, in this study, the differences in maize yields between the various cover crop treatments cannot be explained by GAI or RU, as no significant differences were found in these parameters. Despite the contrasting trial years, the maximum GAI remained consistently high, with average values between 4.69 and 5.18 $m^2 m^{-2}$. This aligns with findings of Earl and Davis (2003), who observed comparable amounts of intercepted radiation by maize, and was thus were unable to explain yield differences. Although drought stress was present during 2022, with high temperatures and low precipitation (Table 1), this did not lead to a measurable reduction in GAI. Teixeira et al. (2014) found that drought could reduce GAI by 37%, but regarding GAI-values in this study, no such impact induced by cover crops was observed. N limitation can be neglected, because maize GAI has often been reported as not highly N-sensitive (Lemaire et al., 2008; Massignam et al., 2011; Teixeira et al., 2014). Furthermore, the treatments were all fertilised sufficiently, to exclude any potential of nitrogen impact. Modelling radiation and water budget of winter wheat at the same study site in winter wheat, (Bukowiecki et al., 2024b) displayed that even under Northern German climatic conditions, reductions in transpiration are relevant for yield formation, and proposed therefore recommended to analyse yield formation rather by a water budget-based than by a radiation budget-based approach.

4.3. Deep-Rooting Effects of Cover Crops on Maize Water Use

Soil water storage patterns varied across layers and throughout the maize growing season, indicating a possible influence of deep-rooting cover crops. In the topsoil, no significant differences in water storage were detected. However, Chen and Weil (2010) found drier soils at 5 and 15 cm depths after fodder radish. In this study, water inflow was likely due to rainfall exceeding plant uptake. In the subsoil (20-110 cm), water storage was positive for all variants until silking. Later in the season, particularly during grain-filling and maturity, significant water reductions appeared, with the highest subsoil water extraction observed in maize after fallow. These patterns suggest that legume-grass and brassica-grass cover crops have a water-conserving effect in the subsoil by enhancing soil porosity and aggregate stability, which improves infiltration and plant-available water (Villamil et al., 2006). Basche et al. (2016) found consistently higher soil water content under maize following a rye cover crop, highlighting this effect in long-term rotations. Niu et al. (2023) confirmed this effect, though primarily at the

maize seedling stage, as cover crop mulch reduced evaporation and conserved water in the topsoil. Using historical data and future scenarios, Li et al. (2021) further supported these findings, showing that cover crops can increase soil water reservoirs by reducing evaporation and drainage across the cropping system.

Only few authors measured the soil moisture in deeper soil layers (Blanco-Canqui, 2024). In this study, an additional deep subsoil depth increment was investigated (110-160 cm). While water withdrawal is low until soil depth of 110 cm and soil water storage recovers during maturity, in the deep subsoil substantial soil water uptake could be shown from across all variants, but the extent varied. In all cover crop mixture variants, maize started water extraction from deep subsoil during stem elongation, while soil water storage of maize after fallow did not change that early. Particularly, maize following legume-brassica mixtures showed the highest uptake, potentially due to a synergistic effect of the deep-rooting species oilseed radish and oilseed rape (Kemper et al., 2020). The addition of brassica species into a cover crop mixture, or more specifically the combination of brassica species with fibrous rooting species, has the potential to result in a reduction in the bulk density of the soil (Saleem et al., 2020; Decker et al., 2022). Furthermore, Chen and Weil (2010) suggest, that tap rooted species facilitate the root growth and thus the access to deeper soil layers for the subsequent cash crop irrespective of the soil compaction or texture. The effect was only significant for legume-brassica but not for brassica-grass variant. Hunter et al. (2021) could not observe an effect of deep soil access caused by tap rooted cover crops. The minimal tillage in the upper soil layers appears to have preserved the biopores formed by the cover crop mixtures, in contrast to the findings of Hunter et al. (2021), who employed deeper tillage machinery.

Regarding the long growing period of alfalfa, it was expected, that water extractions were largest in deep subsoil, due to deeper and thicker root channels. Early studies by Rasse and Smucker (1998) proofed the recolonization of the alfalfa root channels by 41% of maize root biomass. In this study, water uptake in the subsoil was observed at levels comparable to maize grown after fallow, with no significant ΔS detected in deep subsoil. As discussed before, the slower decomposition of alfalfa roots can create competition effects for young maize plants, potentially limiting their early-season growth (Jani et al., 2016). In addition, in deep subsoil layers, the delayed breakdown of alfalfa roots can restrict access to subsoil resources, leading to reduced water uptake and potentially lower yields.

Total averaged WU at harvest date (including the water supply by precipitation) was not significantly different for cover crop variants, which matches the results of Hunter et al. (2021) conducting a very similar trial focussed on monocultures in Pennsylvania, USA. Highest WU

was detected after legume-brassica mixture, whereby water uptake was mostly observed in deep subsoil. WU of legume-grass and brassica-grass variants were lower, matching the water conserving effect, detected in subsoil (20-110 cm). The longer growing period of the perennial cover crop, promised deeper root channels, but led to the lowest water uptake, even resulting in occasional positive ΔS due to temporary inflows (Unger and Vigil, 1998; Florence and McGuire, 2020b). ΔS of maize growing after perennial alfalfa occurred mostly in the subsoil during grain filling. In contrast to the maize after cover crop mixtures, deep subsoil ΔS remained unchanged.

4.4. Responses in Radiation and Water Use Efficiency

As variants had no effect on GAI of maize, but on maize yield, radiation use efficiency (RUE) was significantly different for the regarded cropping systems. RUE values of 3.3, 2.8, and 3.1 g MJ^{-1} for 2021, 2022, and 2023, respectively, align with the findings in literature (Andrade et al., 1993; Bukowiecki et al., 2024a). Bukowiecki et al. (2024a) obtained similar data at the same study site, as well as at additional sites in central Germany with varying growing conditions due to differences in climate and soil texture. The highest RUE values were observed for the fallow and brassica-grass variants, with 3.34 and 3.21 g MJ^{-1}, respectively. The consistently high values are likely attributable to the adequate nitrogen fertilization in the trial, as RUE generally increases with higher leaf nitrogen content (Sinclair and Horie, 1989; Muchow and Sinclair, 1994).

The differences in RUE across trial years further highlight the variability in system performance depending on climatic conditions. Water stress limits the ability of maize to convert absorbed radiation into biomass, as it limits the potential of taking up nutrients (Earl and Davis, 2003; Ullah et al., 2019). In the rather dry season of 2022, the absorbed radiation volume was very high (750.8 MJ), however RUE values were lower across all variants, with the legume-brassica mixture showing the lowest RUE (2.43 g MJ^{-1}). In contrast, in the temperate and more favourable conditions of 2021 and 2023, RUE values for maize after fallow and brassica-grass were notably higher, indicating that these systems are well-adapted.

Alfalfa revealed a significantly lower RUE compared to fallow, with averaged 2.78 g MJ^{-1}. It is important to add here that the alfalfa data set only contains two years (2022 and 2023), due to the enlarged growing period of the perennial cover crop. However, fallow variant still notes a RUE of 3.2 g MJ^{-1}, excluding 2021. Alfalfa's competitive WU especially at the beginning of the season, linked to a slower decomposition rate (Jani et al., 2016) likely induced water stress for maize in particularly in drier years, underscoring how cover crop choice impacts water availability and consequently RUE.

In general, all treatments achieved a high WUE (Fig.) compared to other studies (Bu et al., 2013; Li et al., 2021; Niu et al., 2023), probably due to the low saturation deficit at the experimental

site. Comparable WUE's for silage maize were calculated by Demir et al. (2021) with sufficient nitrogen fertilisation. The highest WUE values were recorded during the year 2023, which experienced higher precipitation levels in late summer, with an average WUE of 9.6 g l^{-1}. This indicates that the maize crop was able to take full advantage of the available water under wetter conditions, leading to more efficient WU and higher yields (Blum, 2009; Wang et al., 2021).

WUE in this study is a simplified estimation, which misses further components of the water balance formula, runoff, drainage to groundwater, upward capillary and lateral groundwater flow. These components can usually not directly measured but have to be simulated via dynamic water balance model (Li et al., 2021).

Cover crop mixtures may decrease the WUE of the succeeding crop (Blum, 2009; Wang et al., 2021), due to a better access to water resources and a consequently higher WU (Blum, 2009). The WUE of the legume-brassica variant was 6.55 g l^{-1}, significantly lower than that of the fallow variant (8.27 g l^{-1}). This was because it used the deep subsoil most effectively, achieving the highest total WU and the lowest yield (Blum, 2009). The brassica-grass mixture produced yields comparable to the fallow variant, while utilizing even less water, indicating improved WUE (8.11 g l^{-1}) closely following the fallow variant. The brassica-grass and legume-grass mixture maintained a relatively high WUE (7.61 and 7.37 g l^{-1} respectively), even under drier conditions in 2022. Li et al. (2021) utilised a system WUE, which includes evapotranspiration, drainage and runoff. In their simulations, the use of wheat cover crop in a soybean-maize rotation increased the WUE of the cropping system due to reduced drainage and evaporation. These findings would match the water conserving effects, measured in the subsoil, for maize after legume-grass and brassica grass.

5. Conclusion

This study aims to explain the varying effects of different deep-rooting cover crop mixtures and perennial alfalfa on yield formation of maize via radiation uptake and water use. The cover crop treatments did not affect total water use but the distribution of water uptake between the soil layers. Water uptake from deep subsoil was significantly higher after cover crops compared to the fallow control. The combinations of brassica-grass but also legume-grass is particularly well-suited to maintaining water use efficiency under drought stress, likely due to complementary rooting systems that optimize water uptake across different soil depths. Brassica-grass and legume-grass mixtures effectively conserved water in the subsoil, while maintaining maize yields comparable to those achieved after fallow. In contrast, the legume-brassica mixture exploited deeper subsoil water reserves the most but used the water least efficiently. Perennial alfalfa, despite its potential of forming deeper root channels due to a longer growing period, resulted in the lowest maize yield and a reduced water use efficiency. For a better understanding of these effects and the hydrological processes driving the observed patterns, crop growth models or water balance models are crucial. The simulation of soil water dynamics of specific site and climate conditions, the underlying causes of water conservation or depletion may be determined, leading to more targeted management strategies for optimizing water use and improving drought resilience in cropping systems.

References

Abdalla, M., Hastings, A., Cheng, K., Yue, Q., Chadwick, D., Espenberg, M., Truu, J., Rees, R.M., Smith, P., 2019. A critical review of the impacts of cover crops on nitrogen leaching, net greenhouse gas balance and crop productivity. Global change biology 25, 2530–2543.

Alonso-Ayuso, M., Quemada, M., Vanclooster, M., Ruiz-Ramos, M., Rodriguez, A., Gabriel, J.L., 2018. Assessing cover crop management under actual and climate change conditions. The Science of the total environment 621, 1330–1341.

Alvarez, R., Steinbach, H.S., Paepe, J.L. de, 2017. Cover crop effects on soils and subsequent crops in the pampas: A meta-analysis. Soil and Tillage Research 170, 53–65.

Andrade, F.H., Uhart, S.A., Cirilo, A., 1993. Temperature affects radiation use efficiency in maize. Field Crops Research 32, 17–25.

Basche, A.D., Kaspar, T.C., Archontoulis, S.V., Jaynes, D.B., Sauer, T.J., Parkin, T.B., Miguez, F.E., 2016. Soil water improvements with the long-term use of a winter rye cover crop. Agricultural Water Management 172, 40–50.

Blanco-Canqui, H., 2024. Do cover crop mixtures improve soil physical health more than monocultures? Plant and Soil 495, 99–112.

Blanco-Canqui, H., Ruis, S.J., 2020. Cover crop impacts on soil physical properties: A review. Soil Sci. Soc. Am. j. 84, 1527–1576.

Blum, A., 2009. Effective use of water (EUW) and not water-use efficiency (WUE) is the target of crop yield improvement under drought stress. Field Crops Research 112, 119–123.

Bretz, F., Hothorn, T., Westfall, P.H., 2011. Multiple comparisons using R. Chapman & Hall/CRC, Boca Raton.

Bu, L., Liu, J., Zhu, L., Luo, S., Chen, X., Li, S., Lee Hill, R., Zhao, Y., 2013. The effects of mulching on maize growth, yield and water use in a semi-arid region. Agricultural Water Management 123, 71–78.

Bukowiecki, J., Rose, T., Holzhauser, K., Rothardt, S., Rose, M., Komainda, M., Herrmann, A., Kage, H., 2024a. UAV-based canopy monitoring: Calibration of a multispectral sensor for green area index and nitrogen uptake across several crops. Precision Agric 28, 345.

Bukowiecki, J., Rose, T., Kage, H., 2024b. Assessment of the impact of accurate green area index, water regime and harvest index on site-specific wheat yield estimation. Computers and Electronics in Agriculture 226, 109429.

Chen, G., Weil, R.R., 2010. Penetration of cover crop roots through compacted soils. Plant Soil 331, 31–43.

Chen, G., Weil, R.R., 2011. Root growth and yield of maize as affected by soil compaction and cover crops. Soil and Tillage Research 117, 17–27.

Daryanto, S., Fu, B., Wang, L., Jacinthe, P.-A., Zhao, W., 2018. Quantitative synthesis on the ecosystem services of cover crops. Earth-Science Reviews 185, 357–373.

de Wit, C.T., 1958. Transpiration and crop yields 64.6, -. https://library.wur.nl/webquery/wurpubs/412958.

Decker, H.L., Gamble, A.V., Balkcom, K.S., Johnson, A.M., Hull, N.R., 2022. Cover crop monocultures and mixtures affect soil health indicators and crop yield in the southeast United States. Soil Sci. Soc. Am. j. 86, 1312–1326.

Demir, Z., Keçeci, M., Tunç, A.E., 2021. Effects of nitrogen fertigation on yield, quality components, water use efficiency and nitrogen use efficiency of silage maize (Zea Mays L.) as the second crop. Journal of Plant Nutrition 44, 373–394.

Deutscher Wetterdienst, 2024. Wetter und Klima - Deutscher Wetterdienst: Kiel-Kronshagen (2565). https://opendata.dwd.de/climate_environment/CDC/observations_germany/climate/multi_annual/mean_91-20/. Accessed 30 September 2024.

Duncan, W.G., 1971. Leaf Angles, Leaf Area, and Canopy Photosynthesis. Crop Science 11, 482–485.

Earl, H.J., Davis, R.F., 2003. Effect of Drought Stress on Leaf and Whole Canopy Radiation Use Efficiency and Yield of Maize. Agronomy Journal 95, 688–696.

Florence, A.M., McGuire, A.M., 2020. Do diverse cover crop mixtures perform better than monocultures? A systematic review. Agronomy Journal 112, 3513–3534.

Hothorn, T., Bretz, F., Westfall, P., 2008. Simultaneous inference in general parametric models. Biometrical journal. Biometrische Zeitschrift 50, 346–363.

Hunter, M.C., Kemanian, A.R., Mortensen, D.A., 2021. Cover crop effects on maize drought stress and yield. Agriculture, Ecosystems & Environment 311, 107294.

Jani, A.D., Grossman, J., Smyth, T.J., Hu, S., 2016. Winter legume cover-crop root decomposition and N release dynamics under disking and roller-crimping termination approaches. Renew. Agric. Food Syst. 31, 214–229.

Kaye, J.P., Quemada, M., 2017. Using cover crops to mitigate and adapt to climate change. A review. Agron. Sustain. Dev. 37, 1–17.

Kemper, R., Bublitz, T.A., Müller, P., Kautz, T., Döring, T.F., Athmann, M., 2020. Vertical Root Distribution of Different Cover Crops Determined with the Profile Wall Method. Agriculture 10, 503.

Kijne, J.W., Barker, R., Molden, D.J., 2003. Water productivity in agriculture: Limits and opportunities for improvement. CABI Publishing In association with the International Water Management Institute, Wallingford, 332 pp.

Kristensen, H.L., Thorup-Kristensen, K., 2004. Root Growth and Nitrate Uptake of Three Different Catch Crops in Deep Soil Layers. Soil Sci. Soc. Am. j. 68, 529–537.

Kühling, I., Mikuszies, P., Helfrich, M., Flessa, H., Schlathölter, M., Sieling, K., Kage, H., 2023. Effects of winter cover crops from different functional groups on soil-plant nitrogen dynamics and silage maize yield. European Journal of Agronomy 148, 126878.

Lemaire, G., van Oosterom, E., Jeuffroy, M.-H., Gastal, F., Massignam, A., 2008. Crop species present different qualitative types of response to N deficiency during their vegetative growth. Field Crops Research 105, 253–265.

Li, Y., Di Tian, Feng, G., Yang, W., Feng, L., 2021. Climate change and cover crop effects on water use efficiency of a corn-soybean rotation system. Agricultural Water Management 255, 107042.

Marcillo, G.S., Miguez, F.E., 2017. Corn yield response to winter cover crops: An updated meta-analysis. Journal of Soil and Water Conservation 72, 226–239.

Massignam, A.M., Chapman, S.C., Hammer, G.L., Fukai, S., 2011. Effects of nitrogen supply on canopy development of maize and sunflower. Crop Pasture Sci. 62, 1045.

Monsi, M., 1953. The light factor in plant communities and its significance for dry matter production. Japanese Journal of Botany 14, 22.

Monteith, J.L., 1977. Climate and the efficiency of crop production in Britain. Phil. Trans. R. Soc. Lond. B 281, 277–294.

Muchow, R.C., Sinclair, T.R., 1994. Nitrogen Response of Leaf Photosynthesis and Canopy Radiation Use Efficiency in Field-Grown Maize and Sorghum. Crop Science 34, 721–727.

Niu, L., Qin, W., You, Y., Mo, Q., Pan, J., Tian, L., Xu, G., Chen, C., Li, Z., 2023. Effects of precipitation variability and conservation tillage on soil moisture, yield and quality of silage maize. Front. Sustain. Food Syst. 7.

Pinheiro, J.C., Bates, D.M. (Eds.), 2010. Mixed-effects models in S and S-PLUS, 2000th ed. Springer, New York, Berlin, Heidelberg, 528 pp.

Puget, P., Drinkwater, L.E., 2001. Short-Term Dynamics of Root- and Shoot-Derived Carbon from a Leguminous Green Manure. Soil Science Soc of Amer J 65, 771–779.

Qin, Z., Guan, K., Zhou, W., Peng, B., Villamil, M.B., Jin, Z., Tang, J., Grant, R., Gentry, L., Margenot, A.J., Bollero, G., Li, Z., 2021. Assessing the impacts of cover crops on maize and soybean yield in the U.S. Midwestern agroecosystems. Field Crops Research 273, 108264.

R Core Team, 2024. R: A language and environment for statistical computing. R foundation for statistical computing, Vienna, Austria.

Rasse, D.P., Smucker, A.J., 1998. Root recolonization of previous root channels in corn and alfalfa rotations. Plant and Soil 204, 203–212.

Saleem, M., Pervaiz, Z.H., Contreras, J., Lindenberger, J.H., Hupp, B.M., Chen, D., Zhang, Q., Wang, C., Iqbal, J., Twigg, P., 2020. Cover crop diversity improves multiple soil properties via altering root architectural traits. Rhizosphere 16, 100248.

Sinclair, T.R., Horie, T., 1989. Leaf Nitrogen, Photosynthesis, and Crop Radiation Use Efficiency: A Review. Crop Science 29, 90–98.

Stipešević, B., Kladivko, E.J., 2005. Effects of winter wheat cover crop desiccation times on soil moisture, temperature and early maize growth. Plant Soil Environ. 51, 255–261.

Szeicz, G., 1974. Solar-radiation for plant-growth. Journal of Applied Ecology 11.

Tanner, C.B., 1981. Transpiration Efficiency of Potato 1. Agronomy Journal 73, 59–64.

Teixeira, E.I., George, M., Herreman, T., Brown, H., Fletcher, A., Chakwizira, E., Ruiter, J. de, Maley, S., Noble, A., 2014. The impact of water and nitrogen limitation on maize biomass and resource-use efficiencies for radiation, water and nitrogen. Field Crops Research 168, 109–118.

Tilman, D., 2013. Functional Diversity. In: Levin, S.A. (Ed.) Encyclopedia of biodiversity, 2nd ed. Academic Press, Amsterdam, pp. 587–596.

Tonitto, C., David, M.B., Drinkwater, L.E., 2006. Replacing bare fallows with cover crops in fertilizer-intensive cropping systems: A meta-analysis of crop yield and N dynamics. Agriculture, Ecosystems & Environment 112, 58–72.

Ullah, H., Santiago-Arenas, R., Ferdous, Z., Attia, A., Datta, A., 2019. Improving water use efficiency, nitrogen use efficiency, and radiation use efficiency in field crops under drought stress: A review. In: ADVANCES IN AGRONOMY, vol. 156. ELSEVIER ACADEMIC Press, [Place of publication not identified], pp. 109–157.

Unger, P.W., Vigil, M.F., 1998. Cover crop effects on soil water relationships. Journal of Soil and Water Conservation 53, 200–207.

Villamil, M.B., Bollero, G.A., Darmody, R.G., Simmons, F.W., Bullock, D.G., 2006. No-Till Corn/Soybean Systems Including Winter Cover Crops. Soil Sci. Soc. Am. j. 70, 1936–1944.

Wang, J., Zhang, S., Sainju, U.M., Ghimire, R., Zhao, F., 2021. A meta-analysis on cover crop impact on soil water storage, succeeding crop yield, and water-use efficiency. Agricultural Water Management 256, 107085.

Williams, S.M., Weil, R.R., 2004. Crop Cover Root Channels May Alleviate Soil Compaction Effects on Soybean Crop. Soil Sci. Soc. Am. j. 68, 1403–1409.

Chapter 4

Estimation of biomass and N uptake in different winter cover crops from UAV-based multispectral canopy reflectance data

---

Katja Holzhauser*, Thomas Räbiger, Till Rose, Henning Kage, Insa Kühling

Institute of Crop Science and Plant Breeding, Agronomy and Crop Science, Kiel University, Germany

* Corresponding author.: holzhauser@pflanzenbau.uni-kiel.de (Katja Holzhauser)

Keywords: remote sensing, Parrot Sequoia, catch crops, sensor calibration, pure and mixed canopies

Published: 10. September 2022 (*Remote Sensing)*

Abstract

Cover crops are known to provide beneficial effects to agricultural systems such as reduction of nitrate leaching, erosion control and increase of soil organic matter. Monitoring of cover crops growth (e.g. green area index (GAI), nitrogen (N) uptake or dry matter (DM)) using remote sensing techniques allows to identify the physiological processes and to optimise management decisions. Based on data of a two-year trial (2018, 2019) in Kiel, Northern Germany, the multispectral sensor Sequoia (Parrot) was calibrated to selected parameters of the winter cover crops oilseed radish, saia oat, spring vetch and winter rye as sole cover crops and combined in mixtures. Two simple ratios (SR_{red}, $SR_{red\ edge}$) and two normalized difference indices (ND_{red}, $ND_{red\ edge}$) were calculated and tested for their predicting power. Furthermore, the advantage of species/mixture-individual compared to universal models was analysed. SR_{red} best predicted GAI, DM and N uptake (R^2: 0.60, 0.53, 0.45, respectively) in a universal model approach. Canopy parameters of saia oat and spring vetch were rather estimated by species-individual models, achieving higher R^2 than with the universal model. Comparing mixture-individual models to universal model revealed low relative error differences below 3%. Findings of the current study serve as a tool for rapid and inexpensive estimation of cover crops canopy parameters that determine environmental services.

1. Introduction

Cover crops gained in importance during the last decade, as they provide ecosystem services such as reduction of nitrate leaching, erosion control and increase of soil organic matter (SOM) (Blanco-Canqui et al., 2011; Abdalla et al., 2019; Nouri et al., 2022). Implementing incentives for growing winter cover crops within the common agricultural policy of the European union encouraged the widespread cultivation (European Commission, 2017). Closing the nitrogen (N) cycle of arable cropping systems is one of the most relevant advantages of cover crops under European conditions. By storing N in the above- and below-ground biomass over winter months, cover crops prevent N leaching losses Thorup-Kristensen et al., 2003; Tonitto et al., 2006; Abdalla et al., 2019; Böldt et al., 2021; Vogeler et al., 2022. A recent meta-analysis estimates a global reduction of N leaching by 69% across all species compared to fallow (Nouri et al., 2022). After termination, N from cover crop biomass might be supplied to succeeding spring cash crops, i.e. maize. The amount of additional N supply to subsequent crops strongly depends on total N amount, the chemical composition (C/N ratio) and on the duration for decomposition and the resulting mineralisation/immobilisation of N (Vogeler et al., 2022). For cover crop residues with wide C/N ratios subsequent N supply can be delayed or reduced (Thorup-Kristensen et al., 2003; Holmes et al., 2019). Recently cover crop established as species mixtures attained a higher recognition in order to reach higher diversity in agricultural land and to combine different functional traits in a beneficial way(Tosti et al., 2014; Florence and McGuire, 2020a).

The application of remote sensing techniques in agricultural science and practice is becoming increasingly important. Monitoring of canopy characteristics such as green area index (GAI), N uptake or dry matter (DM) accumulation during the vegetation period is of major interest to understand physiological processes and to further derive management decisions. Many approaches have been developed for yield prediction, phenotyping, land use monitoring or to estimate further derived ecosystem services (Hively et al., 2009; Hankerson et al., 2012; Bukowiecki et al., 2019; Weiss et al., 2020). Spectral data are either provided by earth orbiting satellites such as Landsat or Sentinel (Clevers and Gitelson, 2013), or can be assessed with multispectral or hyperspectral sensors from handheld devices (Tucker et al., 1981; Gitelson et al., 2003) or mounted on an unmanned airborne vehicle (UAV) (Bukowiecki et al., 2019). Reflectance behaviour of cash crops, such as maize, soybean or wheat have been studied well within the last decades, e.g. by Gitelson (2003; 2004; 2005) and Bukowiecki et al. (2019). However, few authors studied cover crops using satellite imagery, to determine the current growing area and biomass accumulation of cover crops on a large scale (Hively et al., 2015; Goffart et al., 2021). Hively et al. (2009) evaluated the N uptake of cover crops combining on-

field destructive plant sampling with hyperspectral measurements and satellite image analysis. (2015) found a linear relationship between normalized difference vegetation index ($ND_{red,}$ commonly known as NDVI) and percent groundcover of six winter cover crop species at the east coast of the United States using a handheld multispectral radiometer. But so far, there was no study to our knowledge estimating canopy parameters of cover crops on higher resolution using UAV-based multispectral sensors.

The GAI is a canopy parameter directly correlated with chlorophyll amount and consequently can be derived by spectral reflectance of specific wavelengths. Successful estimates of GAI by remote sensing techniques were achieved for example by Kira et al. (2016) for maize and soybean using hyperspectral data and by Bukowiecki et al. (2019) for wheat with UAV-based multispectral data. Further parameters such as DM and N uptake are stated as "secondary variables" by Weiss et al.. Compared to the "primary variable" GAI or fraction of photosynthetically active radiation (FPAR), these are not directly correlated to spectral reflectance. Weiss et al. (2020) recommend the estimation of "secondary variables", based on knowledge about the physiological dynamics in relation to "primary variables". However, other authors estimated further canopy parameters empirically just like "primary" ones. For example, Tucker et al. achieved an R^2 of 0.86 deriving biomass of winter wheat directly from spectral reflectance data using a handheld radiometer.

Canopy reflectance within the spectrum of visual light is the response of the chlorophyll content of leaves. More precisely, green light is reflected by the leaves while red light is absorbed by the chloroplasts used for photosynthesis, hence informative about chlorophyll abundance of the canopy (Curran, 1989; Elvidge, 2007). Within near infrared (NIR) wavelengths, reflection reaches higher ranges and delivers structural information about the canopy (leaf angle, thickness, canopy architecture) (Viña et al., 2011; Kira et al., 2016). Another interesting area of wavelengths within the photosynthetic spectrum is the red edge (RE) band, which records the maximum slope in the reflectance spectra and is sensitive to the chlorophyll content of a plant (Gitelson et al., 2005; Delegido et al., 2013). A widespread approach to combine these informative bands and further gain the contrast of reflection in NIR and absorption in red, is the computation of a vegetation index (VI) (Myneni et al., 1995). Most common indices are the normalised difference vegetation index (ND_{red}, Rouse et al. (1974)) and the simple ratio (Jordan, 1969) based on red light and NIR reflection. Both VIs can be modified replacing red light reflectance with the reflection at RE to gain in precision (Viña et al., 2011; Kira et al., 2016).

Different canopies show variable reflectance behaviour, hence the estimations by species-individual models tend to be more precise, than a universal models (Viña et al., 2011). Another

challenging aspect is the common strategy to cultivate cover crops as mixtures of several species for increasing environmental services in the agricultural system (Chapagain et al., 2020). Due to the expected heterogenous spectral response from different species as well as from different mixtures, a comprehensive comparison of universal and individual models seems necessary for winter cover crops. Another challenge is the season in which cover crops are grown. Due to flat sun angles, radiation incidence is reduced in late autumn and winter months, especially in higher latitudes (Assmann et al., 2019).

The objective of this study was the calibration of the multispectral sensor Sequoia (Parrot) for canopy parameters of pure stands and mixtures of winter cover crops grown in Northern Germany. Therefore, four different VIs (SR_{red}, $SR_{red\ edge}$, ND_{red}, $ND_{red\ edge}$) were tested for the best regression with each cover crop's GAI, DM and N uptake, either as universal or as species- and mixture-individual approach.

2. Material and Methods

2.1. Study site

The study site was located in Northern Germany at the Hohenschulen experimental farm of the Kiel University (10.0 E, 54.3 M, 30 m a.s.l.). Glacial influence led to small scale heterogeneity of soil types. Main soil type is defined as Luvisol with a sandy loam texture in the top soil. The temperate oceanic climate in the study area is characterised by long-term average (1991-2020) mean annual air temperature of 9.3 °C and annual mean precipitation of 797 mm (Deutscher Wetterdienst, 2024).

2.2. Trial designs

Data collection was carried out in two trials (A and B) in 2018 and 2019 with winter cover crops from different functional groups (Table 6). From trial A we used 16 randomised plots with four sole cover crops grown after winter oilseed rape. All cover crop treatments of trial A were unfertilized. Trial B was performed in 32 strips with four cover crops as sole stands and four cover crop mixtures. Variations in biomass growth were achieved by implementing two sowing dates and two different nitrogen levels (with and without N fertilisation, N-level adapted according to sowing date, Table 7). Cover crop mixtures sown in Trial B were all possible combinations of the non-winterhardy species: OR-SO (oilseed radish, saia oats), OR-SV (oilseed radish, spring vetch), SO-SV (saia oat, spring vetch) and OR-SO-SV (oilseed radish, saia oat, common vetch) (Table 6). Winterhardy rye was not included in the mixture combinations.

Table 6 Winter cover crops investigated in this study.

Cover crop	Oilseed radish	Saia oat	Spring vetch	Winter rye
Botanical name	*Raphanus sativus*	*Avena strigosa*	*Vicia sativa*	*Secale cereale*
Family	Brassicaceae	Poaceae	Leguminosae	Poaceae
Abbreviation	OR	SO	SV	WR
Winterhardiness	no	no	no	yes

Table 7 Trial design, sowing dates and N-level of Trial A and B.

Trial	Sowing date	Nitrogen levels (kg N ha^{-1}) (abbreviated as)
Trial A	20.08.2018 23.08.2019	0 (0N)
Trial B	17.08.2018	0 (0N); 60 (60N)
	03.09.2018	0 (0N); 40 (40N)
	24.08.2019	0 (0N); 60 (60N)
	10.09.2019	0 (0N); 40 (40N)

2.3. Reflectance Measurements

Spectral data was collected biweekly with the multispectral camera Sequoia (Parrot), mounted to the eBee-X or eBee-SQ drone. The Sequoia (Parrot) camera comprises four spectral bands covering the wavelength ranges of green (550 nm) and red light (660 nm), red edge (RE, 735 nm), near infrared (NIR, 790 nm). The reflection bands have a bandwidth of 40 nm, except of RE with 10 nm. Radiometric calibration was done by a grey scale target, photographed by the camera before each flight. A light sensor on top of the Sequoia (Parrot) camera measured the incoming radiation. Especially with poorer light conditions coming up in autumn and winter season, those values for incoming radiation became more important for corrections during postprocessing. Flight routes were planned with the software eMotion3 from senseFly. Pixel size was set as 8 cm x 8 cm pixel^{-1}. After each flight, the images recorded with the Sequoia sensor were processed with eMotion3 and Pix4Dmapper software (Pix4D SA., Switzerland). With Pix4Dmapper, recorded images were processed to orthogonal reflection maps for each reflectance-band. Recording an additional image after sampling provided the location and area of the harvested biomass in each plot. Reflectance of the regarded sampling areas was extracted, using QGIS (version 3.22.7) and R 4.0.4 (R Core Team, 2024), using „raster" (Hijmans, 2022) . To avoid bias due to pixels containing soil or shadow, the median of the extracted pixels served as a representative value (Bukowiecki 2020).

2.4. Plant sampling

Within two days after each UAV-flight, destructive plant samplings were made. The parameters green area index (GAI, cm² cm^{-2}), dry matter (DM, g m^{-2}), and N concentration of DM (%) were determined. Therefore, in each plot, 0.5 m² plant material was dug out of the soil. Roots were cut of afterwards, to ensure that the complete above-ground biomass was included in the sample. Remaining biomass was fractionated in green plant material of cover crops, weeds and senescent plant material. Weeds were dominated by plants of voluntary oilseed rape. Senescent material was defined as yellow or brown biomass, which was not photosynthetically active. GAI of the green vegetation (cover crop and weed fraction) was measured by the LI-3100C Area Meter (LI-COR Inc., NE, USA). The sampled biomass of all fractions was oven-dried at 60 °C for five days and weighted subsequently. N concentration of all fractions was assessed with a CN-Analyser (TruMac CN, LECO) and converted to N uptake g m^{-2} of the regarded DM.

2.5. Statistical Analysis

All calculations were done in R (Version 4.0.4, R Core Team, 2021). For canopy parameter prediction, simple ratios (SR) and normalised difference indices (ND) were calculated, combining the spectral bands red and NIR according to *Table 8*.

Table 8 Description of vegetation indices investigated in this study with spectral bands used for calculation (NIR: near infrared, RE: red edge, red: red).

Vegetation index	Abbreviation	Formula	Reference
Simple ratio	SR_{red}	$\frac{NIR}{red}$	Jordan, 1969
Simple ratio red edge	$SR_{red\ edge}$	$\frac{NIR}{RE}$	Sims and Gamon, 2002
Normalised difference vegetation index	ND_{red}	$\frac{NIR - red}{NIR + red}$	Rouse et al., 1974
Red edge normalised difference vegetation index	$ND_{red\ edge}$	$\frac{NIR - RE}{NIR + RE}$	Dong et al., 2015, Gitelson and Merzlyak, 1996

Red: 660 nm; RE: 735 nm; NIR: 790 nm

After selection of the best suitable VI, different model approaches were compared (Figure 13). Measured input data for the canopy parameters referred to the green vegetation. Senescent biomass was excluded, as it showed low spectral response (Prabhakara et al., 2015).One approach was the estimation of cover crop canopy parameters by a universal model (n = 248). Therefore, the best performing vegetation index was correlated with the measured canopy parameters (GAI, DM, N), across all cover crop species. Furthermore, models were generated for each cover crop separately, referred to as species-individual models (n = 65 (OR), n = 53 (SO), n = 65 (SV), n = 65 (WR)).

For mixed stands, the two model approaches were tested as well. First assumption was the calibration of mixture models similar to the species-individual calibration, referred to as mixture-combination model. Secondly, the universal model based on the sole cover crops was applied to the mixture data set. Data set for cover crop mixtures was restricted to DM and N uptake in 2018 (n = 27 for each cover crop mixture). Relative mean absolute error (rMAE) and R^2 were used to assess error of prediction and for performance comparison the VI-models.

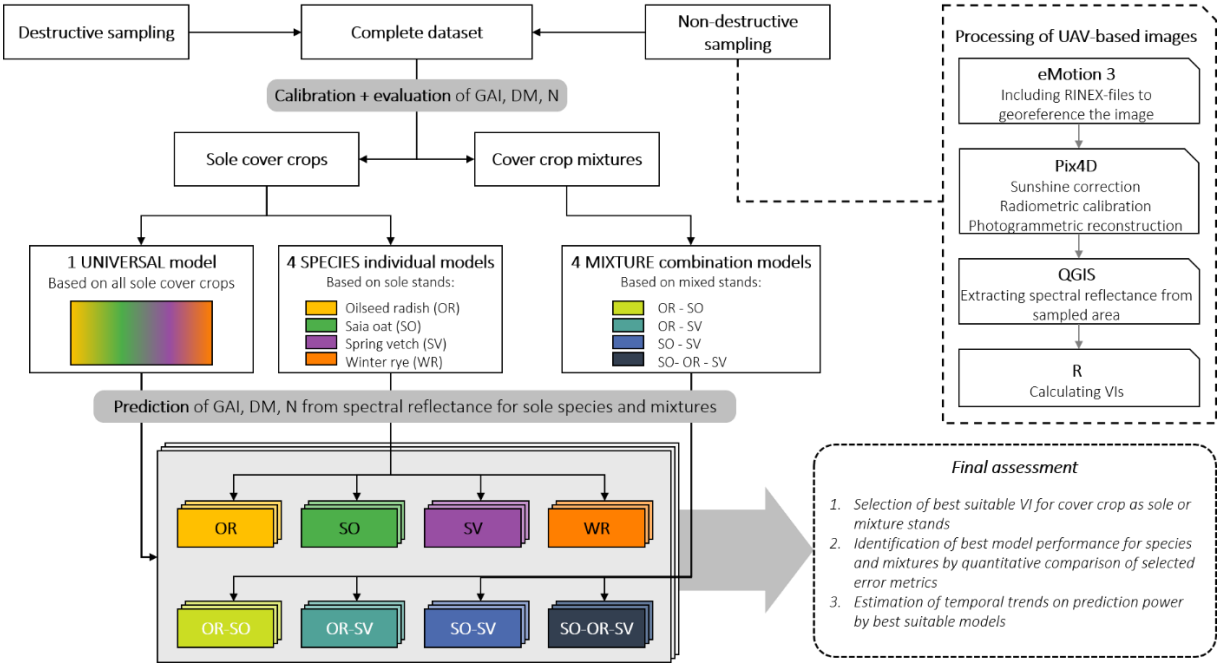

Figure 13: Workflow of the drone-based non-destructive sampling, model calibrations (universal, species- and mixture-individual model) and the prediction possibilities of green area index (GAI), dry matter (DM) and N-uptake (N) of the respected species or mixtures.

3. Results

3.1. Weather conditions

Measured temperature during the observation period ranged from 30 to -1.1 °C in 2018 and 32.1 to -1.3°C in 2019. Frost events (< 0 °C) were documented at 28.11.2018 (-1.1 °C), 31.10.2019 (-1.3 °C) and 01.11.2019 (-0.1 °C). Cumulative PAR saturated towards winter in both years, and reached a sum of 402.9 W m^{-2} in 2018 and 332.7 W m^{-2} in 2019 (Figure 14).

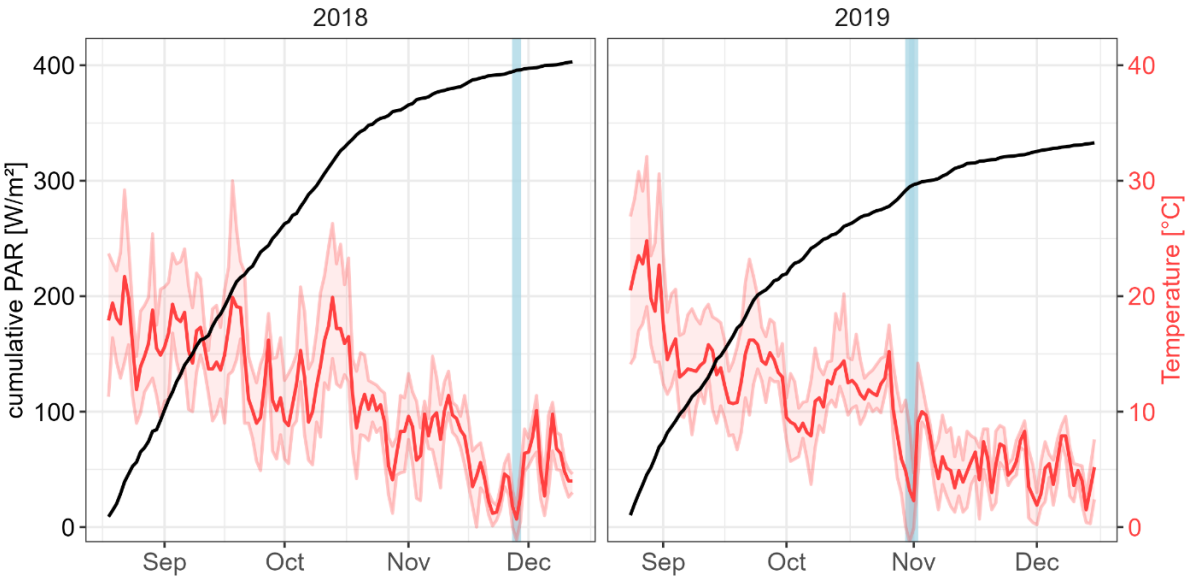

Figure 14: Cumulative photosynthetic active radiation (PAR) (W m^{-2}) (black) and averaged temperature (°C) per day (red) during vegetation periods in 2018 and 2019. Light red area presents the range from minimal and maximal temperature (°C) per day. Frost events are illustrated by a blue vertical line (28.11.2018, 31.10.2019, 01.11.2019).

3.2. Cover crop DM accumulation

Crop growth within the plots turned out to be heterogenous. Biomass varied strongly with each sampling date. After frost events GAI, DM and N uptake decreased or saturated. In 2019, frost events occurred earlier in the season, reducing living biomass even more clearly, especially for SV. Data for cover crop mixtures was restricted to DM g m^{-2} and N uptake g m^{-2} in 2018 (Figure 15).

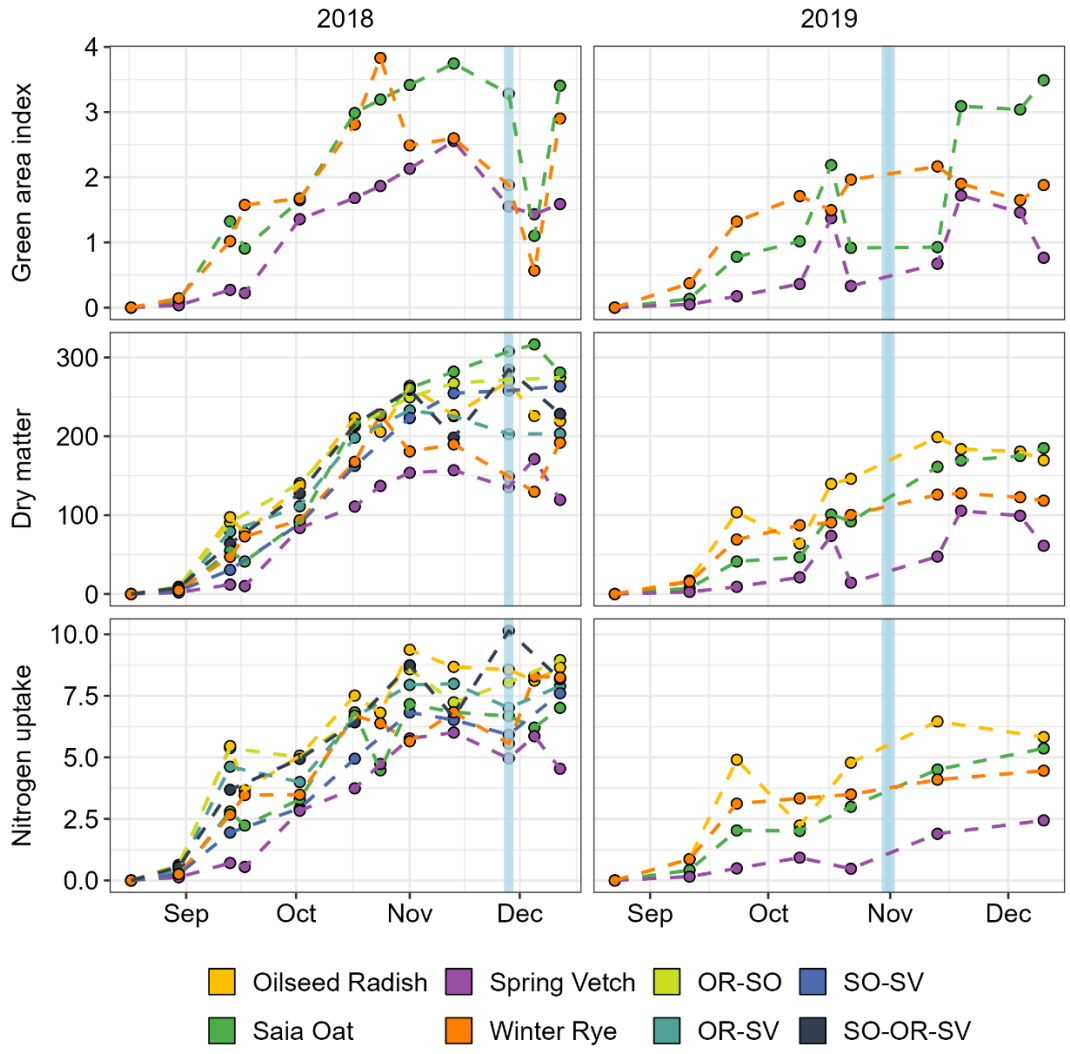

Figure 15: Biomass establishment of sole cover crops and mixtures (OR: oilseed radish, SO: saia oat, SV: spring vetch) presented by green area index (GAI), dry matter (DM) (g m^{-2}) and Nitrogen uptake (g m^{-2}). Blue vertical lines highlight frost events (28.11.2018, 31.10.2019, 01.11.2019). Point: Sampling date, dashed line: linear interpolation between sampling dates.

Senescent biomass increased towards winter month. Highest proportion occurred in WR with 45.7% after a frost event in November 2018. In general, the proportion of senescent plant material was <20% in 2018 and <10% - with little exception of OR – in 2019. SV showed little to none proportions of senescence for both years.

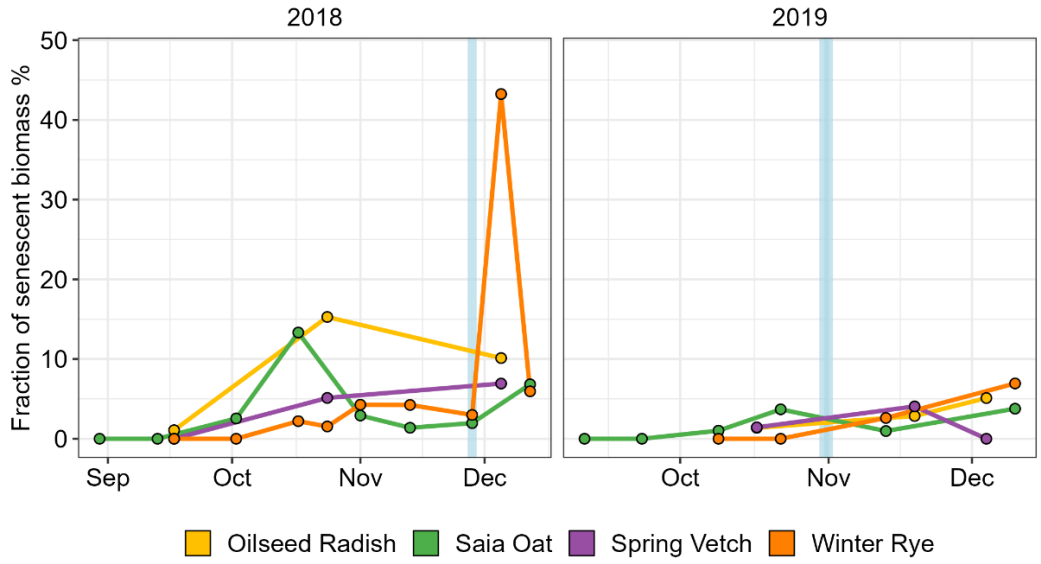

Figure 16: Fraction of senescent biomass (%) in total sampled biomass during the vegetation periods of cover crops in 2018 and 2019. Blue vertical lines highlight frost events (28.11.2018, 31.10.2019, 01.11.2019).

3.3. Universal calibration

Linear models were established for predicting the parameters GAI, DM and N uptake of all sole cover crops together by four VIs (SR_{red}, $SR_{red\ edge}$, ND_{red} and $ND_{red\ edge}$). Regarding rMAE and R^2, the universal calibration using SR_{red} to predict GAI performed best (Figure 17). Furthermore, SR_{red} estimated DM and N uptake more precisely than the other VIs (Table 9). ND_{red}-models assessed a moderate error but saturated at GAI-values >2 (Figure 17). This also applied for DM g m^{-2} and N uptake g m^{-2} (Table 9). Within lower GAI ranges, the ND_{red} estimated negative values (Figure 17). VIs using the RE-band, as $ND_{red\ edge}$ and $SR_{red\ edge}$, showed higher rMAE compared to their red-based counterparts. Performance of RE-based VIs was almost similar for all regarded canopy parameters (Table 9). Towards later time of the year, values of rMAE increased while R^2 decreased (Figure 18) indicating less reliability. Coincidently, proportion of senescent biomass increased during the vegetation period (Figure 16). Winter rye reached the highest amount of senescent biomass in December.

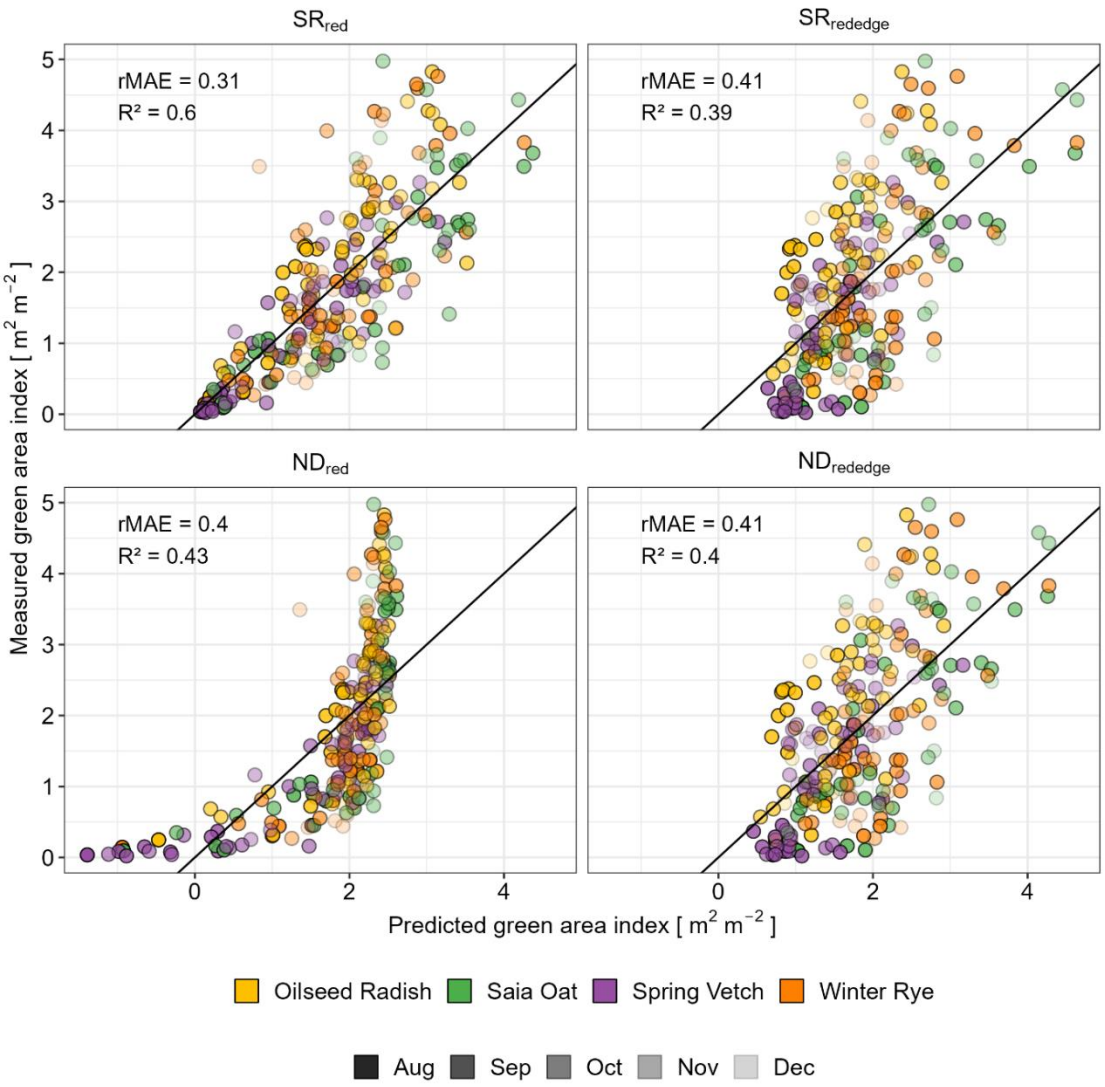

Figure 17 Universal models differing in vegetation indices (Simple Ratio (SR_{red}, $SR_{red\ edge}$,), and normalised difference vegetation indices (ND_{red}, $ND_{red\ edge}$) for estimation of green area index (GAI). Model performance was assessed with relative, mean absolute error (rMAE) (%) and R^2.

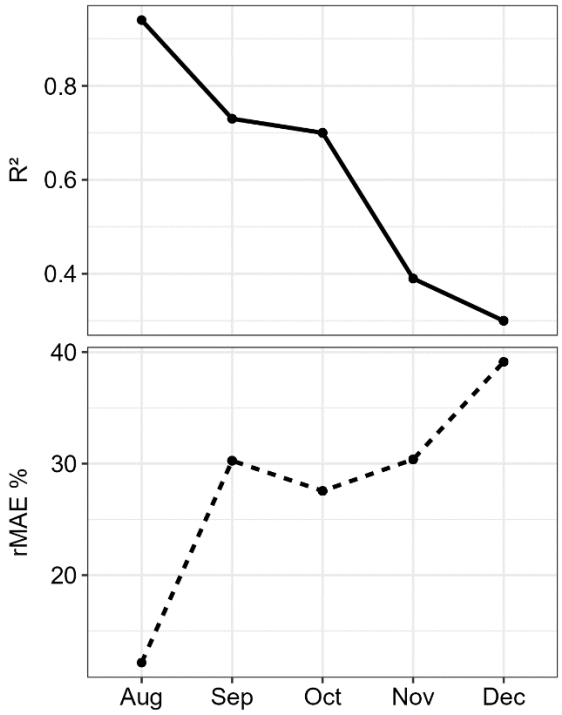

Figure 18: Values of R² and relative mean absolute error (rMAE) (%) of the universal SR_{red}-model predicting green area index (GAI) over growth period of cover crops.

Table 9 Universal models for predicting canopy parameters (green area index (GAI), dry matter (DM) (g m^{-2}) and N uptake (N) (g m^{-2})) of cover crops. For each parameter, four vegetation indices (VIs) (SR_{red}, $SR_{red\ edge}$, ND_{red}, $ND_{red\ edge}$) were tested. Model performance is assessed by relative mean absolute error (rMAE) (%) and R² of the corresponding VI.

Parameter	VI	Equation	rMAE	R²
Green area index	SR_{red}	-0.21 + 0.19 x	31.34	0.60
	$SR_{red\ edge}$	-4.46 + 4.75 x	41.46	0.39
	ND_{red}	-2.46 + 5.51 x	39.91	0.43
	$ND_{red\ edge}$	-0.05 + 13.74 x	40.93	0.40
Dry matter	SR_{red}	-18.51 + 14.56 x	50.37	0.53
	$SR_{red\ edge}$	-361.79 + 377.76 x	63.38	0.36
	ND_{red}	-204.94 + 441.53 x	61.81	0.41
	$ND_{red\ edge}$	-10.66 + 1097.02 x	62.67	0.37
Nitrogen uptake	SR_{red}	0.43 + 0.4 x	35.88	0.45
	$SR_{red\ edge}$	-8.1 + 9.72 x	43.83	0.26
	ND_{red}	-5.72 + 13.6 x	38.91	0.43
	$ND_{red\ edge}$	0.88 + 28.68 x	43.37	0.27

3.4. Species-individual calibration

For each individual cover crop, linear models for all regarded canopy parameters, with the generically best performing VI SR_{red} were established. In general, best results of the species-individual models were achieved for GAI prediction with R^2 of 0.76, 0.63, 0.57 and 0.51 for SV, SO, OR and WR, respectively (Figure 19). Lowest rMAE (25.87 %) were calculated for GAI prediction of SV. Prediction of DM and N uptake were less accurate than GAI (Figure 19). Calibration of SV outperformed the other species by an average lower rMAE of 3.68 % and a higher R^2 for all canopy parameters. Lowest accuracy was found for prediction in WR across all canopy parameters. Comparing species-individual with universal model outputs by rMAE, predictions for all cover crops except of WR were better using the species-individual models (Figure 20, Table 10). With minor differences, WR's DM and N uptake was rather predicted by universal model. In general, differences of rMAE for GAI prediction were small (OR: 1.49 %; SO: 2.50 %; SV: 2.63 %; WR: -0.63 %). Comparison for DM prediction resulted in larger differences in favour for species individual models, especially for SV and WR (32.93 % and 14.45 %, respectively) (Table 9, Figure 19).

Table 10 Comparison of the two model approaches prediction performance (species-individual vs. universal models) for green area index (GAI), dry matter (DM) and N uptake (N) by relative mean absolute error (rMAE) (%) for each cover crop (oilseed radish, saia oat, spring vetch, winter rye), separately.

		rMAE %	
Parameter	Species	species-individual	universal
Green area index	Oilseed Radish	26.91	28.4
	Saia Oat	30.16	32.66
	Spring Vetch	25.87	28.5
	Winter Rye	36.11	35.48
Dry matter	Oilseed Radish	32.28	33.26
	Saia Oat	35.49	45.18
	Spring Vetch	31.18	64.11
	Winter Rye	36.6	51.05
Nitrogen uptake	Oilseed Radish	31.3	33.79
	Saia Oat	28.39	38.27
	Spring Vetch	31.25	39.1
	Winter Rye	36.86	34.47

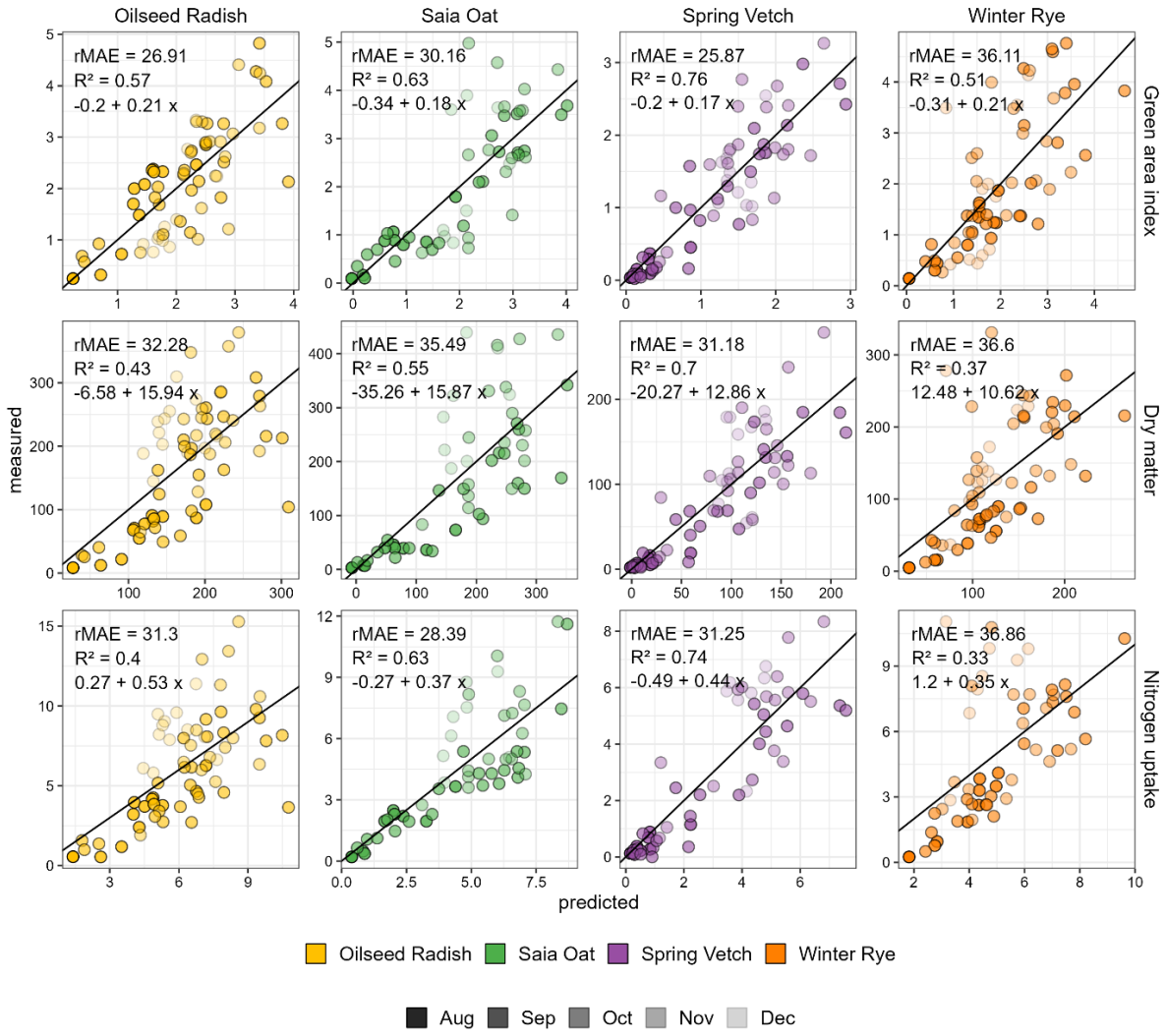

Figure 19: Species-individual models using SR_{red} for estimation of green area index (GAI), dry matter (DM) (g m^{-2}) and N uptake (g m^{-2}). Model performance was assessed with R^2 and the relative mean absolute error (rMAE) (%). Calibration formula is noted for each species and each canopy parameter.

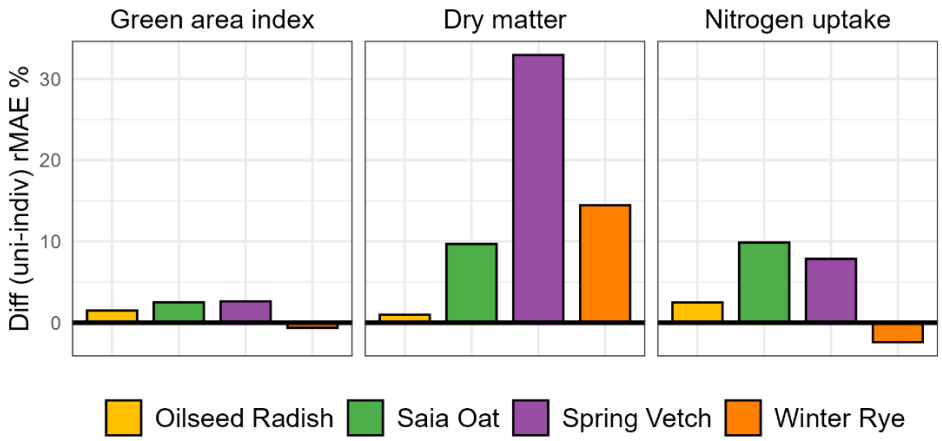

Figure 20 Comparison of the two model approaches prediction performance for green area index (GAI), dry matter (DM) and N uptake (N) by relative mean absolute error (rMAE) (%). Illustrated is the difference (Diff) of the universal model (uni) calibrated with the sole cover crop data set and species-individual models (indiv) of each cover crop (oilseed radish, saia oat, spring vetch, winter rye), separately.

3.5. Mixture calibration

In order to predict N uptake g m^{-2} of cover crop mixtures, two model approaches were compared. Mixture-individual model was related to the spectral reflectance of each cover crop mixtures (Figure 13). Second approach was the estimation by the universal model, generated with the sole cover crops (OR, SO, WR, SV) based on SR_{red} (Figure 13, Table 6). As shown in Figure 21 both, the mixture-individual and universal models did not differ in their performance of estimating DM g m^{-2} and N uptake g m^{-2} for mixtures, with relative error differences below 3%. DM g m^{-2} of OR-SO and SO-SV were rather preferably predicted with the mixture-individual model due to a higher rMAE of the universal model prediction. For N uptake g m^{-2} estimation for OR-SV, SO-SV and SO-OR-SV by mixture-individual models were more precise, while N uptake g m^{-2} for OR-SO was rather predicted by universal model. According to R^2 best estimation for DM and N was achieved by the three-component mixture (SO-OR-SV) with 0.5 and 0.44, respectively (Table 11).

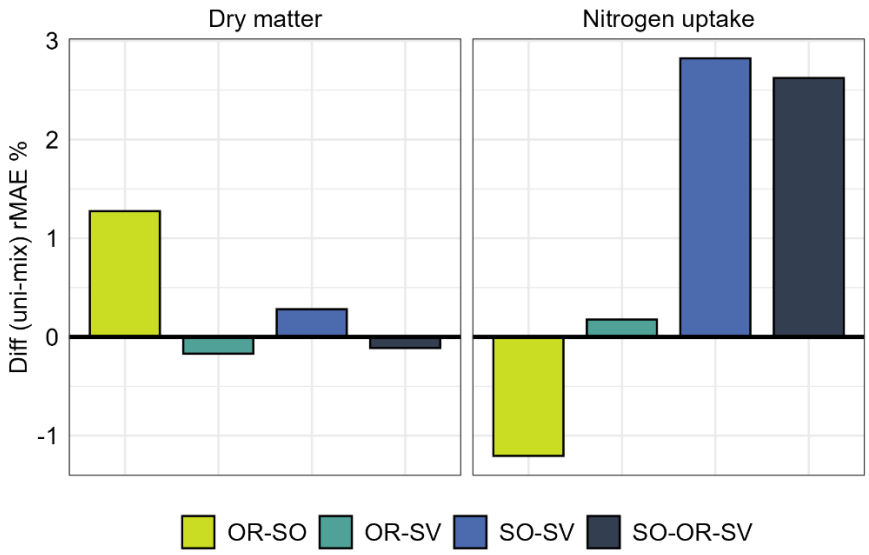

Figure 21: Comparison of the two model approaches prediction performance for dry matter (DM) and N uptake (N) by relative mean absolute error (rMAE) (%). Illustrated is the difference (Diff) of the universal model (uni) calibrated with the sole cover crop data set and mixture-individual models (mix) of each cover crop mixture (OR: oilseed radish, SO: saia oat, SV:spring vetch), separately.

Table 11 Mixture-individual models based on SRred for predicting canopy parameters (dry matter (DM) (g m-2) and N uptake (N) (g m-2)) of cover crop mixtures (OR: oilseed radish, SO: saia oat, SV: spring vetch). Model performance was assessed the relative mean absolute error (rMAE) (%) and R^2. Calibration formula is noted for each mixture and each canopy parameter.

Parameter	Mixture	Equation	rMAE	R^2
Dry matter	OR-SO	-5.18 + 15.51 x	30.71	0.3
	OR-SV	-19.56 + 15.23 x	29.18	0.37
	SO-SV	-3.78 + 13.15 x	49.04	0.25
	SO-OR-SV	-46.26 + 17.42 x	30.3	0.5
Nitrogen uptake	OR-SO	1.68 + 0.37 x	27.00	0.25
	OR-SV	1.53 + 0.38 x	27.18	0.25
	SO-SV	0.58 + 0.32 x	33.6	0.35
	SO-OR-SV	0.38 + 0.47 x	25.18	0.44

4. Discussion

4.1. Universal model approach

Generating universal models based on SR_{red} including all cover crops was the first approach to estimate GAI, DM g m^{-2} and N uptake g m^{-2} using the entire data set consisting of 248 measurements for 18 dates. Best results were achieved for canopy parameter GAI with R^2 of 0.60 (Figure 17, Table 9). GAI directly correlates with the chlorophyll amount of the leaves and thus with the spectral reflectance. Estimation of DM g m^{-2} and N uptake g m^{-2} were less accurate with R^2 up to 0.53 and 0.45, respectively (Table 9). Canopy features such as N uptake or DM do not directly correlate to spectral reflectance, like GAI (Weiss et al., 2020), but species specific correlations between GAI and these secondary traits indirectly lead to more or less close correlation to Vi's. Prediction power for the "secondary variables" (Weiss et al., 2020) is lower than for GAI, but modelling the physiological dynamics was in our study not superior to directly estimated ones (data not shown). However, empirical derivation and thus direct derivation from reflectance data was achieved by several authors for winter wheat. For example, Chen (2015) predicted the biomass of with several VIs, reaching a maximal R^2 of 0.86 using NDVI. In addition Feng et al. (2016) found correlations for the leaf N concentration of winter wheat with a large range of VIs. Earlier studies of Tucker et al. (1981) showed a good biomass prediction power of the common SR based on NIR and red (R^2: 0.76).

4.2. VI selection

In this study, two different approaches for prediction of winter cover crop canopy parameters were examined. Both, universal and species-individual models of predictions in sole stands based on a simple ratio (SR_{red}) were most precise, compared to the other tested VIs. Typically, implementing the RE band into VIs estimations increased the precision, due to the strong correlation of chlorophyll content within the RE wavelengths (Clevers and Gitelson, 2013; Delegido et al., 2013; Kira et al., 2016). Dong et al. (2015) compared the performance of conventional VIs, such as SR_{red} and ND_{red}, to RE-based VIs estimating FPAR of wheat and maize. For both crops, their linear correlations were more stable implementing RE into the indices. However, in our case neither SRs nor NDs performed better when using RE. Considering, that most studies observed crop growing periods during spring and summer months (Bukowiecki et al., 2019), implementing RE may probably not appropriate for the predominant light conditions during winter season (Figure 14, Figure 17). Another explanation might be, that Sequoia's RE band (10 nm) is narrower than the other bands (40 nm) of the sensor. Due to the heterogenous reflectance of the plants caused by the poor light conditions of autumn and winter, reflectance received in wavelength of RE in our measurements might be more inaccurate.

Regarding the most common used ND_{red}, predictions for GAI did not exceed values of 2.6 for canopies with GAIs up to 4.9 (Figure 17). Saturation effects using ND_{red} were also found by Nguy-Robertson et al. (2014), predicting GAI of maize, soybean, wheat and potato. Modifications of ND_{red} towards sensitivity of dense stands were partially successful with the wide dynamic range vegetation index (WDRVI), which includes a weighting factor of the vegetative fraction (Gitelson, 2004; Nguy-Robertson et al., 2014). Prabhakara et al. (2015) found a linear correlation between ND_{red} and groundcover percentage, studying the reflectance behaviour of winter cover crops by using a handheld multispectral radiometer. Groundcover percentage describes mostly the top of the canopy, while GAI, measured in the current study, includes all green area within the canopy structure of the respected biomass. Specifically, for further derived parameters as DM accumulation and N uptake of cover crops, a detailed knowledge of GAI as primary driver is more important than a rough estimation of % ground cover which might be sufficient for estimations of erosion protection potential. In general, ND_{red} is not sensitive to structures beneath the canopy surface, hence saturates with higher biomass (Myneni and Williams, 1994). Therefore, from quantitative empirical results as well as from theoretical aspects the SR based on red band was the preferable VI to estimate functional parameters from spectral information in winter cover crops.

4.3. Universal vs. species-individual and mixture-individual approach

Besides the universal model approach including all cover crops, species-individual models were applied in a second step. Comparing the model approaches universal and species-individual model resulted in high differences in favour of species-individual models, especially for DM and N uptake. GAI estimations showed little differences. SV plots in 2018 were strongly influenced by rapeseed volunteers, which limits the results performed by SV-models in terms of the tested species characteristics. Corresponding data points were not excluded from the calculations, as a motivation of the study was to reflect real environmental conditions of winter cover crop cultivation in common cropping sequences. Nevertheless, SV as a phenological small plant was easier to calibrate than plants reaching higher values of GAI. WR-individual model did not perform better than universal model for GAI and N uptake (Figure 20), which can be traced back to the high amounts of senescent plant material, disturbing the reflectance signal (Figure 16).

Typically, VI's are derived from the reflectance of the wavelength in visible light as well as NIR. The information delivered by NIR- reflectance is mostly about the structural properties of a canopy, such as leaf angle and canopy architecture, while visible light is more about the activity of absorbers, such as chlorophyll, in the canopy (Myneni et al., 1995; Kira et al., 2016). Viña et al. (2011) evaluated the performance of multiple VIs for a general correlation to GAI of soybean and maize. Except for RE Chlorophyll Index (CI red edge), all investigated VIs differentiated

between both crop types, soybean and maize. The authors quoted the differences in chlorophyll distribution within the leaf as main source for the different depth of absorption in the red light. Additionally, diverse canopy structures led to higher reflection in NIR, compared to homogenous vegetation coverage (Viña et al., 2011). Hence, sensor calibration for each species individual, seems to be most appropriate.

The canopies of the winter cover crops observed were partly mixed with weeds and rapeseed volunteers competing for resources, mainly radiation. Canopy structure was not as homogenous as in a pure wheat or maize canopy, and thus also the spectral reflection. Amount of absorbers and reflectance of radiation differs for each leaf shape and plant type (Myneni et al., 1995). Consequently, in heterogenous canopies high precision of canopy parameter estimation should not be expected.

In cover crop mixtures, the combination of several plants with different characteristics, such as growth behaviour, canopy structure, leaf size etc., leads to a diverse reflectance throughout the season and within the canopy. Competition between the species makes the emergence and the share of the single crops in the final biomass of a mixed stand unforeseeable, even it is a well-studied seed mixture. Focussing on cover crops, composition of a mixture canopy depends on management preferences, soil type and weather conditions and is usually independent from the ratio of the sown seeds as the only given measure. As the results showed, sensor calibration for a specific mixture was possible, but its applicability is questionable (Figure 21, Table 11). A more reliable approach might be to utilize the universal calibration for mixtures with only slightly reduced performance compared to mixture-individual models.

In general, estimations by species-individual models achieve more precise results than by universal model. Regarding mixture-individual models, results did not differ fundamentally. Nevertheless, universal model approach is based on a larger data base than individual models, which makes it more reliable. In addition, universal model was successfully predicting the independent data set of cover crop mixtures.

4.4. Seasonal challenges

Observing vegetation during autumn and winter using the used Sequoia sensor turned out to be challenging. R^2 decreased to 0.28 in December, while rMAE increased towards 39.12 % (Figure 18). The inaccuracy in winter month can be explained by the low irradiance. PAR saturated in November and December and was even lower in 2019 (Figure 14). Consequently, the sensor receives only little reflectance of the leaves. A second mitigation source is the low sun angle. Assmann et al. (2019) found that variation in sun angle leads to uncertainties on ND_{red} estimates, testing the same Sequoia sensor with several flights in diurnal solar motion in

the arctic tundra. At higher latitudes such as Northern Germany, the variation of the sun angle during a year is up to 40°, resulting in large changes in the incoming radiation. Especially the growth period of winter cover crops covers almost the maximum range of the sun's angle. Therefore, the scattering of raw data as well as canopy parameter estimates during winter months might be explainable due to the drastic decline in light incidence. Moreover, our measurements during the respected season were frequently influenced by clouds casting shadows on the study area, as documented by Assmann et al. (2019) in north-western Canada, by Stow et al. (2019) in south-central Scotland and reviewed by Aasen et al. (2018).

Low temperatures in winter, furthermore, result in a not neglectable and increasing proportion of senescent plant material over time, especially with non-winter-hardy cover crops such as OR, SO or SV. In the current study, WR – defined as winter hardy cover crop – recorded the highest amount of senescent plant material in both years, especially after frost events (Figure 16). Disturbance of the reflectance signal due to senescence was mirrored in the species individual calibration of WR. The amount of destructive sampled senescent plant material explained a part of the scattering effects in spectral reflectance. Spectra of yellow leaves differ from green leaves, as reflection in red and green light increases, and decreases in the range of NIR (Elvidge, 2007; Royimani et al., 2021). Influence of senescent leaves on estimates was also shown by Di Bella et al. (2010) for ND_{red} in a canopy of Italian ryegrass.

Another source of error is the effect of saturation of the pixel values. Illumination geometry adjustments has been studied by Olsson et al. (2021), stating that the sunshine sensor of Sequoia (Parrot) is inaccurate, if there is a high contrast in pixel values of the image. Saturation occurs over bright areas like bare soil, in-between and around the observed vegetation, influencing the reflectance and the extracted pixel values. At a few sampling dates bare soil surrounded the crops or was visible through a sparse stand and led to noticeable increase in error values (data not shown). Sorting out single images with saturated pixel values even before pre-processing by Pix4D, made the reflectance maps more reliable and reduced scattering.

5. Conclusion

The estimation of cover crop canopy parameters can promote the estimation of their effect on N supply to following cash crops and thereby improve nitrogen use efficiency of cropping systems. Remote sensing techniques brought a huge development in agricultural science, thus to the practice. This study revealed opportunities and challenges for utilisation of such methods in winter cover crops dealing with vegetative growth periods characterised by low irradiance and substantial fractions of senescent biomass.

Applying a universal model for winter cover crops, seemed to be a sound solution. Species-individual models resulted partly in more precise predictions but were based on smaller sub-datasets. Dealing with cover crops involves a huge variation in species and heterogenous canopies, compared to cash crops, managed as homogenous as possible. SR_{red} was the most sufficient VI tested in this study, irrespective of the used model approach and consistently superior to the widely used ND_{red}. In contrast to often described advantages of implementing of RE instead of red band for main crops, this did not improve the prediction accuracy in our observed winter cover crops

Nevertheless, winter cover crops are mostly cultivated for their functional attributes, such as the reduction of nitrate leaching and the improvement of soil properties. Therefore, small inaccuracies in the estimation of GAI, DM g m^{-2} or N uptake g m^{-2} can be tolerated. The main agronomic focus is to estimate the rough performance of the cultivated winter cover crops in terms of biomass growth and N uptake. Therefore, the findings should serve as a tool for rapid and inexpensive estimation of environmental and rotational services of cover crops.

References

Aasen, H., Honkavaara, E., Lucieer, A., Zarco-Tejada, P., 2018. Quantitative Remote Sensing at Ultra-High Resolution with UAV Spectroscopy: A Review of Sensor Technology, Measurement Procedures, and Data Correction Workflows. Remote Sensing 10, 1091.

Abdalla, M., Hastings, A., Cheng, K., Yue, Q., Chadwick, D., Espenberg, M., Truu, J., Rees, R.M., Smith, P., 2019. A critical review of the impacts of cover crops on nitrogen leaching, net greenhouse gas balance and crop productivity. Global change biology 25, 2530–2543.

Assmann, J.J., Kerby, J.T., Cunliffe, A.M., Myers-Smith, I.H., 2019. Vegetation monitoring using multispectral sensors — best practices and lessons learned from high latitudes. J. Unmanned Veh. Sys. 7, 54–75.

Blanco-Canqui, H., Mikha, M.M., Presley, D.R., Claassen, M.M., 2011. Addition of Cover Crops Enhances No-Till Potential for Improving Soil Physical Properties. Soil Science Society of America Journal 75, 1471–1482.

Böldt, M., Taube, F., Vogeler, I., Reinsch, T., Kluß, C., Loges, R., 2021. Evaluating Different Catch Crop Strategies for Closing the Nitrogen Cycle in Cropping Systems—Field Experiments and Modelling. Sustainability 13, 394.

Bukowiecki, J., Rose, T., Ehlers, R., Kage, H., 2019. High-Throughput Prediction of Whole Season Green Area Index in Winter Wheat With an Airborne Multispectral Sensor. Frontiers in plant science 10, 1798.

Chapagain, T., Lee, E.A., Raizada, M.N., 2020. The Potential of Multi-Species Mixtures to Diversify Cover Crop Benefits. Sustainability 12, 2058.

Chen, P., 2015. A Comparison of Two Approaches for Estimating the Wheat Nitrogen Nutrition Index Using Remote Sensing. Remote Sensing 7, 4527–4548.

Clevers, J., Gitelson, A.A., 2013. Remote estimation of crop and grass chlorophyll and nitrogen content using red-edge bands on Sentinel-2 and -3. International Journal of Applied Earth Observation and Geoinformation 23, 344–351.

Curran, P.J., 1989. Remote sensing of foliar chemistry. Remote Sensing of Environment 30, 271–278.

Delegido, J., Verrelst, J., Meza, C.M., Rivera, J.P., Alonso, L., Moreno, J., 2013. A red-edge spectral index for remote sensing estimation of green LAI over agroecosystems. European Journal of Agronomy 46, 42–52.

Deutscher Wetterdienst, 2024. Wetter und Klima - Deutscher Wetterdienst: Kiel-Kronshagen (2565). https://opendata.dwd.de/climate_environment/CDC/observations_germany/climate/multi_annual/mean_91-20/. Accessed 30 September 2024.

Di Bella, C.M., Paruelo, J.M., Becerra, J.E., Bacour, C., Baret, F., 2010. Effect of senescent leaves on NDVI-based estimates of f APAR: Experimental and modelling evidences. International Journal of Remote Sensing 25, 5415–5427.

Dong, T., Meng, J., Shang, J., Liu, J., Wu, B., 2015. Evaluation of Chlorophyll-Related Vegetation Indices Using Simulated Sentinel-2 Data for Estimation of Crop Fraction of Absorbed Photosynthetically Active Radiation. IEEE J. Sel. Top. Appl. Earth Observations Remote Sensing 8, 4049–4059.

Elvidge, C.D., 2007. Visible and near infrared reflectance characteristics of dry plant materials. International Journal of Remote Sensing 11, 1775–1795.

European Commission, 2017. Report from the comission to the European parliament and the council: On the implementation of the ecological focus area obligation under the green direct payment scheme, Bruessels, 14 pp. Accessed 22 March 2022.

Feng, W., Zhang, H.-Y., Zhang, Y.-S., Qi, S.-L., Heng, Y.-R., Guo, B.-B., Ma, D.-Y., Guo, T.-C., 2016. Remote detection of canopy leaf nitrogen concentration in winter wheat by using water resistance vegetation indices from in-situ hyperspectral data. Field Crops Research 198, 238–246.

Florence, A.M., McGuire, A.M., 2020. Do diverse cover crop mixtures perform better than monocultures?: A systematic review. Agron.j. 112, 3513–3534.

Gitelson, A.A., 2004. Wide Dynamic Range Vegetation Index for remote quantification of biophysical characteristics of vegetation. Journal of plant physiology 161, 165–173.

Gitelson, A.A., Merzlyak, M.N., 1996. Signature Analysis of Leaf Reflectance Spectra: Algorithm Development for Remote Sensing of Chlorophyll. Journal of plant physiology 148, 494–500.

Gitelson, A.A., Viña, A., Arkebauer, T.J., Rundquist, D.C., Keydan, G., Leavitt, B., 2003. Remote estimation of leaf area index and green leaf biomass in maize canopies. Geophys. Res. Lett. 30, n/a-n/a.

Gitelson, A.A., Viña, A., Ciganda, V., Rundquist, D.C., Arkebauer, T.J., 2005. Remote estimation of canopy chlorophyll content in crops. Geophysical Research Letters 32.

Goffart, D., Curnel, Y., Planchon, V., Goffart, J.-P., Defourny, P., 2021. Field-scale assessment of Belgian winter cover crops biomass based on Sentinel-2 data. European Journal of Agronomy 126, 126278.

Hankerson, B., Kjaersgaard, J., Hay, C., 2012. Estimation of Evapotranspiration from Fields with and without Cover Crops Using Remote Sensing and in situ Methods. Remote Sensing 4, 3796–3812.

Hijmans, R.J., 2022. raster: Geographic Data Analysis and Modeling.

Hively, W.D., Duiker, S., McCarty, G., Prabhakara, K., 2015. Remote sensing to monitor cover crop adoption in southeastern Pennsylvania. Journal of Soil and Water Conservation 70, 340–352.

Hively, W.D., Lang, M., McCarty, G.W., Keppler, J., Sadeghi, A., McConnell, L.L., 2009. Using satellite remote sensing to estimate winter cover crop nutrient uptake efficiency. Journal of Soil and Water Conservation 64, 303–313.

Holmes, A.A., Thompson, A.A., Lovell, S.T., Villamil, M.B., Yannarell, A.C., Dawson, J.O., Wortman, S.E., 2019. Nitrogen provisioned and recycled by cover crops in monoculture and mixture across two organic farms. Nutr Cycl Agroecosyst 115, 441–453.

Jordan, C.F., 1969. Derivation of Leaf-Area Index from Quality of Light on the Forest Floor. Ecology, 663–666.

Kira, O., Nguy-Robertson, A.L., Arkebauer, T.J., Linker, R., Gitelson, A.A., 2016. Informative spectral bands for remote green LAI estimation in C3 and C4 crops. Agricultural and Forest Meteorology 218-219, 243–249.

Myneni, R.B., Hall, F.G., Sellers, P.J., Marshak, A.L., 1995. The interpretation of spectral vegetation indexes. IEEE Trans. Geosci. Remote Sensing 33, 481–486.

Myneni, R.B., Williams, D.L., 1994. On the relationship between FAPAR and NDVI. Remote Sensing of Environment 49, 200–211.

Nguy-Robertson, A.L., Peng, Y., Gitelson, A.A., Arkebauer, T.J., Pimstein, A., Herrmann, I., Karnieli, A., Rundquist, D.C., Bonfil, D.J., 2014. Estimating green LAI in four crops: Potential of determining optimal spectral bands for a universal algorithm. Agricultural and Forest Meteorology 192-193, 140–148.

Nouri, A., Lukas, S., Singh, S., Singh, S., Machado, S., 2022. When do cover crops reduce nitrate leaching? A global meta-analysis. Global change biology. https://doi.org/10.1111/gcb.16269.

Olsson, P.-O., Vivekar, A., Adler, K., Garcia Millan, V.E., Koc, A., Alamrani, M., Eklundh, L., 2021. Radiometric Correction of Multispectral UAS Images: Evaluating the Accuracy of the Parrot Sequoia Camera and Sunshine Sensor. Remote Sensing 13, 577.

Prabhakara, K., Hively, W.D., McCarty, G.W., 2015. Evaluating the relationship between biomass, percent groundcover and remote sensing indices across six winter cover crop fields in Maryland, United States. International Journal of Applied Earth Observation and Geoinformation 39, 88–102.

R Core Team, 2024. R: A language and environment for statistical computing. R foundation for statistical computing, Vienna, Austria.

Rouse, J.W., Haars, J.R.H., Schell, J.A., Deering, D.W., 1974. Monitoring vegetation systemsin the Great Plains witherts. Proceedings of the 3rd ERTS Symposium, Washingston, DC, USA.

Royimani, L., Mutanga, O., Dube, T., 2021. Progress in Remote Sensing of Grass Senescence: A Review on the Challenges and Opportunities. IEEE J. Sel. Top. Appl. Earth Observations Remote Sensing 14, 7714–7723.

Sims, D.A., Gamon, J.A., 2002. Relationships between leaf pigment content and spectral reflectance across a wide range of species, leaf structures and developmental stages. Remote Sensing of Environment 81, 337–354.

Stow, D., Nichol, C., Wade, T., Assmann, J., Simpson, G., Helfter, C., 2019. Illumination Geometry and Flying Height Influence Surface Reflectance and NDVI Derived from Multispectral UAS Imagery. Drones 3, 55.

Thorup-Kristensen, K., Magid, J., Jensen, L.S., 2003. Catch crops and green manures as biological tools in nitrogen management in temperate zones. Advances in Agronomy, 227–302.

Tonitto, C., David, M.B., Drinkwater, L.E., 2006. Replacing bare fallows with cover crops in fertilizer-intensive cropping systems: A meta-analysis of crop yield and N dynamics. Agriculture, Ecosystems & Environment 112, 58–72.

Tosti, G., Benincasa, P., Farneselli, M., Tei, F., Guiducci, M., 2014. Barley–hairy vetch mixture as cover crop for green manuring and the mitigation of N leaching risk. European Journal of Agronomy 54, 34–39.

Tucker, C.J., Holben, B.N., Elgin, J.H., McMurtrey, J.E., 1981. Remote sensing of total dry-matter accumulation in winter wheat. Remote Sensing of Environment 11, 171–189.

Viña, A., Gitelson, A.A., Nguy-Robertson, A.L., Peng, Y., 2011. Comparison of different vegetation indices for the remote assessment of green leaf area index of crops. Remote Sensing of Environment 115, 3468–3478.

Vogeler, I., Böldt, M., Taube, F., 2022. Mineralisation of catch crop residues and N transfer to the subsequent crop. The Science of the total environment 810, 152142.

Weiss, M., Jacob, F., Duveiller, G., 2020. Remote sensing for agricultural applications: A meta-review. Remote Sensing of Environment 236, 111402.

Chapter 5

General Discussion

Part I – Exploring dynamics of cover crop growth period

In Chapter 2, the effects of different cover crop mixtures on silage maize were explored, with a particular focus on observations within maize vegetation period. Legume-brassica mixture and alfalfa were found to have a significant yield-reducing effect on maize. All tested cover crop mixtures facilitated water uptake from deeper soil layers, with the legume-brassica mixture showing the most pronounced effect. However, maize yield after brassica-grass and legume-grass cover crop mixtures remained at the same level. Possible explanations for these findings include the specific rooting characteristics of the different cover crop mixtures, the role of components within the mixtures, which appear to support yield stability, and their effect on the initial growth conditions of maize (see discussion in Chapter 2). The possible explanations were further analysed by having a closer look at the cover crop growing season.

Belowground complementarity of cover crops

The cover crop mixtures used in the trial were designed based on the principle of niche complementarity. But contrastingly to the majority of literature, the selection of functional traits was focussed on traits, which may increase the belowground ground biomass production and consequently enhance soil physical properties (Blanco-Canqui, 2024). Our approach combines shallow-rooting cover crops with deep-rooting ones to maximize resource utilisation across different soil layers. This approach of belowground niche complementarity has its origins in the American polyculture "three sisters", combining maize bean and squash, with their contrasting root architectures (Zhang et al., 2014). By growing both rooting types together, each component is encouraged to occupy its specific ecological niche, reducing belowground competition for resources such as water and nutrients. This strategic pairing aims to improve overall system efficiency, as shallow-rooting species primarily exploit resources in the upper soil layers, while deep-rooting species access nutrients and water from deeper layers. This combination was done for each functional group (legume, grass and brassica), but also within each mixture, by combining these contrasting groups. In a one-year trial we analysed the root growth of each cover crop mixture and its components grown as sole stands. The investigated cover crops are listed in Chapter 3 (Table 4). The questions raised were:

- Is there a niche complementary effect in the mixtures or even within a functional group?

- Does the rooting depth of the cover crop mixtures explain the effects observed in Chapter 3?

The study was designed in a randomised block design, including four repetitions for each variant. The method applied was the core break method (Böhm, 1979), twice, in winter (2021) and in spring (2022), until a depth of 120 cm, split into 10 cm steps (first 10 cm were neglected). Each 10 cm soil sample, was broken by hand in its middle. All emerging roots from the broken surface were counted and transformed to the surface area, resulting in root counts per cm² (RC). Similar to the analysis in Chapter 3, the soil depths were grouped into three soil layers, by hierarchical clustering (R Core Team, 2024). Resulting clusters were topsoil 10 – 30 cm, subsoil 30 – 70 cm and deep subsoil 70 – 120 cm (first 10 cm were excluded from the measurements, as there was a lot of non-root material, disturbing the measurements). To compare RC among the components within each cover crop mixture, three datasets were compiled, each consisting of one mixture and its four respective components grown as sole stands. RC's were log-transformed. To stabilise variance with a small constant (half of the minimum RC) added to avoid issues with the logarithm of zero. RC was analysed using a linear mixed-effects model (Pinheiro and Bates, 2010). Soil measurement depth was included as a continuous covariate, while the cover crop variant and the clustered soil layers were included as fixed factor along with their interaction to evaluate whether the effect of soil layer varied among cover crop variants. The random structure accounted for repetition nested within sampling date to model variability due to experimental setup and temporal factors. Post-hoc pairwise comparisons among variants within each layer were performed using estimated marginal means (Hothorn et al., 2008; Bretz et al., 2011).

The topsoil layer (0-30 cm) shows the highest RC across all variants and for both sampling dates. Thereby oilseed radish exhibits the greatest RC with 1.1, followed by legume-grass and brassica-grass mixtures, both with a RC of 1.0. Red and white clover display comparatively lower RC, with 0.7 and 0.5 counts per cm². Within subsoil (30-70 cm) tap rooted variants (oilseed radish, oilseed rape, mixtures including brassicas) maintain high root presence while other variants decline stronger, especially the grasses tall fescue and ryegrass with both 0.1 roots per cm². RC's are low in all variants in the deep subsoil (70-120 cm). However, the brassica-mixtures and brassica sole stands show root presence. This is in line with literature, as Kemper et al. (2020) investigated these functional groups on their rooting characteristics, confirming deep root growth by tap rooted species (Chen and Weil, 2010). Kristensen and Thorup-Kristensen (2004b) stated a root growth of brassica species until 1.5 m, depending on the length of the growing period. Grasses and legumes were identified as shallow rooting and

highly abundant in the topsoil. In our results, especially the grasses had high RC in the topsoil layer, too (Figure 22).

Is there a niche complementary effect in the mixtures or even within a functional group?
By combining the functional groups an overall increased rooting, by a favourable rooting of shallow rooting components in the topsoil and deep rooting components in deeper soil layers, was expected. The mixture brassica-grass consists of oilseed radish, oilseed rape, ryegrass and tall fescue. Both, ryegrass and tall fescue differed significantly to brassica-grass mixture, but also from the sole stands of oilseed radish and oilseed rape, except of ryegrass, which is not different to oilseed rape (Figure 22). Regarding the mixture legume-brassica, consisting of red and white clover plus the brassica variants, similar patterns have been observed. Both, red and white clover are significantly lower than the mixture legume-brassica and oilseed radish as sole stand. A significant difference is also observed between oilseed rape and white clover, but not for red clover (Figure 22). RC of the mixture legume-grass did not differ to any of its components. An interaction of variants with the clustered soil layers was not observed for any of the mixture comparison (Figure 22). Saleem et al. (2020) found enhanced root architectural traits by increasing the diversity and species richness of cover crop mixtures, in a pot experiment. However, under field conditions, the postulated niche complementary effect was not found, as the mixtures did not confirm a higher RC in any soil layer, than the most productive mixture component grown as sole stand. Notably, differences were found within the functional groups (brassicas, legumes, grasses); however, oilseed rape shows no significant difference compared to red clover and ryegrass, unlike oilseed radish. This finding may suggest that oilseed radish tends to root slightly more extensively than oilseed rape. Additionally, ryegrass and red clover may root more extensively than tall fescue and white clover, as they do not differ significantly from the tap rooted oilseed rape.

Does the rooting depth of the cover crop mixtures explain the effects observed in Chapter 3?
A significantly greater reduction in soil water in the deep subsoil under the legume-brassica mixture suggested increased root growth, particularly in the deeper soil layers. Brassica-mixture including legumes did not root more intense than mixture with grass, regardless of the soil layer. However, root length density (RC) did not show significant differences between the three cover crop mixtures in the upper soil layers (up to 70 cm). In the deep subsoil (70–120 cm), mixtures containing brassica species exhibited significantly higher RC compared to the legume-grass mixture. The observed effects in Chapter 3 can therefore only be partially explained by preformed root pores, as maize following all cover crop mixtures extracted water

from deep soil layers. No clear differences in rooting behaviour between the mixtures could be identified, except the higher RC by brassica-mixtures. It appears that the tested cover crop mixtures generally contribute to higher soil porosity, which likely facilitates deeper water uptake by the subsequent crop.

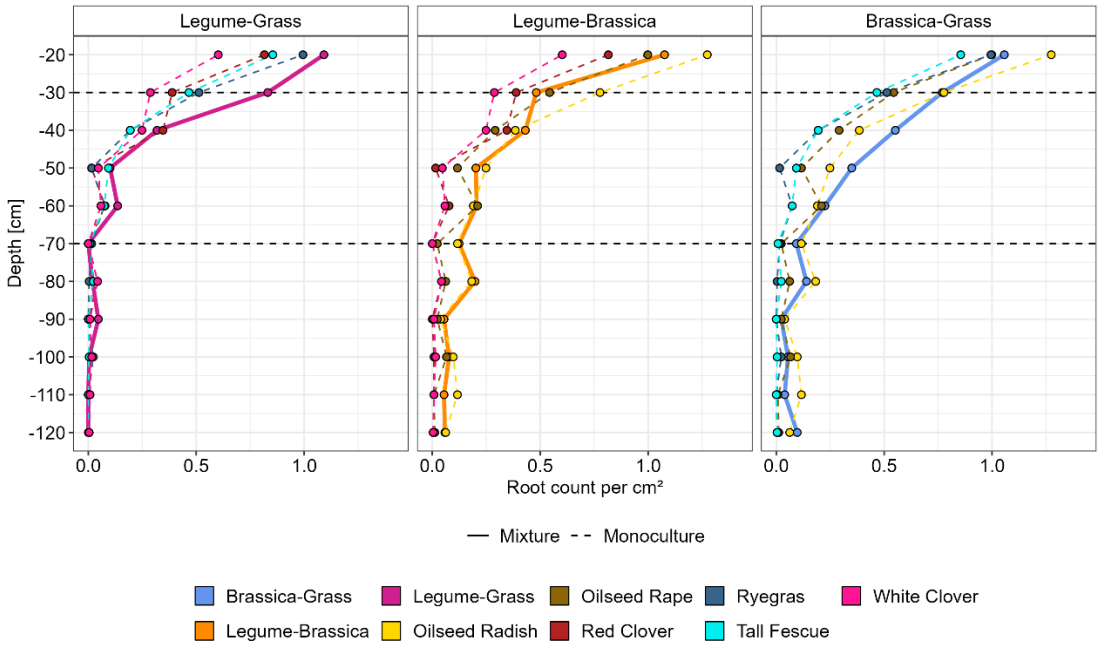

Figure 22 Root counts [roots per cm²] along the soil depth for each tested cover crop mixture (solid line, legume-grass, legume-brassica, brassica-grass). Root counts of the components of each mixture, grown as a sole stand are depicted in each respective facet (dashed lines). Soil depth is divided into three layers (topsoil 0-30 cm, subsoil 30-70 cm, deep subsoil 70-120 cm).

Above ground biomass of cover crop mixtures

To assess above-ground biomass growth, mixture-individual models were established, as documented in Chapter 3. By means of those calibrations the development of the GAI over time for three cover crop mixtures was monitored in all three trial years (Figure 23). All mixtures pause growth in winter due to frost, which causes a decline in GAI. The legume-grass mixture shows a low GAI throughout, as the legumes and grasses produce less biomass than brassicas. The brassica-grass mixture had a higher GAI, but declined more, as it includes non-winterhard oilseed radish. The brassica-grass mixture had the highest GAI.

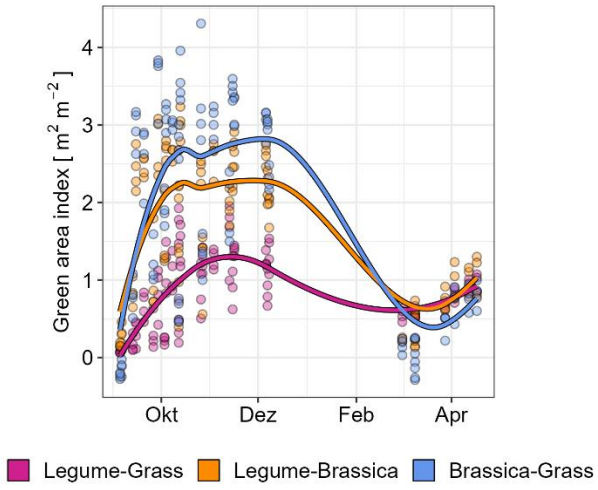

Figure 23 Spectrally derived green area index (GAI, m² m^{-2}) averaged over the three vegetation periods (2020/2021, 2021/2022, 2022/2023) of the cover crop mixtures legume-grass, legume-brassica and brassica-grass (colourful).

As the vegetation peak occurs before the first frost events in winter, destructive samples were collected at that timepoint. The mixtures involving brassicas showed superior dry matter yields before vegetation pause in winter, with averaged 212.9 and 221.8 g m^{-2} for legume-brassica and brassica-grass, respectively. Legume-grass displayed a notably lower yield, approximately 96.9 g m^{-2}. The latter differed significantly from the mixtures containing brassica. These DM yields of the cover crop mixtures, do only include the actual sown cover crops emerged. Table 12 provides an overview of the total biomass emerged and the percentage of its components. Within legume-grass variant, the grasses were the dominant component in the legume-grass mixture with 50.5% of the total emerged biomass. Furthermore, the legume-grass mixture exhibited a notable prevalence of weeds, accounting for 27.3% of the total biomass. The ecosystem service of weed suppression is one of the traits, which are hypothesised to be enhanced using cover crop mixtures, instead of sole stands (Chapagain et al., 2020). However, Florence et al. (2019) and Smith et al. (2014) did not find an effect by mixtures on weed suppression. A high biomass production is linked to the weed suppression, too (Finney et al., 2016; Finney et al., 2017), which is rather achieved by brassica species.

In legume-brassica and brassica-grass mixtures, the brassicas formed the highest proportion of the biomass with 91.7 and 93.5%, respectively. Legumes and grasses were almost negligible components of those mixtures. Wortman et al. (2012) and Couëdel et al. (2018) also stated that brassica species dominated in mixtures. Complementary mixtures were promoted to be more productive than increasing species richness, especially species with different phenological characteristics would be more likely to compete with each other (Chapagain et al., 2020). The expansive foliage of the brassica species effectively excludes the smaller clover and grass

species from the available light, particularly due to the rapid emergence of the brassicas. Florence et al. (2019) investigated functional richness in cover crop mixtures and found an increase about 29% in biomass productivity. But the authors discuss these results carefully. The increase in productivity by cover crop mixtures is not due to niche complementarity. At low diversity, small low-yielding species pull the average down. At high diversity, high-yielding species compensate for the low-yielding variants on average. These findings are consistent with the observed share of cover crop components in the brassica mixtures. However, Finney et al. (2017) did not confirm a productivity increase by mixing complementary cover crop species.

Table 12 Dry matter proportion [%] of cover crop mixture components, sum of sown cover crops emerged, weeds and senescent material. Proportions are averaged over three trial years (2020-2022). Sampling was conducted shortly before end of vegetative period in winter.

Components	Legume-grass	Legume-brassica	Brassica-grass	Alfalfa
Brassica		90.5	90.2	
Legume	19.4	1.2		79.4
Grass	50.5		3.3	
Sown cover crops	69.9	91.7	93.5	79.4
Senescence	2.8	6.1	6.1	7.2
Weeds	27.3	2.2	0.4	13.4

As discussed in Chapter 3, maize yield was only negatively affected by legume-brassica mixture. However, total biomass production of legume-brassica mixture was not significantly different to brassica-grass mixture, which was maintaining maize yield. Furthermore, the share of grasses and legumes in the mixtures including brassica were marginal, as brassica species are very dominant cover crops in mixtures (Wortman et al., 2012; Couëdel et al., 2018). The differences in yield cannot be explained by mixtures biomass production nor emerged mixture compositions.

Starting conditions for silage maize

As discussed previously, the differences in maize yield, may also be related to different starting conditions of the treatments. Especially, young maize plants suffer under dry soil conditions. A late termination date should prevent losses due to evaporation before sowing (Stipešević and Kladivko, 2005). Soil samples (0-90 cm) were collected shortly after cover crop termination in spring. The samples were analysed for mineral N (SMN) and gravimetric soil moisture. The boxplots in Figure 24 show key soil properties at the start of maize cultivation averaged over

the years 2021, 2022, and 2023. The left panel displays SMN (kg ha⁻¹), while the right panel shows gravimetric soil moisture content (mm) under the investigated cover crop variants. N-levels under legume-grass were lowest among all treatments, indicating a high N uptake by the cover crop mixture. Legumes commonly have a high N content and a consequently low C:N ratio. Additionally, due to N fixation, legume cover crops usually provide more N to the soil (Couëdel et al., 2018). However, the legume component in this mixture accounted for only 19.4%, while grasses made up 50.5% of the biomass (Table 12). Grasses, in contrast to legumes, have a relatively high C:N ratio, delaying the decomposition and consequently deplete the N pool at maize sowing (Ranells and Wagger, 1997; Ramírez-García et al., 2015). Comparably, higher SMN of brassica-mixtures is due to early mineralisation of non-winterhardy oilseed radish, as indicated by the amount of senescent material, which was highest for mixtures containing brassica (Table 12). Nevertheless, these starting conditions do indicate a yield reducing effect of legume-brassica mixture and perennial alfalfa. Furthermore, soil moisture was similar for all cover crop variants and fallow, with higher variability for legume-grass mixture, indicating no varying moisture conditions for maize emergence.

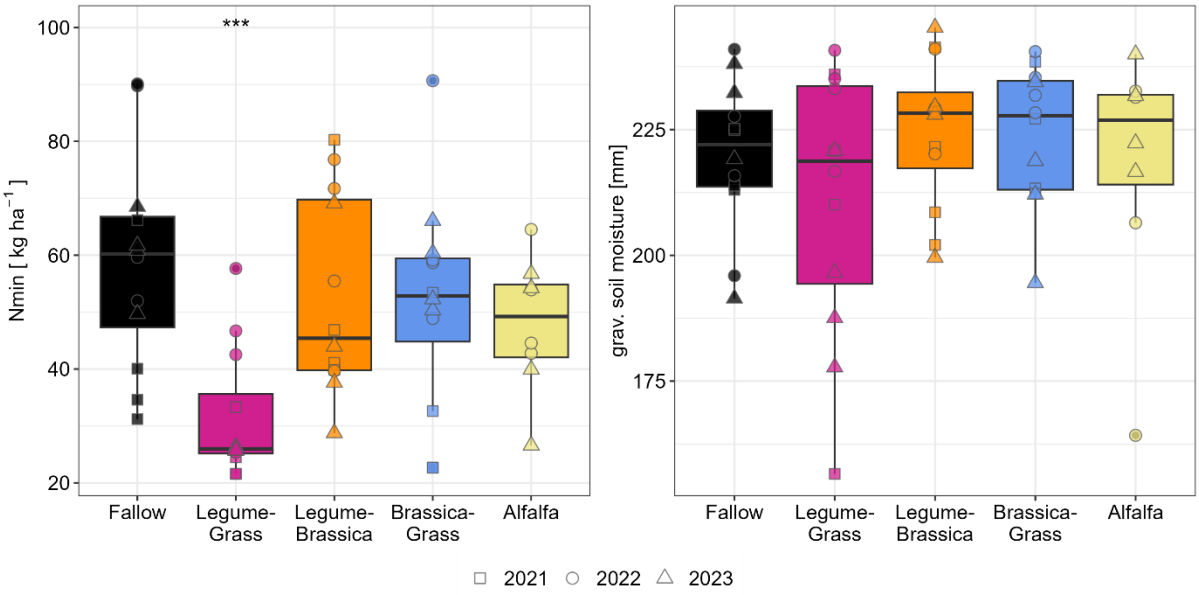

Figure 24 Soil properties after cover crop termination under different cover crop variants and fallow as control, including data of the trial years 2021, 2022, and 2023. Left panel: *Mineral nitrogen (SMN, kg ha⁻¹).* Right panel: *Gravimetric soil moisture (mm). Data points represent individual years (□ 2021, ○ 2022, △ 2023).*

Part II – Estimating silage maize yield response to N availability

In Chapter 2 of this thesis, the HUME-Maize crop growth model was presented and evaluated. It was found to reliably model plant growth under different weather conditions and soil textures. However, effects of varying N availability are so far not included. Also, in the field trial presented in Chapter 3, the effects of winter cover crops on subsequent silage maize were analysed while excluding N stress. However, the potential of N supply by cover crop species is known to be variable, depending on the immobilisation and mineralisation of their residues (Kristensen and Thorup-Kristensen, 2004b). Kühling et al. (2023) found increased N availability in silage maize after a freezing non-leguminous winter cover crop, but only minor effects on yield. Conversely, Möller and Reents (2009) observed positive yield effects subsequent to freezing legumes, which enhance net mineralisation in silage maize (Bukowiecki et al., under review). The German Fertiliser Ordinance (DüV, 2017) also considers differences in site-specific N availability in its N fertiliser recommendations and suggests lower N input after the cultivation of leguminous cover crops.

Hence, to display all yield-relevant effects of cover crops on the following maize, especially with regard to a fertilisation strategy, the HUME-Maize model had to be developed further to exhibit a fundamental sensitivity to N availability. The first steps taken in this direction are reflected below. The dataset used for calibration is the same as in Chapter 2 (Table 1), extended by the N fertilisation levels 0 and 120 kg N ha^{-1} (0N, 120N).

Adding N limitation to HUME Maize via organ-specific dilution curves

Preliminary considerations

N concentration (N_{conc}) of a plant decreases during crop growth as a consequence of self-shading within the canopy (Sinclair and Horie, 1989) and an increase in biomass, particularly structural organs such as stems and cobs (Caloin and Yu, 1984). Self-shading can lead to an uneven distribution of N within the canopy. The upper leaves would have a higher N_{conc}, to better perform photosynthesis (Bertheloot et al., 2008). As the structural plant organs stem and cob perform less photosynthesis, the N_{conc} is lower within these tissues than the leaf N_{conc} (Lemaire and Gastal, 1997). For modelling approaches, it is not appropriate to consider N uptake at the whole plants level only, because N inputs not only affect the absolute amount of N in the crop, but can also cause distinct allocation patterns within the plant. Thus, total N uptake reduces after silking, while N_{conc} within the plant remains constant. However, distinct allocation processes result in a shift of N_{conc} from the leaves to the cob (Figure 1), which leads to the senescence of leaf tissue and a reduction in the photosynthetic active green area. The application of N fertiliser can influence these processes: As depicted in Figure 25, higher N

fertilisation levels lead to a generally higher N content in the leaves, while the lowest fertilisation level (0 kg/ha) results in the lowest N content. Additionally, the decrease in N proportion is more pronounced with N limitations. Similar to the leaves, the N content in the stem decreases with increasing DM. Again, higher fertiliser levels have a positive effect on N partitioning to the stem, but the differences between N-levels are smaller than for the leaves. In contrast to the leaf and stem, the N proportion in the cob tends to increase with increasing DM, resulting from the translocation processes from vegetative organs to the generative organ. At the beginning of cob growth, cob's N proportion is highest without N fertilization, indicating, a prioritisation of cob growth under N limitation.

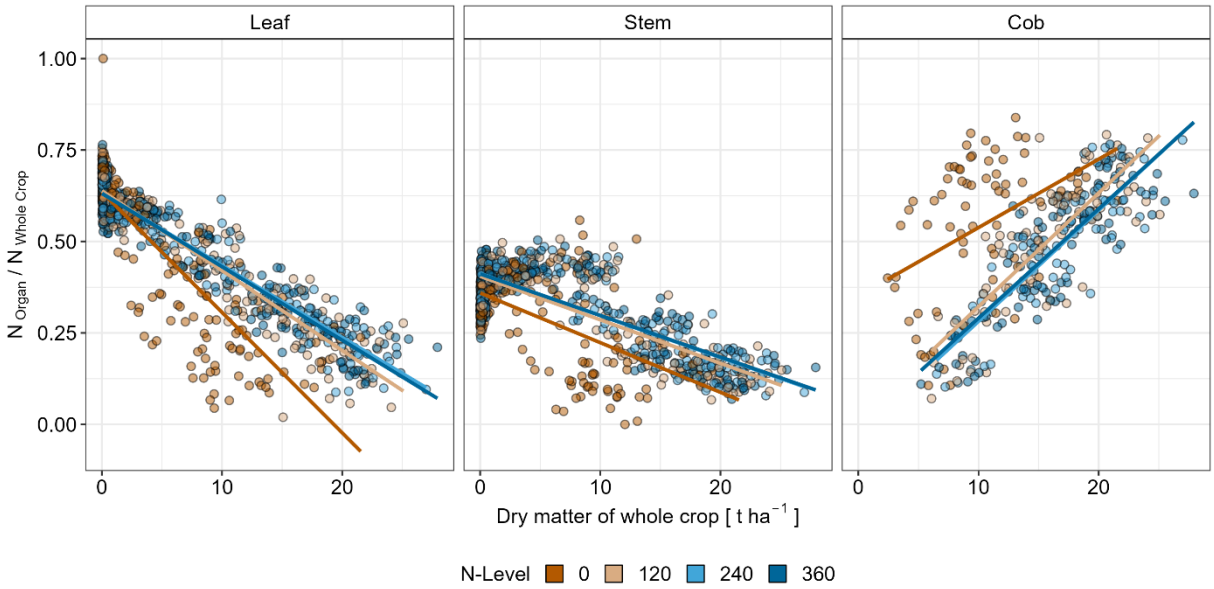

Figure 25 Relationship between the dry matter yield of the whole plant (t ha^{-1}) and the proportion of N in different plant organs (leaf, stem, cob) relative to the total plant N.

Critical N (N_{crit}) dilution curves are used to analyse the N status of crops, assuming a relationship between N_{conc} and DM growth, that determines the optimum N supply for the regarded crop (Lemaire and Salette, 1984). These curves are based on the concept of N_{crit} (Ulrich, 1952; Greenwood. et al., 1991), which is the minimum N_{conc} required to achieve the maximum DM growth. These N_{crit} dilution curves have been established for various crops, e.g. wheat (Justes et al., 1994) , oilseed rape (Colnenne, 1998) , barley (Zhao, 2014), rice (Ata-Ul-Karim et al., 2017) and sunflower (Debaeke et al., 2012). N dilution curve for maize was first established by Plénet and Lemaire (1999) and further extended by Herrmann and Taube (2004) until silage maturity. In addition to the European studies, specific dilution curves for maize were also drawn up in China and Canada (Ziadi et al., 2008; Yue et al., 2014). However, these studies concentrated on the N concentration of the whole plant instead of the single organs.

N_{crit} describes the minimum N_{conc}, at which the maximum DM is reached without additional N fertilisation significantly increasing DM – even if the plants N uptake continues to increase. Determination of N_{crit} was calculated according to Justes et al. (1994), via linear-plateau function for each available sampling date, further illustrated in Figure 26. For some of the sampling dates, it is was not possible to fit a linear plateau (e.g. Figure 25A: only three N_{crit} could be calculated for the trial year 2007 at site "Hohenschulen"). These sampling dates were not included into the further process of N dilution curve development. The final N dilution curve fits the resulting critical N_{conc} and is commonly described by a quadratic function with a plateau for dry matter (DM) values >1 t ha^{-1} (Plénet and Lemaire, 1999; Herrmann and Taube, 2004):

$$N_{conc} = \begin{cases} a & | \ DM < DM_{crit} \\ a * DM^{b} & | \ DM \geq DM_{crit} \end{cases} \quad \text{(E1)}$$

With the coefficient a representing the N_{conc} for DM smaller than DM_{crit}, illustrating the initial plateau of the function. Coefficient b represents the decrease of N_{conc} with DM growth. In this study the plateau DM_{crit} was also fitted.

Regarding whole plant's N dilution curve, parameters are slightly different to the results of Plénet and Lemaire (1999) and Herrmann and Taube (2004) ($3.4*DM^{-0.37}$ and $3.4*DM^{-0.39}$, respectively). Coefficient a in this study is about 4.89 until a DM_{crit} of 0.52 t ha^{-1}. The threshold was fitted with the available data, while the coefficient a of the above-named studies was set to a DM threshold of 1 t ha^{-1}. However, the coefficient b, controlling the decrease of the function, fits well to the results of the Plénet et al. (1999) and Herrmann et al. (2004). Yue et al. (2014) found rather smaller coefficients ($27.2\ DM^{-0.27}$) for maize grown in North China Plain, discussing shorter vegetation duration caused by higher temperatures resulting in lower amount of accumulated N compared to the European studies. However, climatic conditions or vegetation period of the current dataset were at least similar to those of Herrmann and Taube (2004), investigating silage maize in Germany.

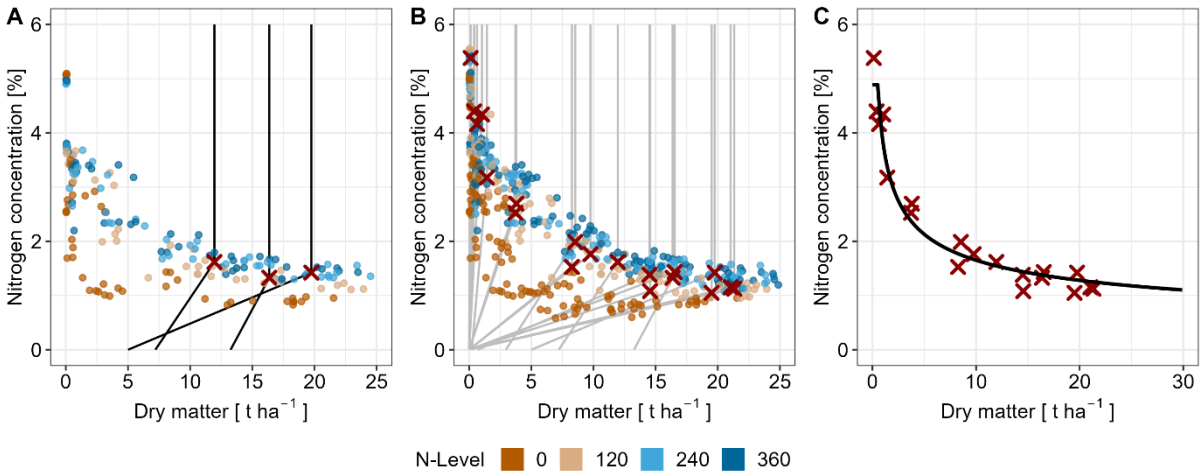

Figure 26 Development of dilution curve for the whole plant. A: calculation of critical N_{conc} (%, red cross) of one sampling date (2021) via linear-plateau function. B: Calculation of critical N_{conc} for all available sampling dates (trial years: 2007, 2008, n=19). C: fitting N dilution curve through the calculated critical N_{conc} (N_{crit}).

In the next step, calculations for N_{crit}'s were applied at the organ level (Figure 3). N_{conc} of the leaves is highest, starting with a plateau at 5.36, compared to the structural organs stem and cob (Figure 27, Table 13). For stem dilution, the best fit was obtained with an exponential function. The plateau was almost negligible (DM_{crit} 0.001 t ha^{-1}). Sieling and Kage (2021) recently worked with the same set of data, calculating distinct coefficients, e.g. 3.17 $W^{-0.34}$ for leaf N_{conc}, suggesting a level and a stronger decrease of N_{conc} in the leaf dry matter. However, they were not following the workflow proposed by Justes et al. (1994), which may cause the deviations.

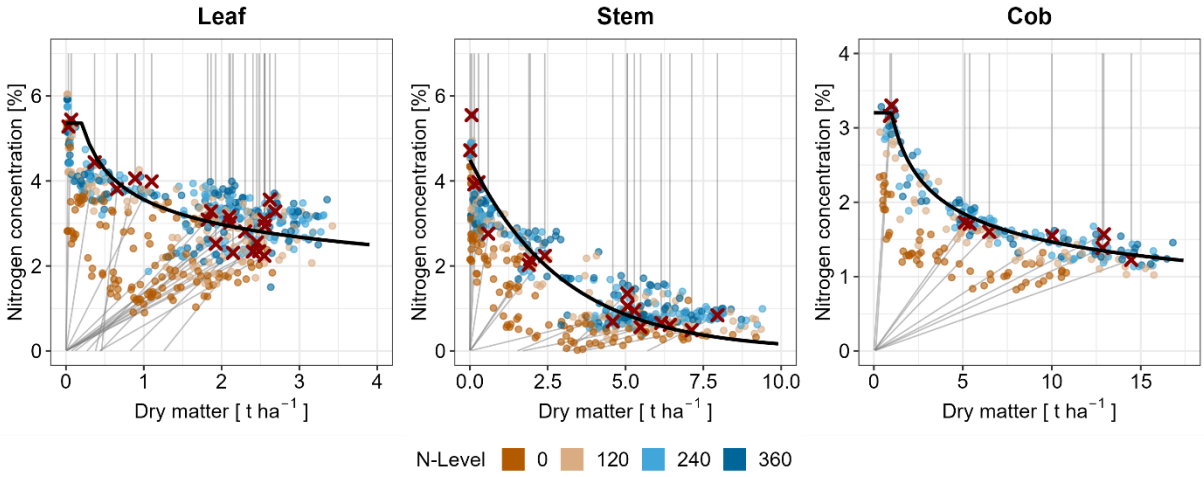

Figure 27 N dilution curves of organs (leaf, stem, cob, solid line) as the relation between N concentration (%) and dry matter (t ha^{-1}) with datapoints coloured for specific N-levels and critical N concentrations (red cross). The latter was calculated via linear-plateau functions (grey lines, Justes et al. (1994)) for each available and computable sampling date.

Table 13 N dilution curves (E1) for whole maize crop and each organ (leaf, stem, cob), with the dry matter threshold W_{crit} [t ha^{-1}] under the function remains in a constant plateau (a, E1) and above, the function. For stem, an exponential function without plateau fit best.

Organ	W_{crit} [t ha^{-1}]	$W < W_{crit}$	$W \geq W_{crit}$	n
Whole plant	0.52	4.89	$4.89 * W^{-0.37}$	19
Leaf	0.21	5.36	$5.36 * W^{-0.26}$	21
Stem	0.001	4.50	$4.50 * e^{-0.33 * W}$	17
Cob	0.98	3.20	$3.20 * W^{-0.34}$	9

To detect N stress of a plant, nitrogen nutrition index (NNI) can be derived from the N dilution curves, as the ratio between actual N_c and N_{crit}. The N status of the plant is also accurately reflected by leaf DM or even leaf area index (Ata-Ul-Karim et al., 2017; Zhao et al., 2017; Zhao et al., 2018; Sieling and Kage, 2021), as the N_{conc} is highest in the leaf. If there is an organ-specific approach made, both NNI assumptions can be introduced as yield reducing factor in the crop growth model HUME-Maize. For this data set, there were negligible differences between NNI variants. In Figure 28 NNI derived by dilution curve based on whole plant (NNI_{Plant}) is compared with the NNI based on leaf dilution curve (NNI_{Leaf}). Both NNI's are depicted throughout the growth period of maize in 2007 and 2008. NNI is reduced to 0.4 and 0.3 for 0N variant in 2007 and 2008, respectively. Thereby, NNI_{Leaf} is slightly lower during the early growth period. The reduction at the beginning of the season happens in all N-levels, indicating the highest growth rate during leaf and stem development. NNI_{Leaf} is lower at maize harvest, in all variants, probably due to maturity induced leaf senescence at the end of the season.

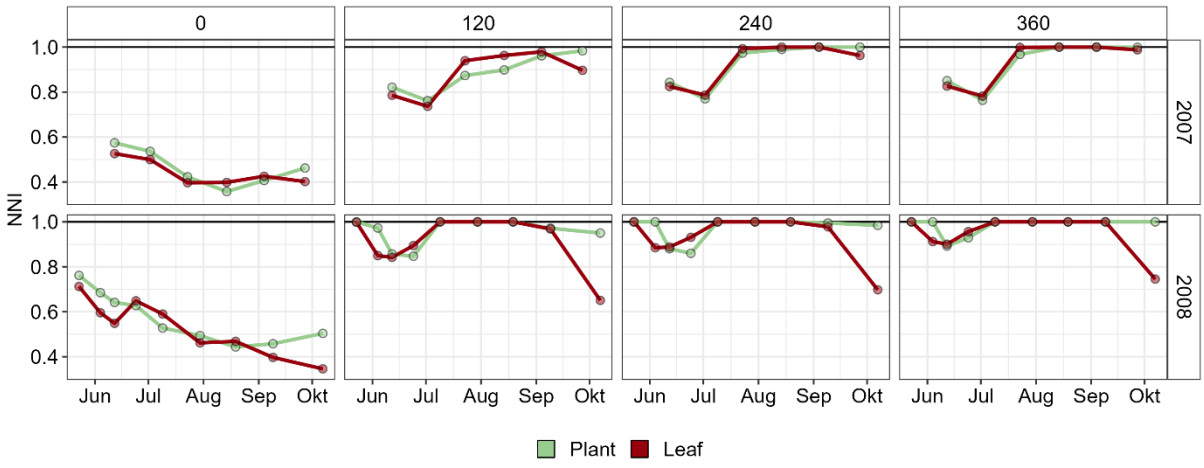

Figure 28 Comparison of nitrogen nutrition index (NNI) derived by dilution curve based on (whole) plant (red) and on leaf (green) N concentrations. The facets show the N-levels 0, 120, 240 and 360 [kg N ha^{-1}] for the years 2007 and 2008.

Implementation in HUME-Maize

The HUME-Maize model was extended by N uptake component, which required an extension of the soil water component about N dynamics, as well. Latter was adopted from HUME-Wheat, e.g. Ratjen and Kage (2015). To provide flexibility, the above described organ-specific N dilution curves have been implemented as an option (Figure 27). At daily level, the N_{crit} is calculated for the current DM of the regarded organ, using the respective N dilution curve described above (Table 13). Subsequently, the N demand is calculated as the difference between the optimal N content derived by the previously calculated N_{crit} and the organs actual N content (N_v). This gap represents the amount of N the organ requires to reach its optimal N status:

$$\text{N Demand}=\left((DM_v+DM_c)*N_{crit}\right)-N_v \quad | \, DM_c>0 \tag{E2}$$

Where the subscript "v" stands for the current status and "c" for the growth occurring at the regarded day. The formula can be applied to all organs, respectively. Additionally, the demand of each organ is summarised to a plants total N demand.

The amount of N that can be taken up is limited by the N supply provided by the soil on that specific day which is composed of N storage, N fertiliser added at the beginning of the growth period and mineralised N. Therefore, N uptake cannot exceed the daily N availability, ensuring a realistic representation of soil-plant nitrogen interactions.

$$\text{Supply-Demand-Ratio (S:D)}=\frac{\text{N Supply}}{\text{N Demand}} \tag{E3}$$

At a specific timepoint, leaf and stems daily DM increase (DM_c) turns negative. They cease to take up N and begin to reallocate accumulated N to other parts of the plant. This N translocation primarily targets the cob, supporting generative growth. During this phase, a negative N demand is calculated based on the leaf's or/and stem's specific daily growth or reduction rates of DM:

$$\text{N Demand}=DM_c*Nc_v \quad | \, DM_c<0 \tag{E4}$$

The surplus nitrogen is moved to a translocation pool (N_{trans}). If the cob's N demand exceeds the N supplied directly by the soil, the deficit is fulfilled using N from the translocation pool. This ensures that the cob's N needs are met efficiently, even under soil N limitations.

Analog to Chapter 2, the new model component was calibrated with the dataset from 2007 and 2008, and evaluated with data from 2021 and 2022. Due to the distribution of these N levels, the evaluation dataset appears to be more suitable for estimating critical N concentrations.

However, the number of sampling dates, particularly during the early growth stages, was very limited.

The calibration of the model component achieved an R^2 of 0.86, 0.78, 0.71 and 0.68 for whole plant, leaf, stem and cob N content, respectively. However, evaluating the model, the whole plant's N content (which is the sum of the organs N content) fits with an R^2 of 0.61. For the 0N and 60N levels, the N content is mostly underestimated, whereas 240N level tend to be overestimated. However, 120 and 180N align well with the model in the example of Hohenschulen 2021 in (Figure 29, top row). Considering the overall dataset, the model slightly overestimated higher N content values for the whole plant. This overestimation was more pronounced for leaf N content. This can be either traced back to inaccuracies in DM partitioning of Chapter 3 and/or indicating a cultivar-specific effect. The cultivars registration dates used in this study were more than 10 years apart from each other. Breeding progress has since worked on the efficiency of the varieties. Taube et al. (2020) identified leaf characteristics as leave number, length and orientation, as main factors driving the yield progress of maize since the 1970's. (Ciampitti et al., 2021) recently reviewed all available N_{crit} data for maize to analyse the differences in parameters. They revealed small differences for parameter b discussing cultivar specific differences between North American and Asian cultivars. Thereby also an interaction with management effects in the contrasting environments may possibly cause the differences.

The translocation processes were well captured by the model for leaf and stem, as the general course of the curve is accurately reflected (Figure 29, top row). The slopes of the 1:1-comparisons in Figure 29 (bottom row) for stem and cob N content were close to one, with R^2 values of 0.42 and 0.64, respectively. Particularly, 120 and 180N matched well with the model prediction. The elevated fertilization level (240N) was not fully represented by the model for leaf N, as illustrated in the example of Hohenschulen 2021 (Figure 29, top row). The underestimation of low N-levels across all regarded fractions (organs and whole plant) could indicate an underestimation of N soil supply. In line with Carpenter-Boggs et al. (2000) and Mahal et al. (2019), Bukowiecki et al. (under review) identified net N mineralisation was highest in the absence of N fertilisation, while N fertilisation was found to reduce net N mineralisation. Despite the implementation of a N recovery factor of 0.8 in HUME, which reduces the N supplied by N fertilisation to 80%, the feedback loop between the two processes may be more complex and therefore not adequately depicted. Moreover, during the 14-year period between the field trials, when calibration and evaluation took place, temperatures increased due to climate change. Since temperature is a key parameter driving mineralisation, this may require an adjustment of processes within the soil N supply component (Cassman and Munns, 1980). Alternatively,

higher measured N uptake without N fertilization compared to models' predictions could indicate an increased N efficiency of new cultivars (15 years between release of the used cultivar in calibration and evaluation), possibly by an earlier and deeper root growth. However, Taube et al. (2020) found root biomass in newer cultivars to be not distinctly higher than in old ones.

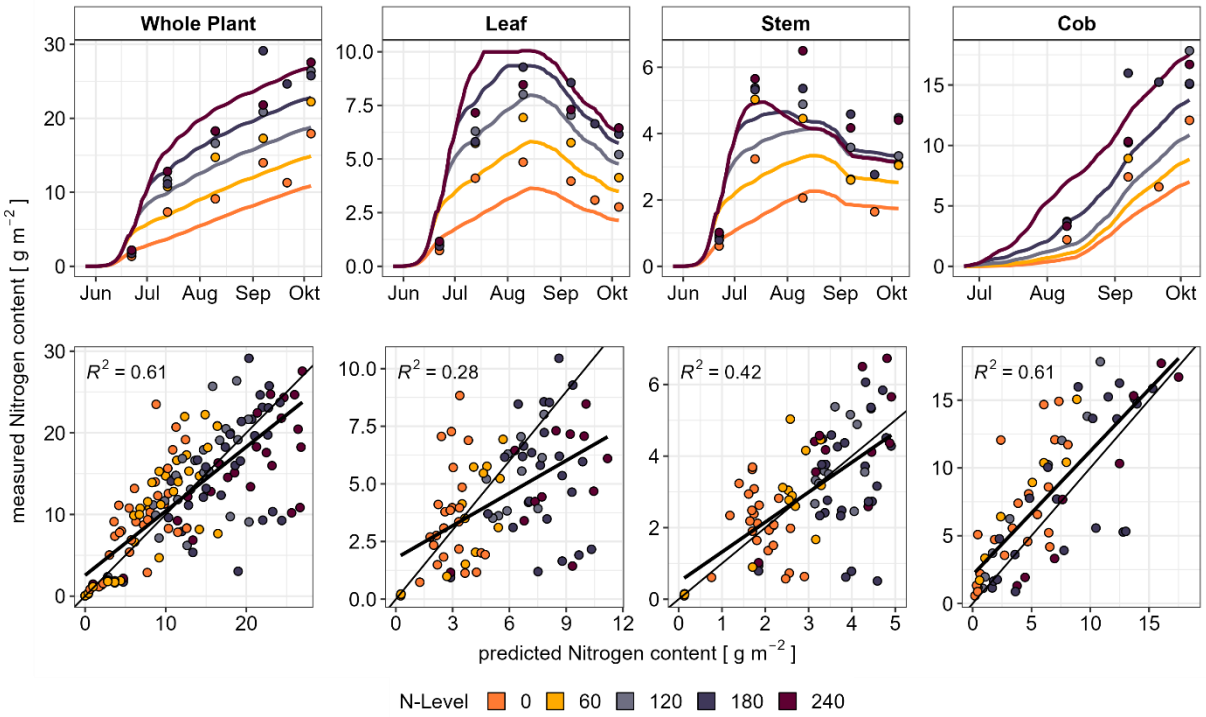

Figure 29 Evaluation of the HUME-Maize nitrogen component, including the fitted N-dilution curves for organs (leaf, stem, cob). On the left side, N content [g m^{-2}] is modelled (line) for Hohenschulen experimental farm in 2021 for each organ and the whole plant (as the sum of the organs), with the measurements as points. On the right side a 1:1 plot for the whole dataset with a regression line for measured vs. predicted N content. Coloured are the N-levels 0, 60, 120, 280, 240.

In summary, the model is now capable of simulating yield responses to varying weather conditions, soil properties, and N availability. Potential for further development lies in improving the soil water component with respect to mineralisation processes, as well as in analysing cultivar-specific differences in nitrogen uptake and distribution patterns.

References

Ata-Ul-Karim, S.T., Zhu, Y., Liu, X., Cao, Q., Tian, Y., Cao, W., 2017. Comparison of different critical nitrogen dilution curves for nitrogen diagnosis in rice. Sci Rep 7, 42679.

Bertheloot, J., Andrieu, B., Fournier, C., Martre, P., 2008. A process-based model to simulate nitrogen distribution in wheat (Triticum aestivum) during grain-filling. Functional plant biology : FPB 35, 781–796.

Blanco-Canqui, H., 2024. Do cover crop mixtures improve soil physical health more than monocultures? Plant and Soil 495, 99–112.

Böhm, W., 1979. Root Parameters and Their Measurement. In: Böhm, W. (Ed.) Methods of Studying Root Systems. Springer Berlin / Heidelberg, Berlin, Heidelberg, pp. 125–138.

Bretz, F., Hothorn, T., Westfall, P.H., 2011. Multiple comparisons using R. Chapman & Hall/CRC, Boca Raton.

Bukowiecki, J., Ullrich, L., Komainda, M., Herrmann, A., Möller, K., Liebisch, F., Manevski, K., Jaufmann, E., Grunert, M., Kage, H., Kühling, I., under review. A closer look at European fertilizer legislations for silage maize: Part I – inaccurate account of net nitrogen mineralization.

Bundesministerium der Justiz und für Verbraucherschutz, 2017. Verordnung über Anwendung von Düngemitteln, Bodenhilfsstoffen, Kultursubstraten und Pflanzenhilfsmittlen nach den Grundsätzen der guten fachlichen Praxis biem Düngen - Düngeverordnung: DüV, 53 pp.

Caloin, M., Yu, O., 1984. Analysis of the Time Course of Change in Nitrogen Content in Dactylis glomerata L. Using a Model of Plant Growth. Ann Bot 54, 69–76.

Carpenter-Boggs, L., Pikul, J.L., Vigil, M.F., Riedell, W.E., 2000. Soil Nitrogen Mineralization Influenced by Crop Rotation and Nitrogen Fertilization. Soil Science Soc of Amer J 64, 2038–2045.

Cassman, K.G., Munns, D.N., 1980. Nitrogen Mineralization as Affected by Soil Moisture, Temperature, and Depth. Soil Science Soc of Amer J 44, 1233–1237.

Chapagain, T., Lee, E.A., Raizada, M.N., 2020. The Potential of Multi-Species Mixtures to Diversify Cover Crop Benefits. Sustainability 12, 2058.

Chen, G., Weil, R.R., 2010. Penetration of cover crop roots through compacted soils. Plant Soil 331, 31–43.

Ciampitti, I.A., Fernandez, J., Tamagno, S., Zhao, B., Lemaire, G., Makowski, D., 2021. Does the critical N dilution curve for maize crop vary across genotype x environment x management scenarios? - a Bayesian analysis. European Journal of Agronomy 123, 126202.

Colnenne, C., 1998. Determination of a Critical Nitrogen Dilution Curve for Winter Oilseed Rape. Ann Bot 81, 311–317.

Couëdel, A., Alletto, L., Tribouillois, H., Justes, É., 2018. Cover crop crucifer-legume mixtures provide effective nitrate catch crop and nitrogen green manure ecosystem services. Agriculture, Ecosystems & Environment 254, 50–59.

Debaeke, P., van Oosterom, E.J., Justes, E., Champolivier, L., Merrien, A., Aguirrezabal, L., González-Dugo, V., Massignam, A.M., Montemurro, F., 2012. A species-specific critical nitrogen dilution curve for sunflower (Helianthus annuus L.). Field Crops Research 136, 76–84.

Finney, D.M., Murrell, E.G., White, C.M., Baraibar, B., Barbercheck, M.E., Bradley, B.A., Cornelisse, S., Hunter, M.C., Kaye, J.P., Mortensen, D.A., Mullen, C.A., Schipanski, M.E., 2017. Ecosystem Services and Disservices Are Bundled in Simple and Diverse Cover Cropping Systems. Agricultural & Env Letters 2, 170033.

Finney, D.M., White, C.M., Kaye, J.P., 2016. Biomass Production and Carbon/Nitrogen Ratio Influence Ecosystem Services from Cover Crop Mixtures. Agronomy Journal 108, 39–52.

Florence, A.M., Higley, L.G., Drijber, R.A., Francis, C.A., Lindquist, J.L., 2019. Cover crop mixture diversity, biomass productivity, weed suppression, and stability. PLOS ONE 14, e0206195.

Greenwood., D., Gastal, F., Lemaire, G., Draycott, A., Millard, P., Neeteson, J., 1991. Growth Rate and % N of Field Grown Crops: Theory and Experiments. Ann Bot 67, 181–190.

Herrmann, A., Taube, F., 2004. The Range of the Critical Nitrogen Dilution Curve for Maize (Zea mays L.) Can Be Extended Until Silage Maturity. Agronomy Journal 96, 1131–1138.

Hothorn, T., Bretz, F., Westfall, P., 2008. Simultaneous inference in general parametric models. Biometrical journal. Biometrische Zeitschrift 50, 346–363.

Justes, E., Mary, B., Meynard, J.M., Machet, J.M., Thelier-Huche, L., 1994. Determination of a Critical Nitrogen Dilution Curve for Winter Wheat Crops. Annals of Botany 74, 397–407.

Kemper, R., Bublitz, T.A., Müller, P., Kautz, T., Döring, T.F., Athmann, M., 2020. Vertical Root Distribution of Different Cover Crops Determined with the Profile Wall Method. Agriculture 10, 503.

Kristensen, H.L., Thorup-Kristensen, K., 2004. Root Growth and Nitrate Uptake of Three Different Catch Crops in Deep Soil Layers. Soil Science Soc of Amer J 68, 529–537.

Kühling, I., Mikuszies, P., Helfrich, M., Flessa, H., Schlathölter, M., Sieling, K., Kage, H., 2023. Effects of winter cover crops from different functional groups on soil-plant nitrogen dynamics and silage maize yield. European Journal of Agronomy 148, 126878.

Lemaire, G., Gastal, F., 1997. N Uptake and Distribution in Plant Canopies. In: Diagnosis of the Nitrogen Status in Crops. Springer, Berlin, Heidelberg, pp. 3–43.

Lemaire, G., Salette, J., 1984. Relation entre dynamique de croissance et dynamique de prelevement d'azote pour un peuplement de graminees fourrageres. I. - Etude de l'effet du milieu. Agronomie 4, 423–430.

Mahal, N.K., Osterholz, W.R., Miguez, F.E., Poffenbarger, H.J., Sawyer, J.E., Olk, D.C., Archontoulis, S.V., Castellano, M.J., 2019. Nitrogen Fertilizer Suppresses Mineralization of Soil Organic Matter in Maize Agroecosystems. Front. Ecol. Evol. 7.

Möller, K., Reents, H.-J., 2009. Effects of various cover crops after peas on nitrate leaching and nitrogen supply to succeeding winter wheat or potato crops. Journal of Plant Nutrition and Soil Science 172, 277–287.

Pinheiro, J.C., Bates, D.M. (Eds.), 2010. Mixed-effects models in S and S-PLUS, 2000th ed. Springer, New York, Berlin, Heidelberg, 528 pp.

Plénet, D., Lemaire, G., 1999. Relationships between dynamics of nitrogen uptake and dry matter accumulation in maize crops: Determination of critical N concentration. Plant Soil 216, 65–82.

R Core Team, 2024. R: A language and environment for statistical computing. R foundation for statistical computing, Vienna, Austria.

Ramírez-García, J., Carrillo, J.M., Ruiz, M., Alonso-Ayuso, M., Quemada, M., 2015. Multicriteria decision analysis applied to cover crop species and cultivars selection. Field Crops Research 175, 106–115.

Ranells, N.N., Wagger, M.G., 1997. Grass–Legume Bicultures as Winter Annual Cover Crops. Agronomy Journal 89, 659–665.

Ratjen, A.M., Kage, H., 2015. Forecasting yield via reference- and scenario calculations. Computers and Electronics in Agriculture 114, 212–220.

Saleem, M., Pervaiz, Z.H., Contreras, J., Lindenberger, J.H., Hupp, B.M., Chen, D., Zhang, Q., Wang, C., Iqbal, J., Twigg, P., 2020. Cover crop diversity improves multiple soil properties via altering root architectural traits. Rhizosphere 16, 100248.

Sieling, K., Kage, H., 2021. Organ-specific critical N dilution curves and derived NNI relationships for winter wheat, winter oilseed rape and maize. European Journal of Agronomy 130, 126365.

Sinclair, T.R., Horie, T., 1989. Leaf Nitrogen, Photosynthesis, and Crop Radiation Use Efficiency: A Review. Crop Science 29, 90–98.

Smith, R.G., Atwood, L.W., Warren, N.D., 2014. Increased productivity of a cover crop mixture is not associated with enhanced agroecosystem services. PLOS ONE 9, e97351.

Stipešević, B., Kladivko, E.J., 2005. Effects of winter wheat cover crop desiccation times on soil moisture, temperature and early maize growth. Plant Soil Environ. 51, 255–261.

Taube, F., Vogeler, I., Kluß, C., Herrmann, A., Hasler, M., Rath, J., Loges, R., Malisch, C.S., 2020. Yield Progress in Forage Maize in NW Europe—Breeding Progress or Climate Change Effects? Front. Plant Sci. 11, 473.

Ulrich, A., 1952. Physiological Bases for Assessing the Nutritional Requirements of Plants. Annu. Rev. Plant. Physiol. 3, 207–228.

Wortman, S.E., Francis, C.A., Lindquist, J.L., 2012. Cover Crop Mixtures for the Western Corn Belt: Opportunities for Increased Productivity and Stability. Agronomy Journal 104, 699–705.

Yue, S., Sun, F., Meng, Q., Zhao, R., Li, F., Chen, X., Zhang, F., Cui, Z., 2014. Validation of a Critical Nitrogen Curve for Summer Maize in the North China Plain. Pedosphere 24, 76–83.

Zhang, C., Postma, J.A., York, L.M., Lynch, J.P., 2014. Root foraging elicits niche complementarity-dependent yield advantage in the ancient 'three sisters' (maize/bean/squash) polyculture. Ann Bot 114, 1719–1733.

Zhao, B., 2014. Determining of a critical dilution curve for plant nitrogen concentration in winter barley. Field Crops Research 160, 64–72.

Zhao, B., Ata-Ul-Karim, S.T., Duan, A., Liu, Z., Wang, X., Xiao, J., Liu, Z., Qin, A., Ning, D., Zhang, W., Lian, Y., 2018. Determination of critical nitrogen concentration and dilution curve based on leaf area index for summer maize. Field Crops Research 228, 195–203.

Zhao, B., Ata-Ul-Karim, S.T., Liu, Z., Ning, D., Xiao, J., Liu, Z., Qin, A., Nan, J., Duan, A., 2017. Development of a critical nitrogen dilution curve based on leaf dry matter for summer maize. Field Crops Research 208, 60–68.

Ziadi, N., Brassard, M., Bélanger, G., Cambouris, A.N., Tremblay, N., Nolin, M.C., Claessens, A., Parent, L.-É., 2008. Critical Nitrogen Curve and Nitrogen Nutrition Index for Corn in Eastern Canada. Agronomy Journal 100, 271–276.

Chapter 6

Overall Conclusion

This study examines key factors for sustainable and resource-efficient silage maize cultivation, with a particular focus on the integration of cover crops and their mixtures. The results demonstrate a precise simulation of silage maize under various climatic conditions, soil types, drought stress scenarios and nitrogen availabilities. Cover crop mixtures facilitated access to deeper soil water reserves and, in some cases, achieved high resource efficiencies of silage maize. The observed effects are crucial for further refinements of the model.

However, the underlying mechanisms behind the increased water use from deeper soil layers following cover crops remain unclear. Further research is needed to determine whether maize roots grow deeper or faster compared to silage maize after winter fallow or whether improved nutrient availability after cover crops plays a crucial role. Understanding these factors is essential for the simulation of root growth and soil dynamics of silage maize cultivation.

Calibration multispectral reflectance of cover crops allows a precise estimation of nitrogen uptake by cover crops, thereby improving predictions of nitrogen availability before maize sowing and enhancing the understanding of nitrogen dynamics within the system. However, a key research gap remains in the understanding of mineralisation processes. This is especially relevant in the context of cover crop cultivation before maize, as nitrogen availability can vary depending on the decomposition rates of above- and below-ground residues.

A deeper understanding of these processes is essential for optimizing nitrogen management and improving the overall sustainability of maize-based cropping systems.

Chapter 7

Summary

Silage maize (Zea mays) is a key crop in European agriculture, with 5-6 million hectares cultivated annually (2024: 5.8 million hectares), including 2 million hectares in Germany. In addition to its use as animal feed, silage maize is also a valuable resource for biogas production. Breeding, optimised management practices, and climate change have led to increasing yields, particularly in the northern growing regions of Europe. Within the framework of the Common Agricultural Policy (2023–2027) promotes sustainable practices that contribute to climate and environmental protection. These include crop diversification through regular crop rotation or the integration of cover crops before spring crops. Cover crops provide important environmental benefits, including replenishment of soil organic matter, in arable soils and improve erosion control and nitrogen retention. In particular, mixtures of different cover crop species are gaining attention, as functional diversity is expected to enhance resource utilisation and system stability. At the same time, the configuration of such mixtures represents a scientific challenge. This study examines key factors for sustainable and resource-efficient silage maize cultivation, with a particular focus on the integration of cover crops and their mixtures.

The HUME-Maize crop growth model was recalibrated for silage maize under northern European conditions. An evaluation using independent data demonstrated realistic yield predictions across various climates and soil types. Additionally, new algorithms were implemented to simulate nitrogen uptake under different fertilization levels. However, further adjustments are needed to account for breeding advancements, such as leaf-stem allometry and radiation use efficiency.

A three-year field experiment in northern Germany investigated the effects of different cover crop mixtures (grasses, crucifers, legumes) and perennial alfalfa on maize growth and yield. The results showed that mixtures comprising grasses supported high maize yields, whereas legume-crucifer mixtures and alfalfa led to yield reductions. Nevertheless, all mixtures facilitated maize access to deep soil water resources, thereby improving drought stress tolerance.

Drone-based remote sensing enabled precise estimation of cover crop dry biomass during the winter months. Universal estimation equations provided practical results for biomass, leaf development, and nitrogen uptake. While mixture- or species-specific models proved more accurate, they were based on smaller datasets.

The field studies, empirical analyses, and process modelling presented in this study provide a comprehensive understanding of the crop rotation sequence involving silage maize and cover crops. In the future, the conditions created by cover crops, particularly improved access to water resources, should be incorporated into the HUME-Maize model. This will enable site-specific yield predictions for maize following cover crops and contribute to more resource-efficient and stable maize production.

Chapter 8

Zusammenfassung

Silage-Mais (Zea mays) ist mit 5–6 Millionen Hektar Anbaufläche jährlich eine der wichtigsten Kulturpflanzen in Europa. Sie wird zur Tierfütterung, sowie als Substrat für Biogas verwendet. Züchtung, verbesserte Anbautechniken und der Klimawandel haben insbesondere in den nördlicheren Anbaugebieten Europas zu steigenden Erträgen geführt. Im Rahmen der Gemeinsamen Agrarpolitik (2023-2027) werden nun nachhaltige Praktiken die zum Klima- und Umweltschutz beitragen gefördert. Dazu gehört zum Beispiel die Diversifizierung von Fruchtfolgen via regelmäßigen Fruchtwechsel oder der Integration von Zwischenfrüchten vor Sommerungen. Zwischenfrüchte tragen zur Reproduktion der organischen Substanz von Ackerböden bei und verbessern die Erosionskontrolle und Stickstoffretention. Mischungen aus verschiedenen Arten können durch funktionale Diversität Vorteile bieten. Die optimale Kombination verschiedener Arten in Mischungen stellt jedoch eine wissenschaftliche Herausforderung dar. Diese Arbeit untersucht zentrale Faktoren für einen nachhaltigen und ressourceneffizienten Silomaisanbau, mit besonderem Fokus auf die Einbindung von Zwischenfrüchten und deren Mischungen.

Das Pflanzenwachstumsmodell HUME-Mais wurde für Silage-Mais unter nordeuropäischen Bedingungen neu kalibriert. Eine Evaluierung mit unabhängigen Daten zeigte realistische Ertragsprognosen des Modells unter verschiedenen Klimata und Bodentypen. In einem weiteren Schritt wurden neue Algorithmen für die Stickstoffaufname unter verschiedenen Düngemengen implementiert. Eine Anpassung zur Abbildung züchterischer Fortschritte, wie z.B. bei der Blatt-Stängel-Allometrie und Lichtnutzungseffizienz, sind noch erforderlich.

Ein dreijähriger Feldversuch in Norddeutschland untersuchte die Effekte verschiedener Zwischenfruchtmischungen (Gräser, Kreuzblütler, Leguminosen) und mehrjähriger Luzerne auf das Wachstum und den Ertrag von Mais. Die Ergebnisse zeigten, dass grashaltige Mischungen hohe Maiserträge ermöglichten, während Leguminosen-Kreuzblütler-Mischungen und Luzerne zu Ertragsminderung führten. Dennoch erleichterten alle Mischungen den Zugang von Mais zu tiefen Bodenwasserressourcen, was die Trockenstresstoleranz steigert.

Drohnengestützte Fernerkundung ermöglichte die präzise Dokumentation der Wachstumsphase der Zwischenfrüchte in den Wintermonaten. Universelle Schätzgleichungen lieferten praktikable Ergebnisse zur Schätzung von Trockenmasse, Blattentwicklung und

Stickstoffaufnahme. Mischungs- oder artspezifische Modelle waren präziser, basieren jedoch auf kleineren Datensätzen.

Die Feldstudien, empirischen Analysen und Prozessmodellierung liefern ein umfassendes Verständnis der Fruchtfolge-Sequenz von Zwischenfrüchten und Silage-Mais. Zukünftig sollen die durch Zwischenfrüchte geschaffenen Bedingungen, insbesondere der verbesserte Zugang zu Wasserressourcen, im HUME-Mais-Modell abgebildet werden. Dies wird die standortspezifische Vorhersage von Maiserträgen nach Zwischenfrüchten ermöglichen und zu einem ressourceneffizienteren und stabileren Maisanbau beitragen.

Curriculum Vitae

Persönliches	
	Katja Holzhauser
	08.02.1995, St.Ingbert
	Sternstraße 2, 24116 Kiel
	holzhauser@pflanzenbau.uni-kiel.de
Ausbildung	
2001 – 2005	Südschule St.Ingbert
2005 – 2013	Leibniz-Gymnasium Allgemeine Hochschulreife
2014 – 2017	Universität Trier Bachelor of Science im Fach Umweltgeowissenschaften
2017 – 2020	Albert-Ludwig-Universität Freiburg Master of Science im Fach Environmental Sciences Schwerpunkt: Landnutzung und Naturschutz
Seit 2020	Christian-Albrechts-Universität zu Kiel Promotion im Fach Agrarwissenschaften
Berufliche Erfahrung	
Seit 2020	Wissenschaftliche Mitarbeiterin Rhizo4Bio (Phase 1 und 2): RootWayS – Deep-rooting cover crop mixtures: Creating highways to subsoil water and nutrient resources Christian-Albrechts-Universität zu Kiel, Abteilung Acker- und Pflanzenbau

Ich möchte mich herzlich bei meinem Doktorvater, Prof. Dr. Henning Kage, für die Betreuung, die zahlreichen Diskussionen und das Vertrauen in den vergangenen Jahren bedanken. Aber auch für die Flexibilität und Freiräume, die er mir gewährt hat, sowie für die Geduld, die er mit mir hatte.

Ich habe viel von Ihnen gelernt und schätze dies sehr.

Ein ebenso großes Dankeschön geht an meine Kollegin und Freundin Josephine für ihre unermüdliche Unterstützung und Rückendeckung, besonders in schwierigen Phasen. Aber auch für die wunderbare Atmosphäre in unserem Büro und die bereichernden Gespräche und Diskussionen danke ich ihr von Herzen.

Meinem engsten Freund und langjährigen Gefährten Julian, für seinen Rat, die stets offenen Ohren und seine Verlässlichkeit in jeder Situation.

Ich danke auch meiner Kollegin Insa für ihr konstruktives Feedback, ihre fachliche Expertise und ihre immer offene Tür.

*Mein Dank gilt außerdem allen Kolleg*innen und Hiwis, die mich in den letzten Jahren unterstützt haben – egal ob bei Wind, Regen oder Schnee, beim Gruben graben, dem Regendachdrama oder dem mühsamen Pulen von Zwischenfrüchten. Ein besonderer Dank geht an Merlin für seine Zuverlässigkeit und die vielen gemeinsamen Ausflüge nach Hohenschulen. Für ihre Unterstützung bei den Laboranalysen und ihre Expertise im Feld danke ich Cotschie, Kirsten, Doris und Gunda.*

Ich bin meiner Familie unendlich dankbar für das Vertrauen, das sie mir entgegenbringt, und für die Freiheit, meinen eigenen Weg zu gehen – selbst wenn uns dieser räumlich so weit voneinander trennt.

*Zu guter Letzt möchte ich meinen Kieler Freund*innen danken, die Kiel für mich zu einem neuen Zuhause gemacht haben und immer für mich da sind. Ein besonderer Dank geht an meine liebe WG in der Sternstraße, die mich nach langen Büro- und Feldtagen stets auffängt und zum Lachen bringt. Ein tief empfundenes Dankeschön geht an Johann – für seine Geduld und seine beständige Gesellschaft in vielen schwierigen Momenten.*

In der Schriftenreihe des Institutes für Pflanzenbau und Pflanzenzüchtung der Christian-Albrechts-Universität zu Kiel sind bisher erschienen:

Heft	Autor	Jahr	Titel
1	Heller, R.	1997	Die genetische Analyse nematodenresistenter Zuckerrüben mit molekularen Markern
2	Schröder, Heidi	1997	Untersuchungen zur Ertragsbildung und Stickstoffverwertung von Wintergerstenbeständen in verschiedenen Produktionssystemen
3	Kornher, Alois Wulfes, Rainer Wachendorf, Michael Taube, Friedhelm	1998	Untersuchungen zur Dynamik der Ertragsbildung und der Qualitätsentwicklung von Extensivgrünland
4	Richter, K.	1998	Die Lokalisation von Genen für die Resistenz gegen die Netzfleckenkrankheit (*Drechslera teres*) in der Gerste
5	Kifle, Sirak	1998	Das *hairy roots*-Transformationssystem zur Expression des Nematodenresistenzgens *HS1* in Zuckerrüben und *Arabidopsis thaliana*
6	Puzio, Stefanie	1998	Untersuchungen zur Überwinterung und zum jahreszeitlichen Verlauf der Ertragsbildung von Weißklee in Abhängigkeit von der Witterung und der Sorteneigenschaft
7	Christen, Olaf	1998	Untersuchungen zur Anbautechnik von Winterweizen nach unterschiedlichen Vorfruchtkombinationen
8	Schacht, Johannes	1998	Beiträge zur Nutzung von Wildformen zur Verbesserung quantitativ vererbter Merkmale am Beispiel Gerste
9	Loges, Ralf	1998	Ertrag, Futterqualität, N_2-Fixierungsleistung und Vorfruchtwert von Rotklee- und Rotkleegrasbeständen
10	Teebken, Tammo	1998	N-Dynamik unter der Fruchtfolge Winterraps-Winterweizen-Wintergerste bei mehrjähriger Rotationsdauer und unterschiedlichen Produktionsintensitäten sowie einfache Ansätze zur N-Bilanzierung
11	Winkelmann, Christoph	1999	Ertragsbildung von Winterweizen in Abhängigkeit von Fruchtfolgestellung, Anbautechnik und Bodenunterschieden
12	Setiawan, Asep	1999	Mapping quantitative trait loci (QTL) for resistance to leaf spot disease (*Cercospora beticola* Sacc.) in sugar beet (*Beta vulgaris* L.)
13	Ruhe, Iris	2000	Winterweizenanbau in stickstofflimitierten Produktionssystemen unter besonderer Berücksichtigung der Ertragsbildung, der organischen Düngung und der mechanischen Beikrautregulierung

14	Oberschmidt, Olaf	2000	Anwendung der *differential display*-Technik zur Isolierung und Analyse von differenziell expremierten Genen in nematodenresistenten Zuckerrüben (*Beta vulgaris* L.)
15	Hühn, Manfred	2000	Universität und Bildungsauftrag. Wirklichkeit oder Farce?
16	Sieling, Klaus	2000	Untersuchungen zu den Auswirkungen unterschiedlicher Produktionssysteme auf einige Parameter des N-Haushaltes von Boden und Pflanze
17	Kaske, Axel	2000	Leistungen unterschiedlich bewirtschafteter Futterleguminosenbestände und deren Auswirkungen auf Ertrag und ausgewählte Kenngrößen des Stickstoffhaushaltes der Folgefrucht Winterweizen
18	El-Mezawy, Aliaa	2001	Fine mapping of the bolting gene from sugar beet (*Beta vulgaris* L.) with molecular markers
19	Gao, Dongjie	2001	Molecular and cytological characterization of a full set of monosomic addition lines from *Beta corolliflora* in *Beta vulgaris* and chromosomal localization of resistance genes to leaf spot (*Cercospora beticola*) and rhizomania disease from wild beets
20	Jacobs, Gunnar	2001	Physikalische Kartierung der Region des Schossgens der Zuckerrübe (*Beta vulgaris* L.)
21	Ingwersen, Bernhard	2001	Einfluss von Bewirtschaftungsmaßnahmen auf die Leistungsfähigkeit von leguminosenbasiertem Dauergrünland unter besonderer Berücksichtigung der Nährstoffbilanzierung
22	Teebken, Tammo Hanus, Herbert	2001	Landwirtschaftliche Produktion und Umweltaspekte – eine Literaturrecherche unter besonderer Berücksichtigung der Produktionsintensität
23	Große-Herrenthey, Ute	2002	Molekulare Analyse der genetischen Variabilität von *Cercospora beticola* Sacc., dem Erreger der Cercospora-Blattfleckenkrankheit bei Zuckerrüben, und Untersuchungen zur Resistenz von *Beta vulgaris* spp. *maritima* gegen *C. beticola* unter Anwendung unterschiedlicher Resistenztestsysteme
24	Tahir, Muhammand Shafique	2002	Reaction of different wheat (*Triticum aestivum* L.) genotypes in response to salt stress and genetic mapping of OTL for salt tolerance using AFLP markers
25	Thurau, Tim,	2002	Der Einfluss stromaufwärts gelegener regulatorischer Sequenzen auf die Transkriptionsintensität des *Hs1^{pro-1}*-Gens für Nematodenresistenz aus der Zuckerrübe
26	Wegelin, Tanja	2002	Bestimmung von Funktion und Wirkungsweise des *Hs1^{pro-1}* Nematodenresistenzgens aus *Beta procumbens*
27	Samuelian, Suren	2002	Identification of genes differentially expressed upon nematode infection by cDNA-AFLP analysis
28	Trott, Hagen Theo	2003	Mittelfristige Auswirkungen einer variierten Bewirtschaftungsform und N-Intensität auf Leistungsparameter und die Stickstoffbilanz von Dauergrünland

29	Treue, Peter	2003	Potenziale und Grenzen teilflächenspezifischer N-Düngung in Schleswig-Holstein/Precision Agriculture
30	Büchter, Manfred	2003	Nitratauswaschungen unter Grünland und Silomais in Monokultur auf sandigen Böden Norddeutschlands
31	Tian, Yanyan	2003	PCR-based cloning of the second nematode resistance gene *Hs1-1*$^{pro-1}$ and resistance gene analogues form sugar beet (*Beta vulgaris* L.)
32	Brase, Thorsten	2003	Einfluss der N-Dynamik in unterschiedlichen Produktionssystemen auf die Ertragsbildung von Raps, Weizen und Gerste sowie die N-Auswaschung
33	Jamsari, Ir.	2003	Construction of high-density genetic and physical maps around the sex gene *M* of *Asparagus officinalis* L.
34	Kelm, Michael	2004	Strategies for sustainable agriculture with particular regard to productivity and fossil energy use in forage production and organic arable farming
35	Wichmann, Stefan	2004	Ertragsleistung, Futterqualitätsentwicklung, N_2-Fixierungsleistung und Vorfruchtwirkung von verschiedenen Körnerleguminosenarten in Reinsaat und Gemenge mit Getreide
36	Gaafar, Reda Mohamed	2005	Fine mapping of the bolting gene of sugar beet (*Beta vulgaris* L) using BAC-derived sequences
37	Lampe, Carola	2005	Effect of nitrogen fertiliser and animal excrements on N_2O emissions from permanent grassland using ^{15}N-labelling
38	Beims, Sandra	2005	Untersuchungen zur N-Effizienz und zum N-Mineralisationspotenzial in langjährig unterschiedlichen Düngungssystemen mit Hilfe von ^{15}N markiertem Mineraldünger
39	Baade, Julia	2005	Untersuchungen zur Futteraufnahme, Futterqualität und –selektion auf Umtriebsweiden mittels einer pflanzenbaulichen Methode
40	Volkers, Karen	2005	Auswirkungen einer variierten Stickstoffintensität auf Leistung und Stickstoffbilanz von Silomais in Monokultur sowie einer Ackerfutterbau-Fruchtfolge auf sandigen Böden Norddeutschlands
41	Dreymann, Sonja	2005	N-Haushalt unterschiedlich bewirtschafteter Rotklee-Bestände und deren Bedeutung für die Folgefrucht Weizen im Ökologischen Landbau
42	Bobe, Janina	2005	Nitratbelastung von Sickerwasser und Grundwasser in Futterbausystemen auf sandigen Böden Norddeutschlands
43	Neumann, Helge	2005	Optimierungsstrategien für den Getreideanbau im ökologischen Landbau: System “weite Reihe” und Direktsaat in ausdauernden Weißklee (“Bi-cropping”)
44	Hamwieh, Aladdin	2005	Development of simple sequence repeat (SSR) and AFLP markers for linkage mapping in lentil (*Lens culinaris* Medik)

45	Kruse, Sandra	2006	Charakterisierung und Modellierung des Abreifeverhaltens von Silomaisgenotypen mittels futterwertbestimmender Parameter
46	Schulte, Daniela	2006	Physische Kartierung und Sequenzierung einer Translokation aus der Wildart Beta procumbens am Zuckerrüben-Chromosom 9
47	Werner, Susanne	2007	Genetische Kartierung von Kohlhernie (*Plasmodiophora brassicae*) - Resistenzgenen in Raps
48	Telgmann-Rauber, Alexa	2007	Untersuchungen zur Struktur des Spargel-Chromosoms L5 mit dem geschlechtsdeterminierten Locus M
49	Treyse, Katharina	2007	Indikatoren für eine nachhaltige intensive Grünlandbewirtschaftung
50	Jung, Christian	2007	Ausgewählte Themen der Pflanzenzüchtung
51	Schiborra, Anne	2007	Short-term effects of defoliation on herbage productivity and herbage quality in a semi-arid grassland ecosystem of Inner Mongolia, P.R. China
52	Endrigkeit, Jessica	2007	Identifikation und Charakterisierung von Genen der Tocopherol-Biosynthese aus Raps (*Brassica napus* L.)
53	Nannen, David	2008	N fluxes in forage production systems as studied by ^{15}N and difference method
54	Henke, Johannes	2008	Entwicklung und Bewertung von Strategien zur Verbesserung der Stickstoffeffizienz im Winterrapsanbau
55	Lange, Tina	2008	Genetische Kartierung und molekulare Identifizierung von Genen für Speicherwurzelbildung in *Brassica napus* L.
56	Mauscherning, Inken	2008	Interseeding catch crops in organic wheat and rape seed production systems
57	Kleen, Jana	2008	Ertragsleistung und Futterqualität verschiedener Leguminosen in binären Gemengen mit Deutschem Weidelgras (*Lolium perenne* L.)
58	Westphal, Derk	2008	Leistung und Vorfruchtwert von Leguminosen-Gras-Beständen im ökologischen Landbau unter Berücksichtigung der Winterbeweidung
59	Eickler, Birgit	2008	Nutritive value of forage legumes with special reference to polyphenol oxidase activity in red clover
60	Keil, Tobias	2008	Selektion von Gerstenherkünften mit Resistenz gegen frei lebende Nematoden der Gattung *Pratylenchus*
61	Müller, Karla	2009	Remote sensing and simulation modelling as tools for improving nitrogen efficiency for winter oilseed rape (*Brassica napus* L.)
62	Fittje, Susanne	2009	Wirkungen des Grünrodens auf Ertrag, Knollenbeschaffenheit und Virusbefall zur Erzeugung von Kartoffelpflanzgut im ökologischen Landbau
63	Kage, Henning & Hollmann, Franz	2009	Norddeutsches Weizen-Forum 2009 – Kurzfassungen der Vorträge
64	Schönbach, Philipp	2009	Grazing effects on productivity and herbage quality of an Inner Mongolian steppe ecosystem – Results of a four-year grazing experiment

65	Gericke, Dirk	2009	Measurement and modelling of ammonia emissions after field application of biogas slurries
66	Taube, Friedhelm	2009	Modelling forage production systems Dedicated to Prof. em. Alois Kornher's 75. birthday
67	Salama, Heba	2010	Process-oriented evaluation of yield performance and nutritive value of perennial rye-grass (*Lolium perenne* L.) genotypes
68	Gong, Xiaoying	2010	Water and nitrogen co-limitation of plant primary production in a semiarid grassland of Inner Mongolia
69	Capistrano, Gina	2010	A candidate sequence for the nematode resistance gene *HS1-2* in sugar beet
70	Lösche, Marc	2010	Nutritive value of perennial ryegrass (*Lolium perenne* L.) with special reference to genotype- and ploidy-related effects
71	Kage, Henning & Hollmann, Franz	2011	Norddeutsches Marktfruchtforum 2011 – Kurzfassungen der Vorträge
72	Abou-Elwafa, Salah	2011	Novel genetic factors affecting bolting and floral transition control in beta vulgaris
73	Büttner, Bianca	2011	Genetic mapping of flowering time genes and functional characterisation of an *FVE* homologue from sugar beet.
74	Bangemann, Lars	2011	Pathogen-nutrient interactions in potato: the case of nitrogen and late blight in organic farming.
75	Krawutschke, Manuel	2011	Qualitätsveränderungen im Zuwachsverlauf und bei der Gärfutterbereitung von Rotklee (*Trifolium pratense* L.) unter besonderer Berücksichtigung der Rohproteinfraktionen
76	Svoboda, Nikolai	2011	Auswirkungen der Gärrestapplikation auf das Stickstoffauswaschungspotential von Anbausystemen zur Substratproduktion
77	Wienforth, Babette	2011	Cropping systems for biomethane production: a simulation based analysis of yield, yield potential and resource use efficiency
78	Wan, Hongwei	2011	Impacts of grazing intensity, grazing system, mowing, and nitrogen fertilization on species dominance and coexistence in typical steppe of Inner Mongolia
79	Weiher, Nina	2011	Variation in the nutritive value of red clover (*Trifolium pratense* L.) with special reference to polyphenol oxidase activity
80	Schmeer, Maria Susanne	2012	Der Einfluss von Bodenverdichtung sowie Grünlanderneuerung auf Stickstoffemissionen und Ertragsleistungen von Futterbausystemen
81	Fritsche, Steffi	2012	Cloning and functional characterization of genes from the tocopherol biosynthesis pathway in rapeseed (*Brassica napus* L.) and candidate gene based association studies of tocopherol content and composition

82	Ren, Haiyan	2013	Impacts of grazing intensity, precipitation and temperature on productivity, forage quality, species composition and diversity in typical steppe of Inner Mongolia
83	Ratjen, Arne Markus	2013	Refined N fertilization of winter wheat: a model supported approach combining statistical and mechanistic components
84	Kage, Henning Sieling, Klaus Hollmann, Franz	2013	Norddeutsches Marktfruchtforum 2013 – Kurzfassungen der Vorträge
85	Pahlmann, Ingo	2013	Entwicklung eines teilflächenspezifischen Düngealgorithmus als Beitrag zur Steigerung der Stickstoffeffizienz und Optimierung der Treibhausgasbilanz im Winterrapsanbau
86	Kardel, Marika	2013	Charakterisierung von Tanninen aus Pflanzenextrakten und deren Einfluss auf pansenphysiologische Parameter
87	Techow, Anna	2013	Leistung und ökologische Effekte von Anbausystemen zur Biogas-/Futtererzeugung
88	Lana, Marcos	2013	Regionalization of climate change impacts and adaptation strategies for maize in Santa Catarina State, Brazil
89	Chen, Shimeng	2014	Sward age and nitrogen determine the quantity and quality of root growth in grass-clover swards
90	Biegemann, Torsten	2014	Grünlandumbruch und Neuansaat: Kurz- und langfristige Effekte auf Treibhausgasemissionen und Ertragsleistungen von Grünlandbeständen
91	Stephan, Helge	2014	Examining the yield potential of winter sugar beet with a process-orientated dynamic simulation model
92	Quakernack, Robert	2014	Biogas cropping systems at a calcareous coastal marsh: productivity, ammonia volatilization, nitrogen use efficiency and soil nitrogen dynamics after fertilization with anaerobic digestates
93	Galal, Ahmed Abdelrahman	2014	Mapping root-leasion nematode resistance QTL in barley (*Hordeum vulgare* L.)
94	Poyda, Arne	2015	Klimarelevanz futterbaulich genutzter Niedermoorböden ind Schleswig-Holstein
95	Rath, Jürgen	2015	Maisgenotypen zur Biogasnutzung: Übersicht, Entwicklung und Validierung eines Modells zur Potenzialabschätzung der Biogasausbeute
96	Weymann, Wiebke	2015	Model-based analysis of weather, soil and management effects on yield formation of winter oilseed rape
97	Ullmann, Ines	2016	The critical phase of stem elongation in perennial ryegrass: a new plant functional trait for understanding yield and forage quality performance
98	Neukam, Dorothee	2016	Modelling wheat canopy temperature: A key to identify plant traits for drought tolerance and to quantify heat stress

99	Biernat, Lars	2016	Ökoeffizienz im ökologischen und konventionellen Marktfruchtbau Schleswig-Holsteins – ein konzeptioneller Ansatz zur Bewertung von Landnutzungssystemen
100	Hamacher, Maike	2016	Potentiale sekundärer Pflanzeninhaltsstoffe in Futterleguminosen und Wiesenkräutern für eine verbesserte N-Verwertung beim Wiederkäuer
101	Komainda, Martin	2017	Catch cropping in silage maize (*Zea mays* L.) – potential with respect to yield and environmental performance under the climatic conditions of northern Germany
102	Schoo, Burkhard Clemens	2017	Comparative eco-physiological analyses in cup plant, maize and lucerne-grass
103	Struck, Inga	2018	No-tillage silage maize (*Zea mays* L.) in ley-arable systems - Crop performance and environmental effects under maritime climates
104	Räbiger, Thomas	2020	Direct and indirect nitrous oxide emissions in oilseed rape production systems: Measurement and simulation
105	Graß, Rikard	2020	High-throughput phenotyping of drought stress resistance in mapping populations of rye: Canopy temperature, radiation interception and stay-green
106	Loza, Cecilia	2021	Examining the impact of different grass-legume mixtures on milk quality and methane emission in pasture-based milk production systems
107	Nyameasem, John Kormla	2021	Diverse forage production systems and their potential for greenhouse gas mitigation
108	Smit, Hendrik Petrus Jordaan	2021	Mitigation strategies to reduce greenhouse gas emissions and nitrogen losses from pasture-based dairy systems
109	Lorenz, Heike	2021	Towards eco-efficiency in dairy farming: the role of pasturing and grass-clover leys
110	Rose, Till	2022	The contribution of functional traits to breeding progress o central European winter wheat
111	Bukowiecki, Josephine	2022	Site-specific yield formation of winter wheat: combining remotely sensed crop data with simulation modeling
112	Verma	2022	Examining the inter- and intraspecies variability in the polyphenolic profile and in vitro antimethanogenic potential of forage species
113	Kemmann, Björn	2022	Assessment of field-derived greenhouse gas mitigation potential in biomass production by replacing maize with cup plant (*Silphium perfoliatum*) in low mountain ranges
114	Peters, Tammo	2023	Plant functional trait analysis and dynamic growth modelling of perennial ryegrass dominated pastures in north-west Europe
115	Rothardt, Steffen	2023	Mitigating N losses and improving N transfer in cropping systems by residue management
116	De Los Rios Mera, Josue	2023	Effects of land use and land use change in agricultural systems on soil carbon sequestration in north-west Europe

117	Brigitte Köhler	2024	Untersuchungen zur quantitativen Erfassung von Masse- und Stoffströmen im Futterbaubetrieb
118	Katja Holzhauser	2025	Cover crops for sustainable silage-maize production: Enhancing resource use efficiency through modelling and remote sensing

ISSN: 1435-2613